2-1-2016

Calcified gelatin nanofibers for guided tissue regeneration using water-based benign solvent: An investigation for periodontal applications

Nihal Abdelnabi Elsayed

Follow this and additional works at: https://fount.aucegypt.edu/etds

www.manaraa.com

THE AMERICAN UNIVERSITY IN CAIRO
الجــامـعة الأمـريكيـة بالقـاهـرة

School of Sciences and Engineering

Calcified Gelatin Nanofibers for Guided Tissue Regeneration Using Water-based Benign Solvent: An Investigation for Periodontal Applications

A Thesis Submitted to
The Biotechnology Graduate Program

In partial fulfillment of the requirements for
The degree of Master of Science in Biotechnology
By

Nihal A. Hassan, B.Sc.

Bachelor of Science, (2008)
Faculty of Science, Ain shams University

Under the supervision of

Dr. Nageh K.Allam, Ph.D

Associate Professor of Physics, Physics Department, the American
University in Cairo

Professor Suher Kamal Zada, Ph.D.

Professor of Immunology, Biology Department, the American University
in Cairo

Fall 2016

<u>Dedication</u>

To my Mother: the only person I am nothing without her. Thank you for making my life brighter and not giving up on me.

Acknowledgment

"All the praise to Allah by whose favor good works are accomplished"

Abstract

Periodontal regeneration, especially guided tissue regeneration (GTR), is one of the expanding applications in the field of tissue engineering. GTR barriers serve an exceptional function in healing various periodontal diseases such as gingivitis, periodontitis and loss of alveolar bone. Healing of periodontal pockets is somehow challenging as epithelial cells originated from the gingiva fill the site of defect and no regeneration takes place. Complete cell occlusion is a critical characteristic in case of pockets healing to obstruct gingival tissue growth, which performed via GTR membrane. Various materials were investigated for the synthesis of GTR membranes with collagen being the desired one among other bioresorbable polymers. Although collagen is renowned for its exquisite properties in mimicking the extracellular matrix (ECM), its high cost recalls for a substitute.

In an attempt to introduce a new composite for GTR membrane, cost effective gelatin was mixed with calcium carbonate at different concentrations and electrospun using a benign solvent. Different concentrations of gelatin solutions were first investigated to obtain smooth fibers using diluted acetic acid, where 40% of gelatin solution was successively electrospun into smooth fibers with diameters ranging from 140-260nm. Experiments were carried out by adding calcium carbonate ($CaCO_3$) at different concentrations. While smooth fibers were successfully obtained at lower concentrations of $CaCO_3$, beaded broken fibers were obtained at higher concentrations. The diameter of the smooth nanofibers was found to increase with increasing the concentration of $CaCO_3$. As gelatin is well known for its poor mechanical properties and stability, crosslinking using gluteraldhyde (GTA) vapors was considered to be a mandatory step. Different crosslinking time intervals were investigated for better stability, with the 20 h crosslinked mats showed enhanced water resistance and increased viability. Although the stability of nanofibers is elevated with prolonged crosslinking time, the pore size distribution among different mats was found to be almost the same (up to 250 nm) with the majority of the pores up to 50 nm.

Crosslinked mats showed distinguished mass increase during both swelling and biodegradability tests, especially with the decrease of calcium concentration among the mats. The presence of calcium within the mats acts as a nucleation site for the growth of Ca-P structures, leading to mineralization of the mats. Not only calcified did gelatin mats show promising results in MTT assay but also overall improved functional and structural properties. In summary, calcified gelatin mats proved to be a good candidate for guided tissue regeneration.

Table of contents:

List of abbreviations

BJH: Barrett-Joyner- Halenda

CaCO₃: Calcium carbonate

Ca-P: Calcium-Phosphate

CIP: Ciprofloxacin

Co-Cr: Cobalt-Chromium

COL: Collagen

Cs: Chitosan

DAA: Diluted acetic acid

DMEM: Dulbecco Modified Eagle's Medium

DMSO: Dimethyl sulfoxide

d-PTFE: High density polytetrafluoroethylene

ECM: Extra-cellular matrix

EDTA: Ethylenediamintetraacetic acid

EDX: Energy dispersive X-ray spectoscopy

Ef: *Enterococcus faecalis* bacterium

e-PTFE: Expanded polytetraflouroethylene

ESM: Egg shell membrane

ESP: Egg shell protein

FESEM: Field emission scanning electron microscopy

FTIR: Fourier transforms infrared spectroscopy

GBR: Guided bone regeneration

Gn: Gelatin

GTA: Gluteraldhyde

GTR: Guided tissue regeneration

HA: Hydroxyapaptite

HFP: 1,1,1,3,3,3-hexafluoro-2-propanol

HNTs: Halloysite aluminosilicate clay nanotubes

HPLC: High performance liquid chromatography

hTERT: Human telomerase reverse transcriptase

HVPS: High voltage power supply

kV: Kilovolt

mA: Milliampere

MET: Metronidazole

MNA: Metronidazole

MTT: 3-(4, 5-dimethylthiazol-2-yl)-2, 5-diphenyltetrazolium bromide

nAp: Nanoapatite

NFs: nanofibers

PBC: Poly(butylene carbonate) polymer

PBS: Phosphate buffer saline

PCL: Polycaprolactone

PDL: Periodontal ligaments

PDS: Polydioxanone

Pg: *Porphyromonas gingivalis* bacteria

PGA: Polyglycolic acid

PisPLLA: Poly isosorbide succinate-co-L-lactide

PLA: Polylactic acid

PLGA: Poly (D, L -lactide-co-glycolide)

PLLA: Poly-L-lactide

PTFE: Polytetraflouroethylene

SEP: Soluble egg shell protein

SPF: Simulated body fluid

Sw %: Swelling percentage

TCPs: Tissue culture polystyrene plates

Ti: Titanium

v%: volume per volume ratio

w%: Weight loss percent

w/v %: weight per volume ratio

XRD: X-ray diffraction

List of Tables

List of Figures

CHAPTER 1

INTRODUCTION AND SCIENTIFIC BACKGROUND

1.1. Tissue engineering:

Tissue engineering is a growing multidisciplinary field of biomedical engineering that utilizes biological tissues, biomaterials and biochemical factors to mimic natural tissues (Berthiaume, Maguire, & Yarmush, 2011) . It aims to enhance or replace a failing tissue for proper functioning (Annabi, Vrana, & Zorlutuna, 2006). The aforementioned functions could be (i) structural support as in bone and cartilage regeneration, (ii) transport related functions as in skin and blood vessels and (iii) secretory function as in liver and pancreas, more details were illustrated in Table 1.1 (Berthiaume et al., 2011).

Table 1.1: An overview of the different applications of tissue engineering with facing challenges (Berthiaume et al., 2011)

Tissue	Function	Approach	Challenges
Skin	Barrier for the body	Matrix implanted to guide regeneration; implants with autologous or allogeneic cells	Lack of appendages, slow process for growing cells, slow vascularization
Cornea	Transparent barrier for the eye	Matrix implants; extracellular matrix generated by cells cultured ex vivo	Maintain transparency and barrier properties of the matrix
Liver	Detoxification, production of liver-specific proteins	Hepatocytes from xenogeneic, allogeneic or stem cell-derived sources, or immortalized hepatoma seeded in implantable matrices, extracorporeal bioreactor systems	Cell source, maintenance of hepatic function, high cell density, vascularization of implants
Pancreas	Secrete insulin to maintain glucose homeostasis	Free or encapsulated islet transplantation	Choice of transplantation site, vascularization, cell source, immune rejection
Cartilage	Critical component of joints	Matrix implanted to guide regeneration; implants with autologous or allogeneic cells	Slow process for growing cells, control of cell differentiation, host integration, long-term durability
Heart	Provides blood circulation	Materials, including decellularized organs, seeded with progenitor and stem cells differentiated into cardiomyocytes	Tumorigenicity, control of cell differentiation, electrical integration
Kidney	Regulates body fluid volume and pH, metabolite excretion	Stem cell–derived nephrons cultured ex vivo	Replicating glomerular selectivity while retaining high hydraulic permeability
Neurons and spinal cord	Send electrical stimuli to control bodily functions	Materials shaped as tubes for axonal guidance and regeneration, sometimes used in combination with anti-inflammatory strategies; neural stem cells	Reconnecting proper axons, controlling proinflammatory environment, preventing scar tissue formation

Several technologies have been developed and investigated in the past decades to overcome the augmentation of various disease incidence that causes a wide range of damage from partial loss of function to complete failure of the organ as shown in Table 1.2 (Berthiaume et al., 2011).

Table 1 .2: Incident number of patients in the United states. (Berthiaume et al., 2011)

Indications	Procedures or patients
Skin	
Burns	2,000,000 total
Pressure sores	144,000 total
Venous stasis ulcers	2,500,000 total
Nervous system	
Spinal cord injury	259,000 total
Alzheimer's disease	5,300,000 total
Eye surgery	5,500,000/year
Ear surgery	900,000/year
Musculoskeletal	
Joint replacement (knee)	326,000/year
Joint replacement (hip)	165,000/year
Bone graft	500,000/year
Musculoskeletal (other)	6,300,000/year
Cardiovascular	
Heart disease	26,800,000 total
Respiratory system surgeries	1,500,000/year
Liver	
Liver cirrhosis	400,000 total
Liver cancer	16,260/year
Hepatitis C	3,200,000 total
Pancreas	
Diabetes	24,000,000 total
Digestive system surgeries	11,000,000/year
Urinary system surgeries	2,500,000/year

There are three main approaches that are usually followed in tissue regeneration: (i) transplantation of isolated cells as stem cells in damage sites, (ii) using biochemical growth factors to induce regeneration and (iii) scaffold implantation seeded with cells within the damaged tissue (Dhandayuthapani et al., 2011).

1.2. <u>Biomaterials</u>

According to Williams dictionary, biomaterials can be defined as any biocompatible material that interfaces a biological system to enhance, regenerate or replace a specific tissue/organ (Bergmann & Stumpf, 2013; Izwan et al., 2012). It acts as a framework to renovate diseased tissues as in sutures and different implants applied in tissue regeneration as previously shown in Table 1.1. (Dhandayuthapani et al., 2011).

Designing and fabrication of three-dimensional scaffolds that mimic the natural extracellular matrix (ECM) is one of the mostly used biomaterials for different tissue engineering applications. Scaffold can be defined as a 3D biomaterial having a porous surface to serve as a substrate for cell attachment, proliferation and differentiation (Dhandayuthapani et al., 2011). These biomaterials aim to resemble the original tissue to regenerate for optimal functioning.

In this chapter: different requirements essential for efficient scaffolding were highlighted, in addition to fabrication methods used and the composition of these scaffolds.

1.2.1. <u>General requirements</u>

Scaffolds should possess specific physical and chemical properties for proper performance, which vary depending on the desired application but there are essential requirements that cannot neglected.

1.2.1.1.<u>External surface and geometry</u>

Scaffolds must simulate the ECM where the external surface together with the architecture plays an important role for cellular attachment. Natural polymers unlike synthetic ones serve binding sites for cellular attachment which enhances the overall regeneration process (Dhandayuthapani et al., 2011). Scaffolds with poor cellular adhesion affect the proliferation rate and finally the success of scaffolding.

1.2.1.2. <u>Pore size and porosity</u>

Porous structures are vital for different type of applications. Its success depends on pore size distribution together with the interconnectivity of the pores, which is crucial for proper vascularization and better functioning. (Dhandayuthapani et al.,

2011; O'Brien, 2011). The importance of scaffold vascularization lies in exchanging nutrients with the surroundings and getting rid of wastes. Pore size can be manipulated depending on the desired function as incase occlusive membranes used in different environmental and biomedical applications which require very small sized pores to entrap particles or cells outside the membrane (Marco C. Bottino et al., 2012).

1.2.1.3. Biocompatibility

On top of all essential requirements remains the biocompatibility of the scaffold the most crucial one. Biocompatibility is the capability of performance with good host response. Biocompatible scaffolds should not provoke the immune system providing a suitable environment for cellular attachment and growth. (Dhandayuthapani et al., 2011; Gunatillake & Adhikari, 2003)

1.2.2. Methods of fabrication

1.2.2.1. Particulate-leaching technique

It is commonly used simple technique for scaffolds synthesis. In this technique, salt having desired size is used for creating pores with the same size.

Salt of desired size will be prepared and then well dispersed in polymeric solution to use. The solution will be casted in a mold and left until the solvent completely evaporated. The salt then removed from the scaffold using water in which it dissolved leaving pores of equal size. The degree of porosity together with the size of the pores can easily manipulated with the concentration of the salt initially added and the size used respectively. (Ma, 2004)

1.2.2.2. Gas foaming

In this technique, carbon dioxide gas is used for creation of pores within the polymeric structure. The gas foamed at higher pressure into the polymer, where it is absorbed within and saturation reached. The dissolved gas upon saturation separates in form of nucleation. Later, the absorbed gas will be converted to pores within the polymer decreasing its density with increasing the occupied volume (Subia, Kundu, & Kundu, 2010).

1.2.2.3. Phase separation

In this technique, temperature used to aggregate the polymeric solution into two phases; one with high concentration of polymer and the other with low concentration. The solvent removed afterwards at the sublimation temperature leaving only the polymer behind. Pores fabricated by using bioactive particles that dispersed before phase separation and will removed after solvent evaporation. Solvent used in this technique was carefully chosen together with the temperature at which the separation took place for desired results (Ma, 2004; Subia et al., 2010).

1.2.2.4. Electrospinning

Electrospinning is a versatile cost-effective technique for fabrication of nanofibers. Different types of polymers were successfully electrospun into nanofibers as shown in Table 1.3. As nanofibers known for their high aspect ratio, they are manifested in wide range of applications shown in Figure 1.1.

Table 1.3 : Synthetic and natural polymers successfully used for nanofibers fabrication (Bhardwaj & Kundu, 2010).

Polymers	Applications	Characterizations
Poly(glycolide) (PGA)	Nonwoven TE[a] scaffolds	SEM[b], TEM[c], *in vitro* rat cardiac fibroblast culture, *in vivo* rat model
Poly(lactide-co-glycolide)(PLGA)	Biomedical applications, wound healing	SEM, WAXD[d], SAXS[e], degradation analysis
Poly(ε-caprolactone) (PCL)	Bone tissue engineering	SEM, *in vitro* rat mesenchymal stem cell culture
Poly(l-lactide) (PLLA)	3D cell substrate	SEM, *in vitro* human chondrocyte culture
Polyurethane (PU)	Nonwoven tissue template wound healing	SEM, *in vivo* guinea pig model
Poly(ethylene-co-vinyl alcohol) (PEVA)	Nonwoven tissue engineering scaffold	SEM, *in vitro* human aortic smooth muscle cell and dermal fibroblast cultures
Polystyrene (PS)	Skin tissue engineering	SEM, *in vitro* human fibroblast, keratinocyte, and endothelial single or cocultures
Syndiotactic 1,2-polybutadiene	Tissue engineering applications	ESEM[f], XRD[g], FTIR[h]
Fibrinogen	Wound healing	SEM,TEM,mechanical Evaluation
Poly (vinyl alcohal)/cellulose acetate (PVA/CA)	Biomaterials	SEM, FTIR, WAXD, mechanical evaluation
Cellulose acetate	Adsorptive membranes/felts	SEM, FTIR
Poly(vinyl alcohol)	Wound dressings	SEM, EDX[i]
Silk fibroin, silk/PEO[j]	Nanofibrous TE scaffold	SEM, FTIR, XPS[k]
Silk	Biomedical Applications	SEM, TEM, WAXD
Silk fibroin	Nanofibrous scaffolds for wound healing	SEM, ATR-IR[l], ^{13}C CP/MAS NMR, WAXD, NMR[m], *in vitro* human keratinocyte culture
Silk/chitosan	Wound dressings	SEM, viscosity analysis, conductivity measurement
Chitosan/PEO	TE scaffold, drug delivery, wound healing	SEM, XPS, FTIR, DSC[n]
Gelatin	Scaffold for wound healing	SEM, mechanical evaluation
Hyaluronic acid, (HA)	Medical implant	SEM
Cellulose	Affinity membrane	SEM, DSC, ATR-FTIR[o]
Gelatin/polyaniline	Tissue engineering scaffolds	SEM, DSC, conductivity measurement, tensile testing
Collagen/chitosan	Biomaterials	SEM, FTIR

Conventional electrospinning setup is made of; high voltage power supply (HVPS), Spinneret, syringe pump and collector as shown in Figure1.2 (A) (Bhardwaj & Kundu, 2010). The range of voltage supported by HVPS differs from one setup to another, which can reach up to 40 KV or even more. The HVPS connects to the spinneret, where the polymer-loaded syringe placed to be electrospun. The spinneret can be stationary or translocatory during the electrospinning process. The solution ejects from the syringe using syringe pump, which controls the flow of the polymeric solution with desired rate. Finally, the synthesized fibers received on grounded collector for removal of charge residuals within the collected mats.
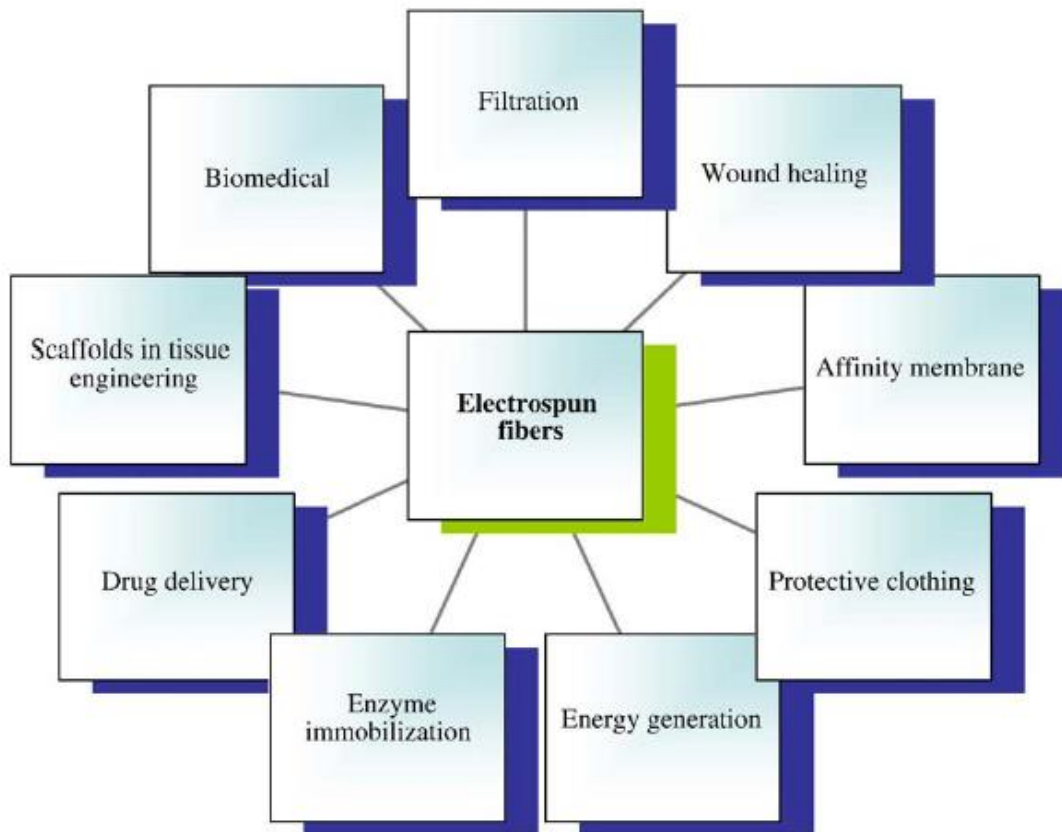
Figure 1. 1: Various applications of nanofibers (Bhardwaj & Kundu, 2010).

There are different types of collectors to be used depending of the final desired architecture and orientation i.e. stationary collector, rotating drum and disc collector as shown in Figure1.2 (A-C) (Bhardwaj & Kundu, 2010; Pham, Sharma, & Mikos, 2006).

7

During the electrospinning process, voltage applied to the polymeric solution ejected through the syringe tip charging the ejected drop. At low voltages, Rayleigh forces dominate leading to droplets formation. On increasing of the applied voltage, the charged drop elongates into a Taylor cone, where Rayleigh instabilities cease as illustrated in Figure 1.3 (A-B). On reaching critical voltage, Rayleigh instabilities disappear and the charged solution overcame the surface tension leading to jet formation as shown in Figure 1.3 (C). The charged jet has undergone whipping and bending forces resulted from repulsive forces within the charged polymer, which caused its acceleration toward the oppositely charged collector. The formed nanofibers are collected, and residual charges are neutralized (Baji, Mai, Wong, Abtahi, & Chen, 2010; Okutan, Terzi, & Altay, 2014).

There are different parameters that affect the success of the electrospinning process in addition to the morphology of the resulted nanofibers. These parameters classified into solution parameters, processing parameters and ambient parameters as illustrated in Table 1.4.
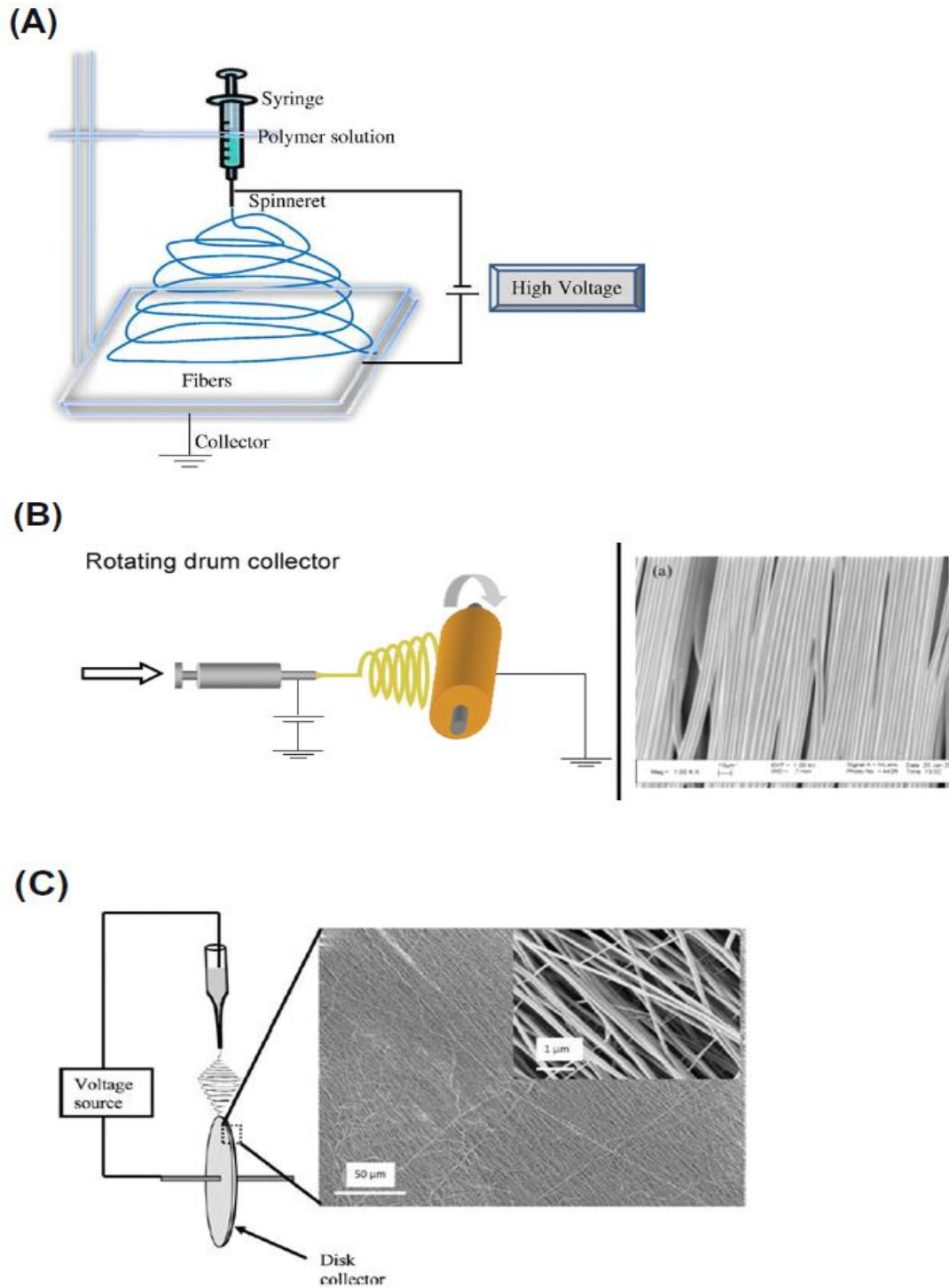
Figure 1. 2: Different collectors used in electrospinning setup; (A) stationary collector, (B) Rotating drum and (C) Disk collector (Baji et al., 2010; Bhardwaj & Kundu, 2010; Pham et al., 2006).
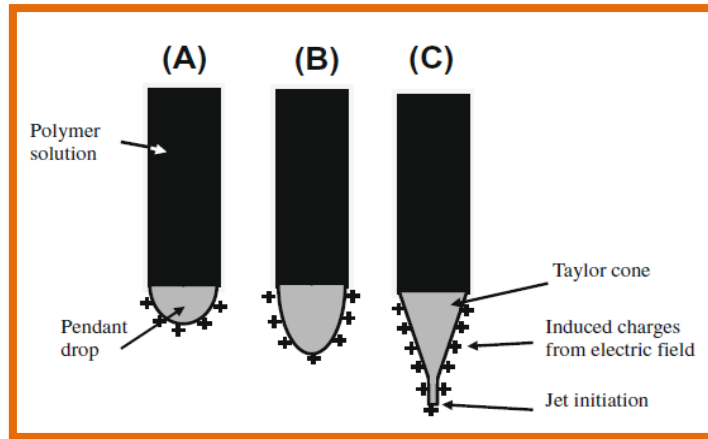
Figure 1. 3: Different stages undergone by the solution ejected drop by drop while increasing the applied voltage; (A) charged drop on voltage application where on increasing the voltage , it expands as illustrated in (B) which is converted to Taylor cone followed by jet ejection as in (C).(Baji et al., 2010)

Table 1.4: Electrospinning parameters: processing and ambient parameters and their effect on the resulting nanofibrous structures. (Baji et al., 2010)

Parameters	Effect on fiber morphology
Solution parameters	
Viscosity	Low-beads generation, high-increase in fiber diameter , disappearance of beads.
Polymer concentration	Increase in fiber diameter with increase of concentration.
Molecular weight of polymer	Reduction in the number of beads and droplets with increase of molecular weight.
Conductivity	Decrease in fiber diameter with increase in conductivity.
Surface tension	No conclusive link with fiber morphology, high surface tension results in instability of jets.
Processing parameters	
Applied voltage	Decrease in fiber diameter with increase in voltage.
Distance between tip and collector	Generation of beads with too small and too large distance, minimum distance required for uniform fibers.
Feed rate/Flow rate	Decrease in fiber diameter with decrease in flow rate, generation of beads with too high flow rate.
Ambient parameters	
Humidity	High humidity results in circular pores on the fibers.
Temperature	Increase in temperature results in decrease in fiber diameter.

1.2.3. Composition

Different materials used for fabrication of wide range of biomaterials for biomedical applications as illustrated in Figure 1.4. Each material has its own characteristics, with its positive and negative aspects that qualify it for a specified effective application (Ramakrishna, Mayer, Wintermantel, & Leong, 2001).

1.2.3.1. Natural grafts

Natural grafts are types of biomaterials, where natural biological tissues harvested and implanted in site of injury. They classified according to the origin of these tissues into three main types as shown in Figure 1.5.

1.2.3.1.1. Autografts

They are biological grafts, where the patient acts as his own donor (Izwan et al., 2012). Cells are harvested from the patient's body and embedded in the site of injury (Freeman & Kwansa, 2008; Izwan et al., 2012). This type of grafts is the gold standard approach in regenerating injuries, as the body will not reject the graft and easily recognize it.

Autografts have a major drawback; the patient has to suffer from a surgical operation to extract these cells, which may be accompanied by site morbidity (Oryan et al., 2014; Izwan et al., 2012). Although it is the most desired approach among other grafts it has limited applications due to anatomical differences between the extracted tissues and the damaged ones (Izwan et al., 2012).

1.2.3.1.2. Allografts

Allografts are biological grafts, where cells were harvested from a donor of the same species as from one human to another (Freeman & Kwansa, 2008). Although it did not proceed by another surgery to harvest the cells as in autografts, it considered an undesired approach. It has major drawbacks; (i) it can be rejected by the receiver, (ii) it can induce the immune system and (iii) have high probability of disease transmission and bacterial infection (Izwan et al., 2012 ;Freeman & Kwansa, 2008).

1.2.3.1.3. Xenografts

They are biological grafts, where cells obtained from one species and transplanted in a receiver from another species. It shares the same drawbacks aforementioned for allografts, which makes it an undesired approach (Oryan et al., 2014).
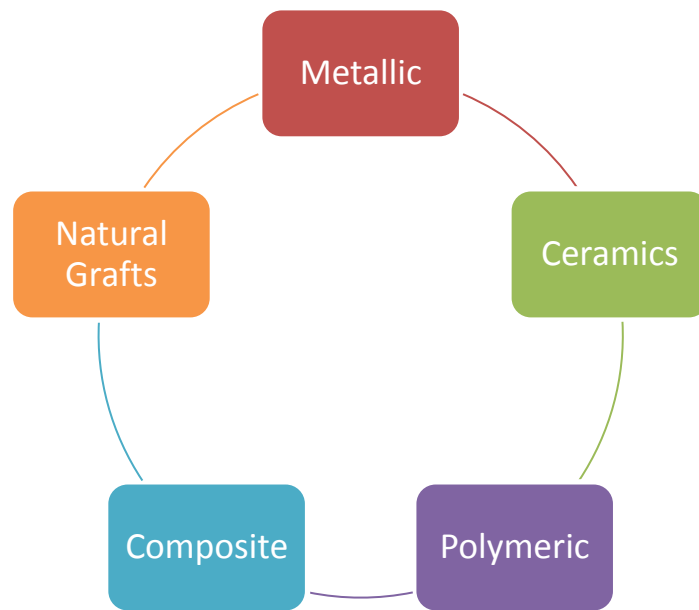
Figure 1.4: Different materials used in biomaterials fabrication for wide range of biomedical applications.
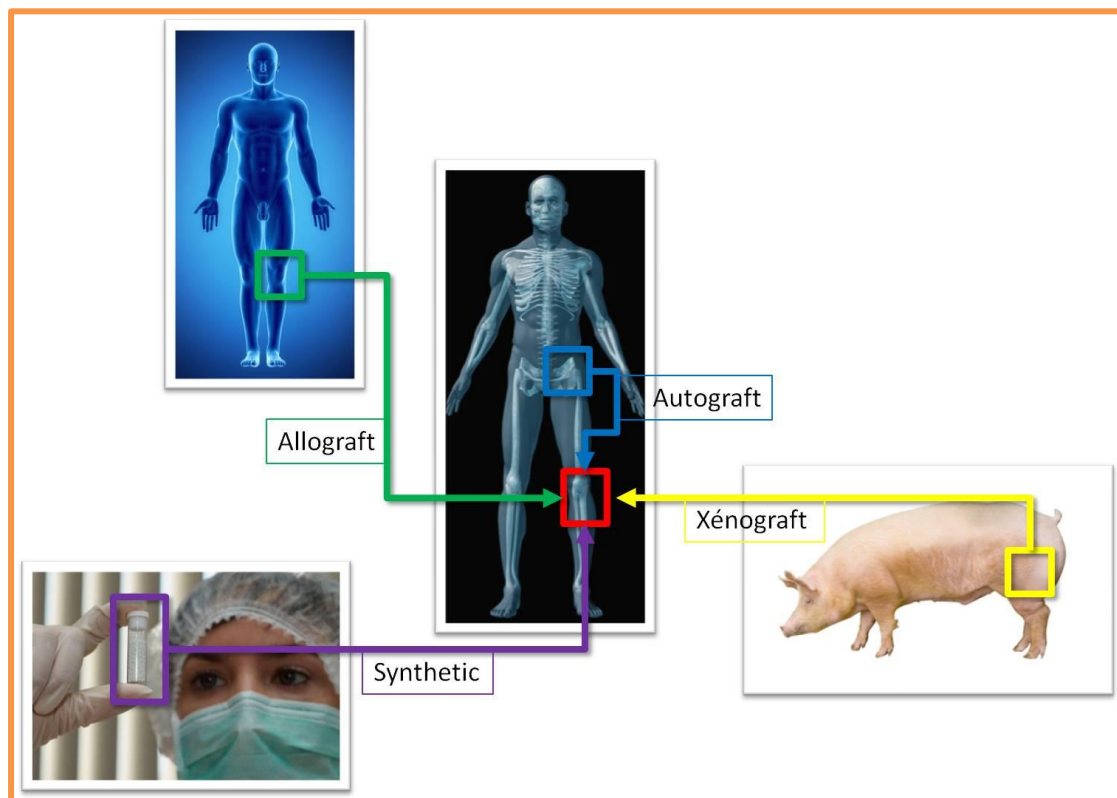
Figure 1.5: Different types of natural grafts used in bone regeneration

1.2.3.2. Metallic biomaterial

Metals have exquisite electrical, mechanical and thermal properties (Pilliar & Metals, 2009). It has free electrons that interacts with the surrounding tissues via metallic bonds that result in its fixation (Kim & Park, 2003). Different shapes of metallic biomaterials can be easily fabricated using different techniques to be used several applications.

It has wide range of applications as it is considered an excellent candidate for hard tissue replacements due to its load bearing properties i.e. in orthopedic replacements (Mediaswanti et al., 2013; Kim & Park, 2003). It is also can be used in neuromuscular application i.e. neuromuscular devices and cardiac pacemakers due to its high electrical conductivity (Pilliar & Metals, 2009).

Alloys of various metals have been synthesized of different composition and amounts that can be tolerated within the body for bone replacements as shown in Table 1.5 (Kim & Park, 2003). The first implant was made of vanadium steel and was used in form of plates and screws applied in humans (Kim & Park, 2003). It revealed two main drawbacks (i) metals can be toxic if it exceeds a certain limit and (ii) the degradation products of these implants resulted from *in vivo* corrosion could be lethal to the surrounding tissues besides decreasing its mechanical properties (Kim & Park, 2003) .

Due to the aforementioned drawbacks, vanadium steel was replaced by other alloys with elevated strength and resistance to corrosion such as stainless steel, cobalt-chromium (Co-Cr) alloy and titanium (Ti) alloy (Nasab & Hassan, 2010; Kim & Park, 2003).

Table 1.5: Different mechanical properties of different metallic alloys implants relative to those of cortical and cancellous bones (Mediaswanti et al., 2013).

Material	Elastic modulus GPa	Tensile strength (10^{-3}) GPa
Cortical bone	20	150
Cancellous bone	3	5
Stainless steel	200	700
Co-Cr-Mo alloys	230	500
Titanium	110	500
Ti-6Al-4V	110	950

1.2.3.3. Polymeric biomaterial

Wide range of scaffolds can be synthesized using variant types of polymers for different biological applications i.e. skin, cartilage, bone, vascular and liver regeneration. Polymers can be classified according to their origin into natural and synthetic polymers as shown in Figure 1.6 where synthetic polymers can be further classified according to their degradability into biodegradable and non-degradable polymers (Patel, Bonde, & Srinivasan, 2011; Seal, Otero, & Panitch, 2001).
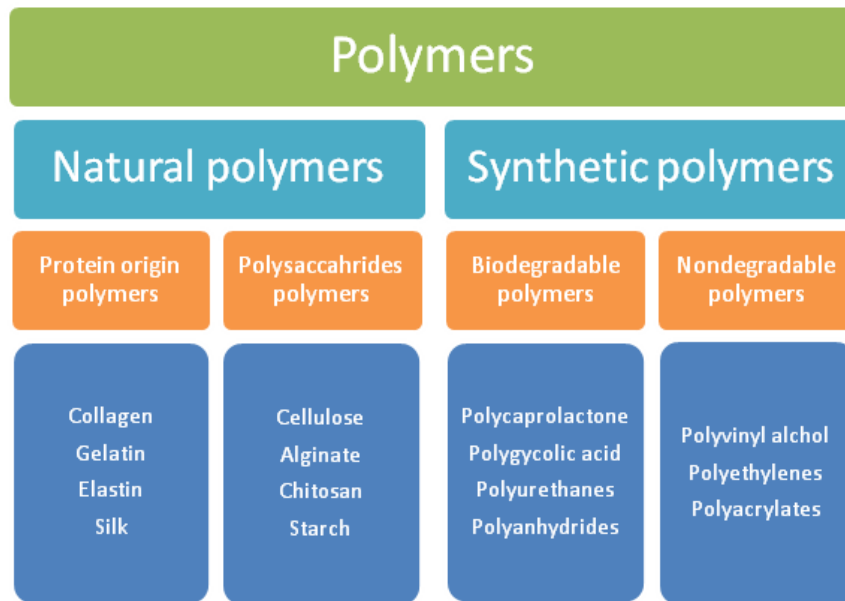
Figure 1.6: Different types of polymers used in different biomedical applications.

1.2.3.3.1. Biodegradable polymers

They are types of polymers that degrades within the body into by product while/after performing a desired function (Chandra & Rustgi, 1998a). These polymers can be classified according their origin into natural polymers and synthetic polymers (Patel et al., 2011).

1.2.3.3.1.1. Natural polymers

Polymers that are naturally exist in different living organisms are known as biopolymers or natural polymers (Chandra & Rustgi, 1998a). There are two main categories of natural polymers (Patel et al., 2011).

A. Protein-based polymers

They are complex arrangements of polypeptides made of variant types of α-amino acids connected by peptide bond (Chandra & Rustgi, 1998a).

A.1. Collagen

There are twenty seven types of collagen abundant among living organisms (Gómez-Guillén, Giménez, López-Caballero, & Montero, 2011). Type I collagen is a unique polymer representing the majority of the ECM of connective tissues (Patel et al., 2011; Oryan et al., 2014). It is composed of triple helix of α-amino acid chains which is supported by different types of intra-chain and inter-chain bonding (Gómez-Guillén, Giménez, López-Caballero, & Montero, 2011). It can be obtained by extraction from different tissues of variant animals such as rat tail tendons, calf bones and porcine skin (Gómez-Guillén et al., 2011).

Collagen is considered to be an outstanding choice for variant biomedical applications due to its high biocompatible, biodegradable and non-cytotoxic properties (Oryan et al., 2014) . It has been used commercially for different biomedical applications i.e. collagen gels used for skin regeneration, collagen sponges for healing long bone fractures and conventional membranes for periodontal applications (Patel et al., 2011; Y. Zhang, Zhang, Shi, & Miron, 2013). Despite the aforementioned biomedical applications of collagen, It has major drawbacks i.e. (i) low mechanical properties which is considered a main concern in some applications (Oryan et al., 2014), (ii) inconsistent rate of degradation (Patel et al., 2011), (iii) difficulty of handling and sterilization (Patel et al., 2011) and (iv) Its elevated price (Oryan et al., 2014). Its mechanical properties and degradation rate were optimized using variant methods such as crosslinking or reinforcement by adding fillers or polymers (Patel et al., 2011).

A.2. Gelatin

Gelatin is a natural polymer produced by partial hydrolysis of collagen (Patel et al., 2011). Collagen was hydrolyzed when heat is applied at temperature greater than 45°C leading to cleavage of hydrogen and covalent bonds which destabilize the triple helix and soluble gelatin was formed (Gómez-Guillén et al., 2011).

It is a polypeptide chain composed of Glycine-X-Y where X and Y usually proline and hydroxyproline. It produced from different sources. Porcine skin is considered the most plentiful origin for gelatin production (up to 50%) followed by bovine hides (almost 30%) and cattle bones and marine resources (Gómez-Guillén et al., 2011).

There are two main types of gelatin that can be produced depending on the hydrolysis process (i) type A; produced from the acidic pretreatment and (ii) type B; produced from the alkaline pretreatment (Gómez-Guillén et al., 2011). Isoelectric point of each type of gelatin varied from 8-9 for type A and 4-5 for type B (Gómez-Guillén et al., 2011).

Gelatin has both acidic and basic functional group due to the presence of carboxylic and amino groups (Patel et al., 2011). It has exquisite gelling properties besides its viscoelasticity that has diversity of applications in food industry, pharmaceuticals, and cosmetics (Gómez-Guillén et al., 2011). It is considered to be a good alternative for collagen due to its low cost, excellent antigenic properties, biocompatibility and bioaffinity (Chung & Park, 2007). Gelatin scaffolds showed great attachment, migration and proliferation in different tissue regeneration applications (Chung & Park, 2007; Patel et al., 2011).

Different gelatin structures were fabricated using different techniques such as freeze drying, lypholization, phase separation, porogon-leaching and 3-D printing as shown in Figures (1.7-1.9) (Irvine et al., 2015; Liu & Ma, 2009). Gelatin nanofibers electrospun using different solvents such as tetrafluoroethanol (Z. M. Huang, Zhang, Ramakrishna, & Lim, 2004), formic acid (Ki et al., 2005), mixture of solvents (Mindru, Mindru, Malutant, & Tura, 2007), ethylacetate dissolved in water (Song, Kim, & Kim, 2008), water (S. Zhang et al., 2009), mixture of acetic acid, tetrafluoroalcohol (Nguyen & Lee, 2010) and diluted acetic acid (Erencia et al., 2015).
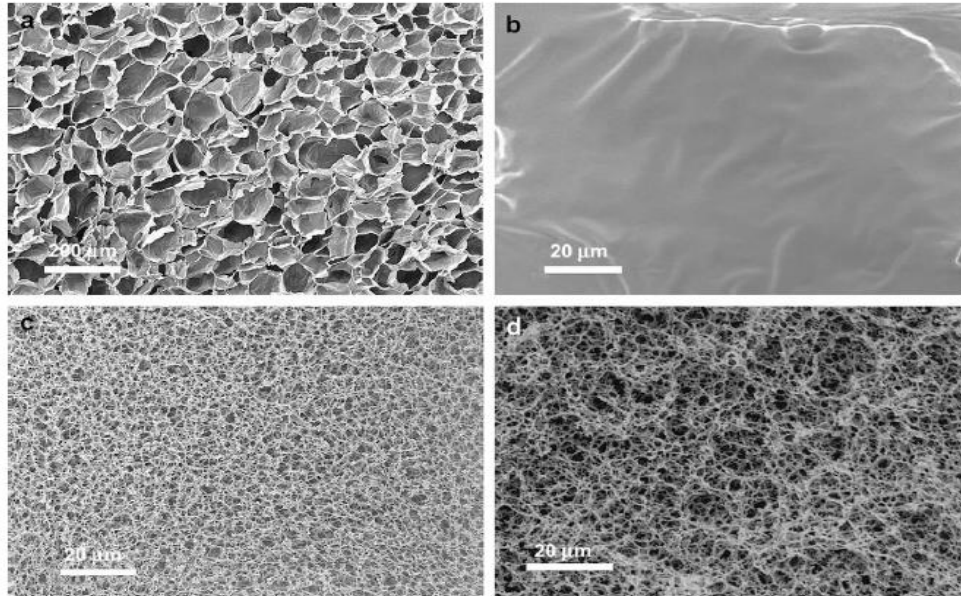
Figure 1.7: SEM images of different gelatin matrices fabricated by different techniques using different solvents; (a-b) lypholization images at low and high magnifications, (c-d) phase separation followed by freeze drying (Liu & Ma, 2009)**.**
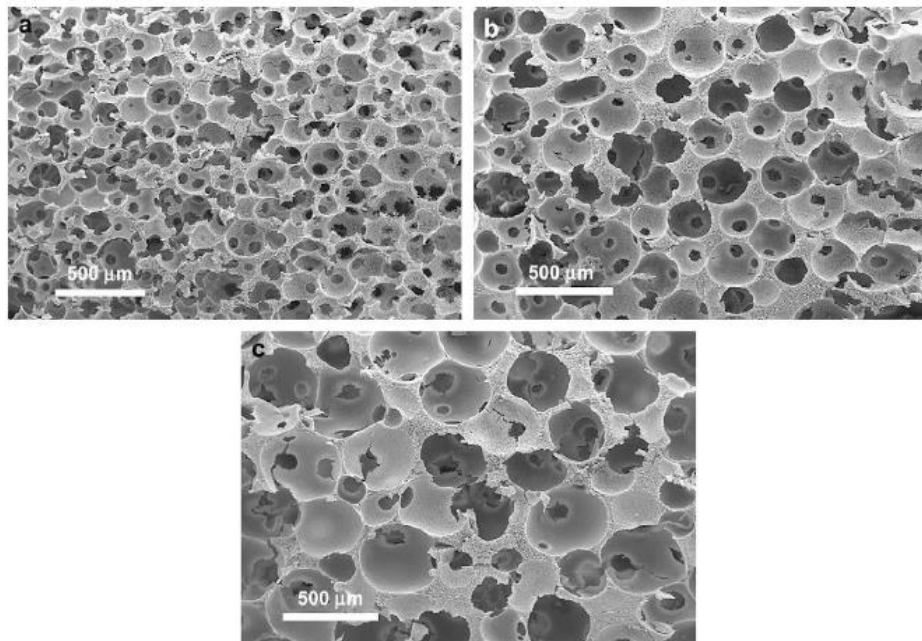
Figure 1.8: SEM images of gelatin scaffold having different pore sizes synthesized using porogen-leaching technique (Liu & Ma, 2009)**.**
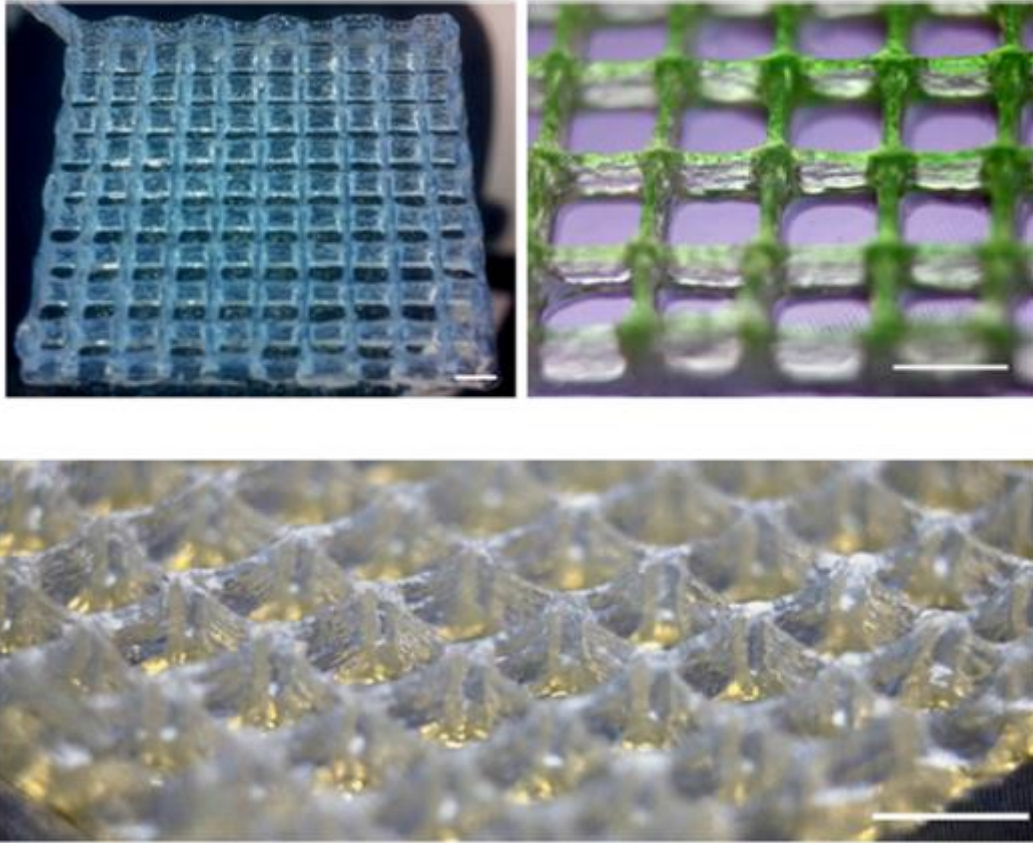
Figure 1.9: Woodpile structure synthesized via 3D printing of gelatin shown at different magnification (Irvine et al., 2015).

A.3. <u>Elastin</u>

Elastin is one of the major elastomeric proteins in the extracellular matrix of variant tissues (Annabi et al., 2013; Oryan et al., 2014). It constitutes almost half of the aortic tissue and the elastic ligaments, almost 32% of main vascular tissues, almost 7% of lungs and skin's dry weight and 4% of tendons (Annabi et al., 2013). It can be extracted from elastin rich tissues such as in animal ligaments or even produced by recombinant technology using different hosts for protein expression (Annabi et al., 2013).

It has variant morphological displays in different tissues with different biological functions. Elastin based biomaterials are considered to be an excellent choice for biomedical applications in elastic tissues i.e. in skin, lungs, blood vessels and vascular tissue regeneration (Annabi et al., 2013).

18

A.4. <u>Silk</u>

Silk is a natural polypeptide produced by variants of arthropods for functional purposes Silk can be produced by some worms i.e. *Bombyx mori* and by different genera of spiders i.e. *Argiope* and *Nephila* (Humenik, Smith, & Scheibel, 2011). It serves different functional purposes as worms silk is used to protect them during metamorphosis while spiders silk is used for weaving webs to catch their prey (Humenik et al., 2011). Despite worms silk is the famed type of silk for its industrial use in textile production, spiders silk is favored for its mechanical properties (Humenik et al., 2011). Certain species of spiders can weave webs made of seven types of silk having variant properties to enable it to catch flying preys (Humenik et al., 2011).

Although different types of silks produced by spiders are considered rich with wide range of properties for industrial uses, its production on large scale have many obstacles. First, spider farming as the majority of spiders cannot survive in large population due to the lack of social instincts. Second, collection and separation of produced silk takes a lot of time and effort. Recombinant technology solved these problems by using hosts for significant genes responsible for silk production as shown in Figure 1.10 (Humenik et al., 2011)

Engineered spiders silk can be used for films, 3D hydrogels, micro/ nano-capsules or even can be used for fibers production for different applications (Humenik et al., 2011).
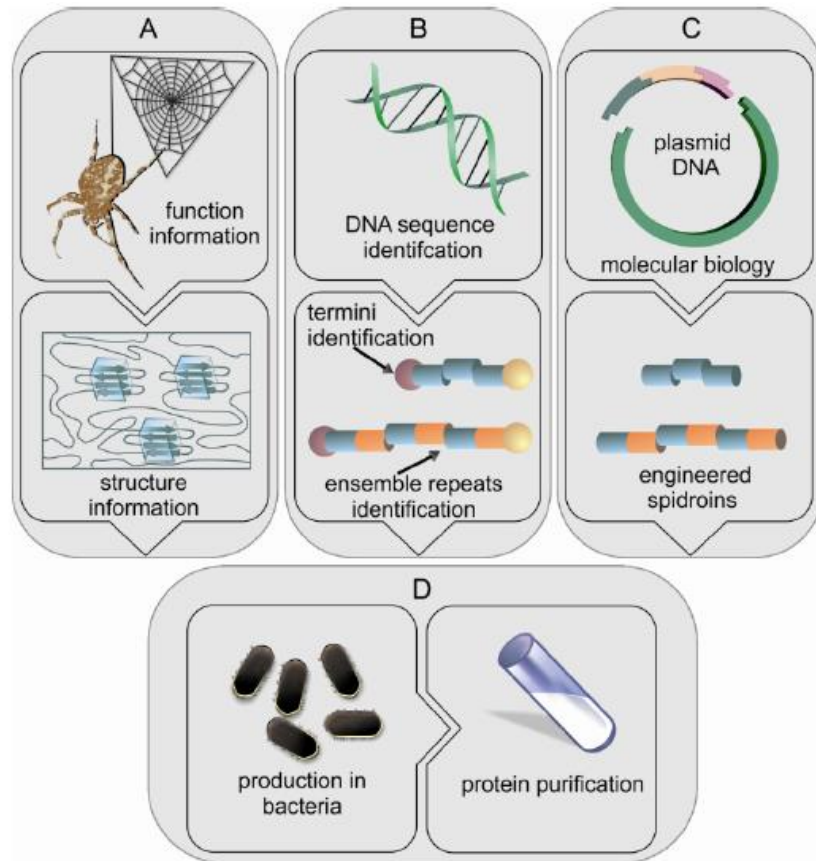
Figure 1.10: Recombinant technology used for silk production: (A) Shows silk structure obtained from previous experimentation using different instrumentations such as FTIR and XRD, (B) all information obtained is used for production of cDNA libraries, (C) known structure genes obtained from saved cDNA libraries inserted into plasmids where synthetic gene expression can be done using hosts such as E.coli , for protein production, (D) produced proteins can be extracted and purified for further applications. (Humenik et al., 2011)

B. Polysaccharide-based polymers

Naturally existing polymers are made of more than one carbohydrate monomer linked by glycosidic linkage (Chandra & Rustgi, 1998a).

B.1. Cellulose

Cellulose is a naturally occurring biomass in plants, bacteria and some marine organisms (Moon, Martini, Nairn, Simonsen, & Youngblood, 2011). Its production reaches 500 billion tons yearly with only two percent being used in industrial applications (Qiu & Hu, 2013).

Cellulose has no color, no odor besides being nontoxic (Qiu & Hu, 2013). It is mainly composed of a six member ring *D*-anhydroglucopyronase units that is linked by glycosidic linkage (Qiu & Hu, 2013). Cellulose is rich with hydroxyl groups along its skeleton which are consequently linked forming intra and inter-molecular bonds

stabilizing the whole structure (Moon et al., 2011; Qiu & Hu, 2013). These molecular bonds promote the insolubility properties of cellulose as it doesn't dissolve neither in water nor in most of the other solvents (Kalia et al., 2011; Kamel, Ali, Jahangir, Shah, & El-Gendy, 2008).

Cellulose consists of two main regions; an arranged crystalline region and an amorphous region where the crystalline region has four polymorphic structures (I, II, III & IV) (Kalia et al., 2011; Moon et al., 2011). The first and the second types (cellulose I and II) are called native cellulose referring to plant cellulose (Kamel et al., 2008). Type I is considered to be the least stable amongst the four types which is converted via chemical treatment to metastable type II (Moon et al., 2011; Kamel et al., 2008).

It is characterized by being nontoxic, biocompatible, hydrophilic biopolymer with thermoplastic properties (Qiu & Hu, 2013). it has great mechanical strength that enables its application in stimuli responsive materials (Qiu & Hu, 2013). It has wide range of applications as it is used industrially for paper and textile production, besides using it medically in blood dialysis (Kamel et al., 2008; Moon et al., 2011)

B.2. <u>Alginate</u>

Alginate is a type of biodegradable natural existing polysaccharides (Sun & Tan, 2013). It is synthesized by certain species of seaweeds i.e. *Laminaria* and *Lessonia* species where its production reaches 38 thousand tons yearly (Andersen, Strand, Formo, Alsberg, & Christensen, 2012). Bacteria is considered to be another source for alginate production via fermentation process especially those belong to *Azotobactar* and *Pseudomonas* genera (Rehm, 2009; Andersen et al., 2012).

Alginate is an unbranched polymer composed mainly of *D*-mannuronic acid and *D*-Guluronic acid residues known as M and G residues (Basu, Jana, Gandhi, & Sen, 2011; Rehm, 2009). These residues can be arranged either individually into G/M blocks or arranged alternatively forming MG dimers as shown in Figure 1.11 (Basu et al., 2011).

It is anionic water soluble polymer characterized by their sol/gel properties besides it biocompatible , biodegradable and non-antigenic properties (Basu et al., 2011; Sun & Tan, 2013). Its sol gel properties is attributed to its G block interaction

with multivalent cations as Ca^{2+} (Kurt I. Draget & Taylor, 2011). Its mechanical properties can be tailored by its molecular weight (Sun & Tan, 2013). Alginate has wide range of biomedical applications i.e. wound dressing, medical stents, microspheres and hydrogels for different tissue regeneration (Kurt I. Draget & Taylor, 2011; Andersen et al., 2012; Sun & Tan, 2013)
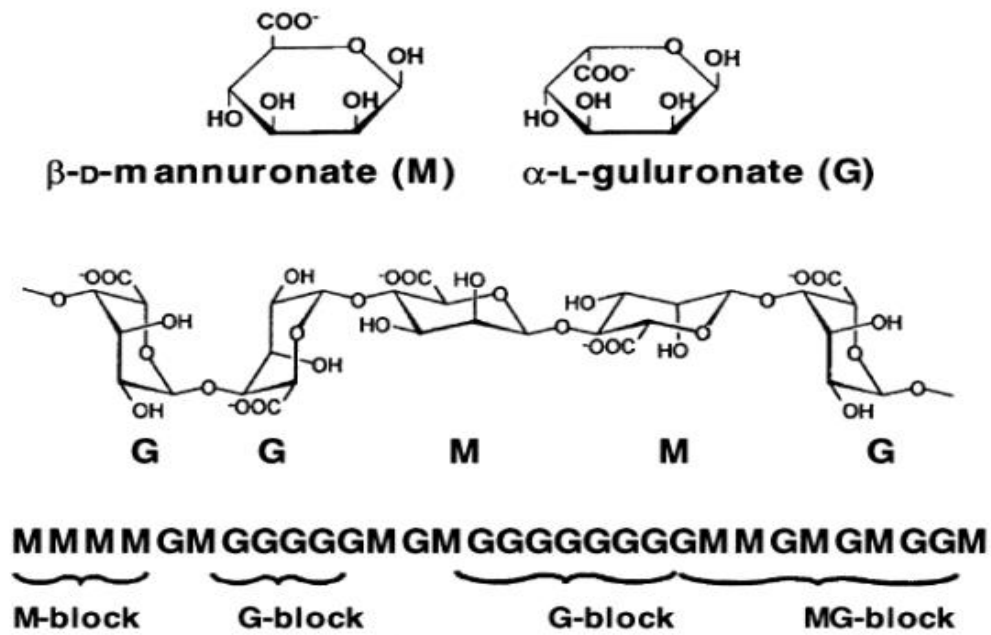
Figure 1. 11: Alginate main residues; M and G monomers which is arranged either into homo-blocks of G/M residues or in MG dimeric block (Draget et al., 2005;Kurt I. Draget & Taylor, 2011).

B.3. Chitosan

Chitosan is the de-acetylated derivative of chitin biopolymer which is originated mainly from crustaceans, fungi and yeast cell walls as shown in Figure 1.12 (Bansal, Sharma, Sharma, Pal, & Malviya, 2011; Di Martino, Sittinger, & Risbud, 2005). Its solubility is pH dependent as it is insoluble in aqueous solutions at pH > 7 and its solubility is enhanced in weak acids below pH=6 (Rinaudo, 2006; Di Martino et al., 2005).

It exists naturally in the cationic form which makes is susceptible to interact with other anionic molecules (Rinaudo, 2006; Di Martino et al., 2005). It has exquisite

characteristics that promotes it for different biomedical and industrial applications as shown in Table 1.6 (Rinaudo, 2006; V & A, 2013). It is a biocompatible polymer with biodegradable, bioresorbable and non-immunogenic properties (Z. Li, Ramay, Hauch, Xiao, & Zhang, 2005). Chitosan has great antimicrobial and hydrophilic properties which enhance the attachment of cells (Di Martino et al., 2005; Bansal et al., 2011).

```
          Crab/Shrimp shells
                  ↓
       Demineralization (dilute)
                  ↓
        Deproteination (dilute)
                  ↓
        Decolourisation (dilute)
                  ↓
               Chitin
                  ↓
      Deacetylation (concentrated)
                  ↓
              Chitosan
```
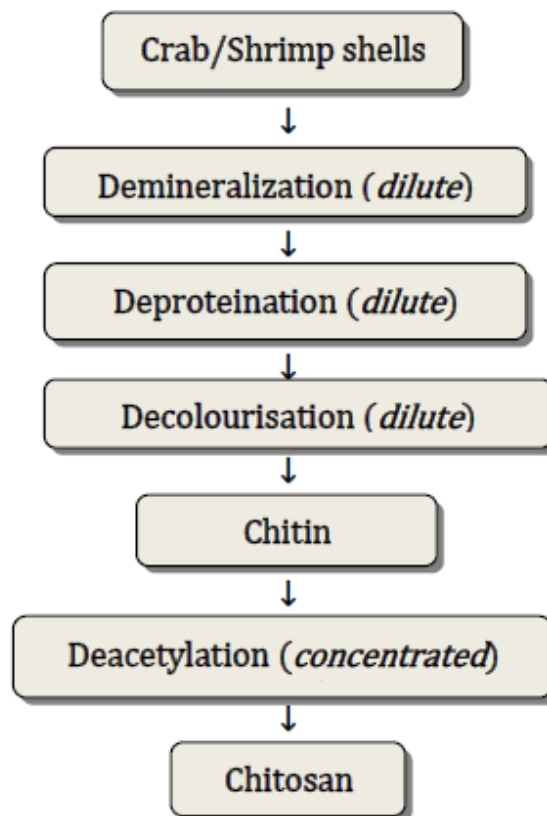
Figure 1.12: The extraction of chitin from crustaceans and its further deacetylation to chitosan (V & A, 2013).

Table 1.6: Applications of chitosan in variant fields (Rinaudo, 2006).

Agriculture	Defensive mechanism in plants Stimulation of plant growth Seed coating, Frost protection Time release of fertilizers and nutrients into the soil
Water & waste treatment	Flocculant to clarify water (drinking water, pools) Removal of metal ions Ecological polymer (eliminate synthetic polymers) Reduce odors
Food & beverages	Not digestible by human (dietary fiber) Bind lipids (reduce cholesterol) Preservative Thickener and stabilizer for sauces Protective, fungistatic, antibacterial coating for fruit
Cosmetics & toiletries	Maintain skin moisture Treat acne Improve suppleness of hair Reduce static electricity in hair Tone skin Oral care (toothpaste, chewing gum)
Biopharmaceutics	Immunologic, antitumoral Hemostatic and anticoagulant Healing, bacteriostatic

B.4. Starch

It is an inexpensive biopolymer with wide applications in plastic industry (Halley & Averous, 2014). It originates from plants cereals and fruits. It is considered to be the main polysaccharide stock in different plant tissues responsible for photosynthesis process (Halley & Averous, 2014). It is composed of two main polysaccharides; (i) unbranched amylose and (ii) nonlinear amylopectin (Babu, O'Connor, & Seeram, 2013).

Starch is considered to be the main lignocellulosic resource that is used in production of bioethanol due to its availability in low cost besides the ease of processing (Mobini-Dehkordi & Javan, 2012). It converts to ethanol by two consecutive steps. First, it undergoes saccharification process using different enzymes such as α-amylase to produce sugars (Viktor, Rose, van Zyl, & Viljoen-

24

Bloom, 2013; Mobini-Dehkordi & Javan, 2012). Second, the produced sugars are fermented using microorganisms i.e. *S.cerevisiae* for ethanol production (Viktor, Rose, van Zyl, & Viljoen-Bloom, 2013; Mobini-Dehkordi & Javan, 2012). It has other applications i.e. in paper, plastics, pharmaceuticals, fabrics and chemical industries (Babu et al., 2013; Halley & Averous, 2014; Mobini-Dehkordi & Javan, 2012)

1.2.3.3.1.2. <u>Synthetic polymers</u>

Synthetic polymers produced via chemical reactions called polymerization. Biodegradable synthetic polymers undergo degradation through the breakage of these chemical bonds either by hydrolysis or enzymatic degradation (Nair & Laurencin, 2007). This type of synthetic polymers has huge impact on industry as it can replace commonly used plastics derived from petroleum products (Vroman & Tighzert, 2009).

Traditional plastic has two main drawbacks; first, it is derived from petrol product and with the inflation of the oil prices, its industry became expensive. Besides its difficulty in biodegradation as it resists degradation by microbes and thus will have a hazardous impact on the ecosystem to its accumulation (Vroman & Tighzert, 2009).

There are various classes of biodegradable synthetic polymers such as polyesters, polyorthoesters, polyurethanes and polyanhydrides (Gunatillake & Adhikari, 2003). These classes have broad range of applications in industrial and biomedical fields; such as degradable sutures, packaging films, cleaning products, orthopedic fixation pins and screws (Vroman & Tighzert, 2009; Gunatillake & Adhikari, 2003).

A. <u>Polyesters</u>

A.1. <u>Polycaprolactone</u>.

Polycaprolactone was first manufactured at the early thirties. It is a synthetic biodegradable polyesters with hydrolysable backbone and slow degradation rate (Puppi, Chiellini, Piras, & Chiellini, 2010). It is soluble in different organic solvents with outstanding degradation rate compared to other resorbable polymers.

It has wide range of applications especially in drug delivery devices due to its controlled releasing rate (Chandra & Rustgi, 1998; Woodruff & Hutmacher, 2010).

Polycaprolactone is well known for its enhanced mechanical properties, which enables great performance in different biomedical applications. Different fabrication techniques applied using PCL that yielded variant structures as shown in Figure 1.13.
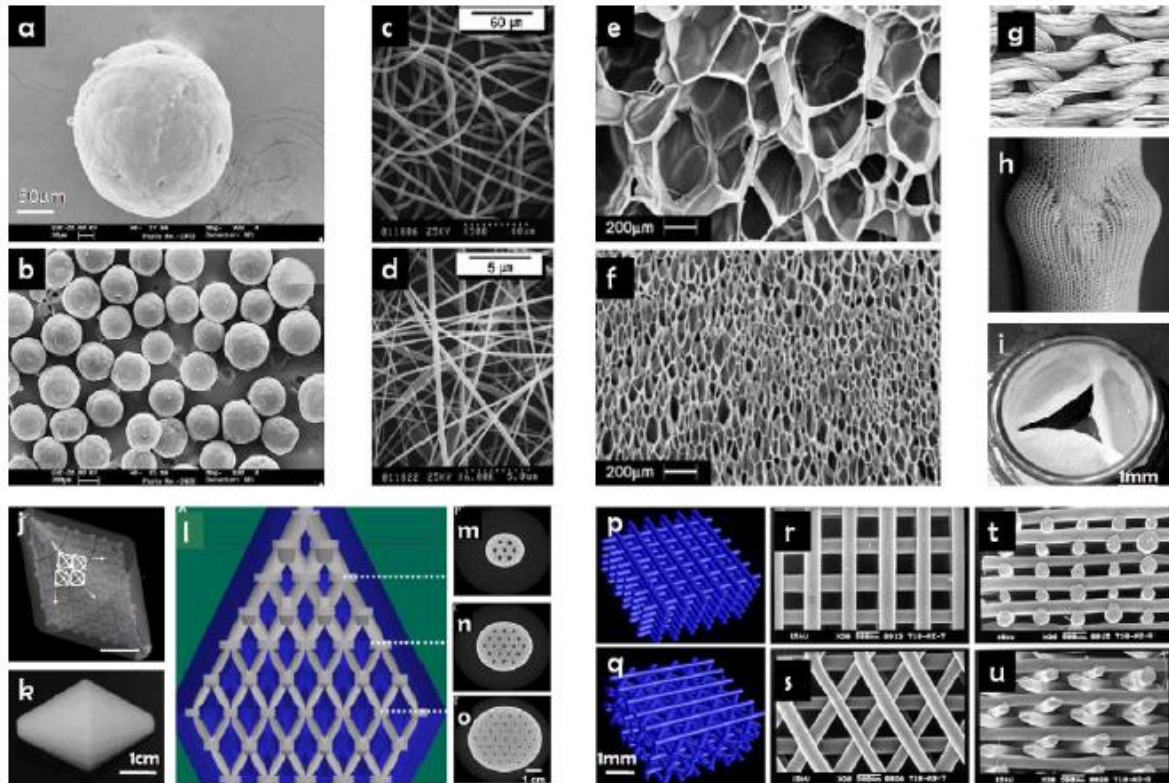
Figure 1.13: Different PCL synthesized structures; (a-b) PCL nanospheres, (c-d) PCL nanofibers, (e-f) PCL foams, (g-i) PCL knitted textiles, (j-l) PCL scaffolds synthesized using laser sintering technique and (p-u) PCL scaffolds formed by fused deposition (Woodruff & Hutmacher, 2010).

A.2. Polylactic acid

Polylactic acid is an aliphatic polyester polymer that chemically synthesized from lactic acid. Lactic acid is widely spread in different natural starch rich renewable sources.

It is used in wide range of applications starting from packaging of food and sanitary products to biomedical applications (Avérous, 2008; Vroman & Tighzert, 2009). Different antimicrobial agents were loaded within PLA for antimicrobial packaging (Tawakkal, Cran, Miltz, & Bigger, 2014). It is considered to be a promising alternative to plastics used that contribute to increased carbon dioxide gas emission accompanied by global warming (Ren, 2010).

Although PLA is popular for its biocompatible and enhanced mechanical properties, it has major drawbacks such as increased hydrophobicity and decreased

bioaffinity. To overcome these drawbacks different composite of PLA in addition to PLA modification were investigated to enhance its rate of degradation and cell adhesion for biomedical applications (Lee, Yoon, Woo, & Choi, 2003).

A.3.   Polyglycolic acid
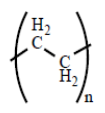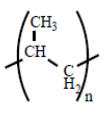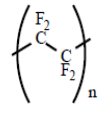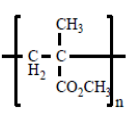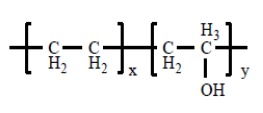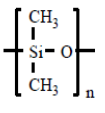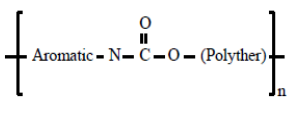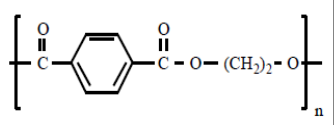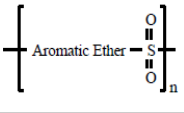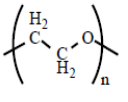
It is a type of polyester polymers, which is used in drug delivery applications in addition to surgical sutures industry. Although it shares different members of polyester polymer their hydrophobic properties, it can be tailored by surface modification for different applications (Lee et al., 2003). PGA yields acidic byproducts upon degradation which limits its applications (Vroman & Tighzert, 2009).

1.2.3.3.2. Nondegradable polymers

There are different types of non-degradable polymers that are used for different types of application as shown in Table 1.7 (Shastri, 2003).

Polytetraflouroethylene polymer (PTFE) is one of the most widely used nondegradable polymers. It is made of fluoro-ethylene monomer (Ham & Miller, 2003). It is a costly crystalline polymer with high chemical resistance properties (Aldousiri, Shalwan, & Chin, 2013). It is widely famous for its application in periodontal membranes, which are merchandized by different brands like Gore-Tex®. These membranes are characterized by their highly manipulated pore size and porosity (Aurer & JorgiE-Srdjak, 2005).

Table 1.7: Different types of non-degradable polymers; chemical structure and possible applications (Shastri, 2003).

Chemical name & Trade name	Chemical Structure	Key Property	Traditional Applications
Poly(ethylene) (PE) (HDPE, UHMWPE)		Strength and lubricity	Orthopaedic implants and catheters
Poly(propylene) (PP)		Chemical inertness and rigidity	Drug delivery, meshes and sutures
Poly(tetrafluroethylene) (PTFE) (Teflon), extended-PTFE (Gore-Tex®)		Chemical and biological inertness and lubricity	Hollow fibers for enzyme immobilization, vascular graft, guided tissue regeneration and barrier membrane in the prevention of tissue adhesions
Poly(methymethacrylate) (Palacos®)		Hard material, excellent optical transparency	Bone cement, ocular lens
Ethylene-co-vinylacetate (EVA) (Elvax®)		Elasticity, film forming properties	Implantable drug delivery devices
Poly(dimethylsiloxane) (PDMS) (Silastic®, silicone rubber)		Ease of processing, biological inertness, excellent oxygen permeability, excellent optical transparency	Implantable drug delivery devices, device coatings, gas exchange membranes, ocular lens, orbital implants
Low MW poly(dimethylsiloxane) (Silicone oil)	Same as above	Gel-like characteristics	Filler in Silicone breast implants
Poly(ether-urethanes) (PU) (Tecoflex®, Tecothane®, BioSpan®)		Blood compatibility and rubber-like elasticity	Vascular grafts, heart valves, blood contacting devices, coatings
Poly(ethylene terphthalate) (PET) (Dacron®)		Fiber forming properties and slow in vivo degradation	Knitted Dacron vascular grafts, coatings on degradable sutures, meshes in abdominal surgery
Poly(sulphone) (PS)		Chemical inertness, creep resistant	Hollow fibers and membranes for immobilization of biomolecules in extra-corporeal devices
Poly(ethyleneoxide) (PEO, PEG)		Negligible protein adsorption and hydrogel forming characteristics	Passivation of devices toward protein adsorption and cell encapsulation

CHAPTER 2

LITERATURE REVIEW

2.1. <u>General overview</u>

Tissue engineering scaffolds generally used to act as an extracellular matrix for cellular attachment, migration and proliferation (Jafari et al., 2015; Sachlos & Czernuszka, 2003). There are characteristic properties that are crucial for successful scaffolding. Although these characteristics vary according to the desired function, they should be basically porous biocompatible architectures permitting vascularization and act as a hydrophilic mechanical support for the attached cells (Chan & Leong, 2008; Jafari et al., 2015; Rucker et al., 2008; Sachlos & Czernuszka, 2003).

Periodontal regeneration especially guided tissue regeneration (GTR) is one of the expanding application of tissue engineering field which started after its usage clinically in the mid of eighties (Scantlebury & Ambruster, 2012; Y. Zhang et al., 2013). GTR/GBR barriers serve an exceptional function in healing various periodontal diseases such as gingivitis, periodontitis and loss of alveolar bone (Fujihara, Kotaki, & Ramakrishna, 2005; Rakhmatia, Ayukawa, Furuhashi, & Koyano, 2013).

Periodontal ligaments (PDL) are dynamic connective tissue attached to the cementum of the teeth from one side and to the alveolar bone in the gingiva from the other side (Marco C. Bottino et al., 2012; L. Huang et al., 2016). It has numberless of exquisite functions besides holding all parts together. First, it is highly responsive to mechanical stresses, where it protects the teeth by stress dissipation (L. Huang et al., 2016). Second, It serves a unique regenerative machinery as they act as a reservoir for both differentiated and the peregrinator cells which is essential for regeneration of different periodontal tissues (Aurer & JorgiE-Srdjak, 2005; Pellegrini, Pagni, & Rasperini, 2013b). Third, it supplies nutrition to various dental cells in addition to other functions.

Although gum inflammation known as gingivitis is considered to be a tolerable disease that occur basically due to simple bacterial infection, it can finally lead to teeth loss (Nagarajan, Miller, Dawson, Al-Sabbagh, & Ebersole, 2015). It all starts when untreated gingivitis progresses to periodontitis where loosening of the alveolar bone from the PDL took place creating dental pockets (Srivastava et al., 2015).

Plaques and debris accumulate within these pockets and consequently it can turn to severe periodontitis, where loss of alveolar bone and periodontal ligaments takes place leading teeth loss.

Healing of periodontal pockets is somehow challenging as epithelial cells and fibroblast originated from the gingiva grow at higher rates compared to that originated from periodontal ligaments. In consequence the site of defect will be filled by the gingiva rather that regenerated by the periodontal ligaments and thus no regeneration takes place (Pellegrini, Pagni, & Rasperini, 2013a; Shue, Yufeng, & Mony, 2012; Wang et al., 2016).

Loss of teeth can be hindered if periodontal defects were filled with membranes that facilitate regeneration. GTR/GBR membranes should have key characteristics for optimal functioning besides being biocompatible and other basic properties mentioned earlier (Aurer & JorgiE-Srdjak, 2005). Complete cell occlusion is a critical characteristic in case of pockets healing to obstruct gingival tissue growth through the membrane and thus easing regeneration process by PDL. Occlusive GTR/GBR can be formed by pore size manipulation to be small enough to hinder the undesired growth but permits vascularization at the same time (Rakhmatia et al., 2013; Rispoli L, Fontana F, Beretta M, 2015).

Periodontal pockets requires require up to six weeks for PDL regeneration and up to 6 month in case of bone replacement and ridge augmentation so the rate of degradability of the membrane is a key characteristic for its success (Marco C. Bottino et al., 2012; Wang et al., 2016).

The first attempt for dental regeneration was launched by Nyman et.al where Millipore cellulose acetate filter was used and since then various types of synthesized membranes have been tested (Y. Zhang et al., 2013). Synthesized membrane barriers can be classified into three main generations, where various types are commercially available as illustrated in Table 2.1 (Rakhmatia et al., 2013; Sam & Madhavan Pillai, 2014)

First generation of membrane barriers were nonresorbable membranes usually made of polytetrafluorethylene (PTFE) or titanium reinforced PTFE (Aurer & JorgiE-Srdjak, 2005; Sam & Madhavan Pillai, 2014). Commercially available PTFE membranes are made either of expanded PTFE (e-PTFE) known as Gore-Tex® or high density PTFE (d-PTFE) like those merchandized as cytoplast® (Aurer & JorgiE-Srdjak, 2005; Y. Zhang et al., 2013). Although first generation membrane barriers are distinguished for its mechanical and biocompatible properties ,surgical procedure after a month for its removal is considered to be a major drawback (Aurer & JorgiE-Srdjak, 2005; Sam & Madhavan Pillai, 2014). Not only PTFE removal is considered to be unpleasant costly experience for the patient, but also it may leads to bacterial infection and consequently regeneration failure (Aurer & JorgiE-Srdjak, 2005; Y. Zhang et al., 2013).

Table 2.1: Different commercially available GTR/GBR membranes (Rakhmatia et al., 2013).

Commercial name	Properties (pores; thick)
Non resorbable expanded polytetrafluoroethylene (e-PTFE)	
Gore-Tex®	0.5–30 μm. Discontinued
Non resorbable high dense polytetrafluoroethylene (d-PTFE)	
Cytoplast™ (GBR; TXT)	Less than 0.3 μm
Cytoplast® Non Resorb	Less than 1.36 μm
TefGen FD™	0.2–0.3 μm
Nonresorbable ACE	<0.2 μm; 0.2 mm
Non resorbable titanium mesh	
Frios® BoneShields	0.03 mm; 0.1 mm
Tocksystem Mesh™	0.1–6.5 mm; 0.1 mm
M-TAM™	1700 μm; 0.1–0.3 mm
Ti-Micromesh ACE	1700 μm; 0.1 mm
Resorbable collagen (origin type of collagen; resorption time)	
BioGide®	Porcine (I and III); 24 weeks
BioMend®	Bovine (I); 8 weeks
Biosorb® Membrane	Bovine (I); 26–38 weeks
Neomem™	Bovine (I); 26–38 weeks
OsseoGuard®	Bovine (I); 24–32 weeks
Ossix	Porcine (I); 16–24 weeks
Resorbable synthetic (origin; resorption time)	
Atrisorb®	Poly-DL-lactide; 36–48 weeks
Biofix®	Polyglycolic acid; 24–48 weeks
Epiguide®	Poly-DL-lactic acid; 24–48 weeks
Resolut XT	Poly-DL-lactide/Co-glycolide; 8 weeks
OsseoQuest®	Hydrolyzable Polyester; 16–24 weeks
Vicryl	Polyglactin 910 mesh; 8 weeks

First generation drawbacks gave rise to a second generation of bioresorbable membrane barriers, where both natural and synthetic polymers employed. Although synthetic polymers showed enhanced mechanical properties compared to natural polymers, they possess some properties considered challenging points to be solved (Marco C. Bottino et al., 2012). Finally the third generation was on leach, where resorbable membranes were fabricated as drug delivering machinery in order to enhance regeneration (Sam & Madhavan Pillai, 2014).

Here I will spot the light on different polymers used for the synthesis of bioresorbable GTR membranes for periodontal applications using electrospinning technique.

2.2. <u>Second generation membranes</u>

Polyesters polymers such as polycaprolactone (PCL) are synthetic polymers characterized by their high mechanical properties and prolonged degradation rate. They considered good candidates for periodontal regeneration and widely employed for membranes fabrication. Although their exquisite mechanical properties they have two main concerns for their application as they possess poor cell adhesion and prolonged degradation. To overcome these drawbacks and make use of their exquisite mechanical properties an approach of mixing natural polymers which is well known for its high cell adhesion and degradability with polyesters to get the advantages of both polymers where the membrane will attain good mechanical properties supplied by the synthetic polymer but with increased cell attachment and degradation rate.

Different ceramics were incorporated together with PCL to test its effect on enhancement of PCL for periodontal applications. Fujihara et al. investigated the effect of calcium rich PCL membranes resulted from the addition of calcium carbonate nanoparticles to enhance the osteoconductive properties of membranes used for GTR (2005). In this approach the hydrophobic properties of PCL was balanced with the addition of nano-calcium carbonate particles, as nano-architectured surfaces showed to enhance cell adhesion and proliferation. Two concentrations of PCL-$CaCO_3$ mixtures were prepared (1:3 and 3:1) where the initial

concentration of PCL was added to these two mixtures varied from 3 to 7.5 wt%. Smooth nanofibers were obtained using 5% PCL in PCL-CaCO$_3$ (1:3) and 7% PCL in PCL-CaCO$_3$ (3:1) solution. As PCL is famous for its poor hydrophilic properties, the fabricated nanofibrous membranes were treated with plasma to increase the hydroxyl groups on its surface and thus enhancing its hydrophilicity. PCL membranes having lower concentration of calcium carbonate (PCL-CaCO$_3$ = 3:1) showed better results in both mechanical testing and cell proliferation. The increase of calcium carbonate within the mats lowered the mechanical properties by elevating the mat's brittleness. PCL nanofibers containing nanosized calcium carbonate is considered to be a promising approach to increase cell attachment and proliferation (Fujihara et al., 2005).

Another approach for using PCL polymer for periodontal application was reported by Yang et al., where nanoapatite (nAp) was used instead of calcium carbonate for improving its bioactivity (2009). PCL together with nAP were successfully electrospun into smooth nanofibers using diluted trifluroethanol as electrospinning solvent. The mats revealed great mineralization results when immersed in simulated body fluid (SPF) for two and four weeks compared to PCL mats that lacked mineralization. The presence of nAp within the mats releases calcium on degradation, which acts as a nucleation sites for apatite growth on the surface of the mats appeared as needle like structures after 2 weeks of immersion and progressed to cauliflowers on week 4. Although mineralization of the mats together with the apatite presence usually enhances cellular growth, PCL-nAp mats experienced ceased cellular growth up to 28 days of incubation. Yang et al. explained the aforementioned cellular growth by the early differentiation of the osteoblasts decreasing the proliferation rate (Yang et al., 2009).

Egg shell protein (ESP) is a cost effective, naturally existing protein extracted from egg shell membrane (ESM) located between egg white and egg shell. It consists of different types of collagen (I, V and X) in addition to other proteins (Jia, Liu, Guo, Yu, & Duan, 2012). It has outstanding mineralization characteristics enabling biomineralization within 24 h. Natural ESM has been investigated by Dupoirieux et

34

al. to be used as a periodontal membrane which revealed decreased space maintaining ability (Dupoirieux, Pourquier, Picot, & Neves, 2001). Soluble egg shell protein (SEP) extracted from ESM was further investigated by mixing it with various synthetic polymers for enhancement of mechanical properties. SEP together with poly (D, L -lactide-co-glycolide) (PLGA) polymer was prepared by Jia et al. at three different concentrations; 9:1, 7:3 and 1:1 (2012). Different concentrations of SEP-PLGA were electrospun into beads free nanofibers, where the thickness decreased with the SEP content. Blending of SEP together with PLGA enhanced the hydrophilicity of the mats, where contact angle was decreased with the concentration of SEP added. Not only has the increase of SEP concentration affected the hydrophilic properties but also it decreased the mechanical properties of the mats. SEP-PLGA nanofibers with 7:3 and 1:1 ratios showed better support for cellular growth and adhesion. Briefly, Jia et al. proposed a good candidate simulating ECM for GTR membrane where future optimization is required (Jia et al., 2012).

Other type of polyester polymers that was used for second generation of periodontal membranes is Poly-L-lactide (PLLA). As a member of polyesters, PLLA shared PCL their aforementioned drawbacks. It has different applications in *in vivo* for many years, where by Trejo et al. has used it for healing of intrabony defects. Its hydrophobic natural slows down its degradation rate in addition to ceased cell attachment along its surface. Chen et al. grafted chitosan (Cs) which is well known for its biodegradability and increased cell affinity on PLLA electrospun mats (2013). PLLA mats aminolyzed with Cs revealed better hydrophilic properties, which in turn affected cell attachment and degradation rate. The degradation rate of newly fabricated mats was tested by their immersion in PBS at 37°C and was compared to untreated PLLA mats. The mats found to lose up to 20% of its initial weight compared to only 5% for PLLA mats. The results showed that although grafting of Cs on PLLA mats did not change the external morphology of the mats but it enhanced its rate of degradation. PLLA poor cell adhesion proved to be enhanced with Cs addition, as it added new recognition sites for cellular attachment along the surface. PLLA mats grafted with Cs proved good mineralization and hydrophilic properties which enhanced both cells attachment and degradation rate (S. Chen et al., 2013).

Another trial was performed by replacement of polycaprolactone (PCL) with Poly(butylene carbonate) (PBC) polymer for GBR membranes by Xia et al. (2014). PBC has similar backbone to PCL and its fabrication using electrospinning technique was compared to electrospun PCL nanofibers. As PBC is more hydrophilic compared to PCL, it was expected to stimulate cell adhesion and increase its rate of degradation due to hydrolysis. Electrospinning solutions were prepared by using formic acid as a solvent and electrospinning took place for nanofibers fabrication. Surface contact angle results of both mats revealed that PBS possesses better hydrophilic properties compared to PCL, where the later showed better mechanical properties. Both mats revealed same rate of cellular growth, however PBC mats showed better ALP activity. This enhanced activity considered as a marker for its ability to undergo mineralization and osteogenic differentiation. Xia et al. showed that prepared PBS membrane was a successful prototype compared to pure PCL nanofibers for GBR (Xia et al., 2014).

Electrospun polydioxanone (PDS) polymer was used by Bottino et al. for root pulp healing as a replacement for conventional used therapy of calcium hydroxide or mineral trioxides (2015). They aimed the synthesis of hallow nanofibers for future loading of antibiotic drugs within these structures for antibacterial effect. Halloysite aluminosilicate clay nanotubes (HNTs) were mixed at different concentrations with PDS using 1,1,1,3,3,3-hexafluoro-2-propanol (HFP) as an electrospinning solvent. Hollow structures were synthesized ranging from 300nm up to 1.5um where the thickness was found to increase with the HNTs concentration. Unlike the diameter of the nanofibers, the mechanical properties were found to decrease with HNTs content. Different concentrations of HNTs tested for proliferation assay supported cellular attachment and growth. According to Bottino et al. PDS-HNTs nanofibers showed promising results for future optimization to be used as antibiotic machinery for regenerative endodontitis application (Marco C Bottino et al., 2015).

2.3. Third generation membranes

Third generation membranes; novel membranes of both synthetic and natural composites were synthesized and loaded with different drugs and growth factors to

promote regeneration especially in case of GBR which usually takes from 3 month up to 6 month of healing.

Norowski et al. have developed Chitosan (Cs) mats crosslinked with genipin and loaded with minocycline (2012). As Chitosan was proven to enhance dental pulp healing, it was used together with genipin for nanofibers crosslinking. The mats were then soaked in minocycline solution for drug loading. Crosslinking was performed by genipin dispersion within Cs to ensure high crosslinking efficiency. Although crosslinked mats showed similar swelling results to uncrosslinked Cs nanofibers, bacterial inhibition was observed to increase from 4 days for uncrosslinked mats to 8 days for crosslinked ones. The aforementioned results showed that crosslinking of Cs using genipin improved minocyline retention within the mats and its prolonged release upon degradation which in turn increased the zone of inhibition compared to uncrosslinked mats (Norowski et al. , 2012).

As collagen has exquisite natural properties mimicking the natural ECM its employment for GTR membrane remains on top of natural polymers, Chen et.al developed biocompatible membranes made of electrospun collagen nanofibers loaded with amoxicillin, metronidazole, and lidocaine (D. W. C. Chen et al., 2013). Composite of PLGA together with collagen was prepared by with 2:1 ratio into 1,1,1,3,3,3-hexafluoro-2-propanol (HFP) and was then successfully electrospun as an outer shell of smooth nanofibers where the core was filled with amoxicillin, metronidozole and lidocaine hydrochloride. *In vitro* drug release investigated by soaking samples in PBS solution and analysis of eluents performed using high performance liquid chromatography (HPLC) until the samples completely dissolved within almost 30 days. The experimental results showed that the drug-loaded collagen membranes could provide sustainable release of effective amoxicillin, metronidazole, and lidocaine for 28, 56, and 8 days, respectively. Furthermore, the bioactivity of the released antibiotics remained high, with average bioactivities of 50.5% for amoxicillin against *Staphylococcus aureus* and 58.6% for metronidazole against *Escherichia coli*. The aforementioned continuous release of drugs did not affect the cytotoxicity of the mats, which showed good viability results. The

nanofibrous multipharmaceutical membrane developed in this study may provide a promising solution for regenerative periodontal therapy (D. W. C. Chen et al., 2013).

Polydioxanone (PDS) synthetic polymer was investigated for periodontal applications as for healing of endodontitis; inflammation of dental pulp. Bottino et.al. have prepared different concentrations of PDS. During these preparations, antibiotics such as metronidazole (MET) and ciprofloxacin (CIP) were added each at a time (M C Bottino et al., 2013). Different antibiotic containing PDS solutions were electrospun into nanofibers followed by drug release characterization using high-pressure liquid chromatography (HPLC), mechanical testing, cytotoxicity test and antimicrobial testing. All synthesized mats containing antibiotics possessed good mechanical properties to maintain spacing required for endodontitis regeneration. Mats containing 25% MET showed better results compared to other concentrations of MET and CIP. Due to the difference in molecular weight of antibiotics used the difference in drug release rates was significant where MET release up to 50% during the first two days. Antimicrobial results revealed that electrospinning of PDS into nanofibers loaded with antibiotics did not affect its antibacterial activity. Electrospun nanofibers loaded with CIP showed inhibition of both *P.gingivalis (Pg)* and *E. faecalis (Ef)* even at low concentrations (5%) where MET loaded nanofibers showed inhibition of *Ef*. To sum this up Bottino et al. showed that PDS loaded with antibiotics could be a good competitive to antibiotic paste and other solutions conventionally used (M C Bottino et al., 2013).

Another attempt in synthesis of nanofibers loaded with antibacterial drug was done by Xue et al. (2014). PCL mixed with gelatin (Gn) where used as carriers for metroniadazole (MNA) drug at different concentrations. They succeeded in electrospinning these mixture solutions into smooth fibers and investigated the rate of MNA release. To overcome PCL drawbacks, gelatin was added to enhance both cellular adhesion and the degradation rate of PCL. Different solutions were prepared to test the effect of both gelatin and MNA addition on the degradation of the fabricated membranes and the rate of cell proliferation. Three main solutions were investigated; the first was pure PCL, the second was a mixture of PCL with 30% MNA

and the third was PCL and gelatin (1:1) with MNA concentrations up to 40%. Smooth nanofibers were prepared using different concentration previously mentioned. The diameter of the fibers increased with the concentration of the loaded MNA reaching 2.67 um compared to 470 nm of unloaded fibers. Both MNA and gelatin enhanced the hydrophilicity of the fabricated membranes, which attributed to the both the amine/ carboxyl groups along the gelatin backbone and the hydroxyl/ polar imidazole ring on the MNA surface. The increased hydrophilicity of the membranes together with the surface roughness of the fibers enhanced the cell adhesion and proliferation. The biodegradation results showed that the gelatin loss from the PCL-gelatin membranes was greatly observed within the first day, which affected the total mass loss of the membranes. Mass loss due to both the lost gelatin and MNA release was followed with slow prolonged degradation of PCL together with the continuous release of MNA. PCL-Gn membranes loaded with MNA showed bacterial inhibition zones while those membranes without MNA lack antibacterial effect, which increased with the MNA concentration. In conclusion PCL-Gn membranes loaded with MNA showed to be successful delivery vehicle for MNA, those containing 30% of MNA showed to be the most efficient membranes with the least inflammatory response when tested in rabbits (Xue et al., 2014).

In an attempt to synthesis a novel membrane, Gonçalves et al. (2016) synthesized GBR membrane where one side was completely occlusive for epithelial infiltration and the other side permitted mesenchymal cells for enhancement of dental regeneration. Two different composites were prepared. The first composite was composed of PLLA, collagen (COL) and hydroxyapaptite (HA) while the second was made of poly isosorbide succinate-co-L-lactide (PisPLLA), CoL and HA. The prepared solutions were electrospun and further crosslinked using glutaraldehyde. The mats were compared to that synthesized using PLLA only , PisPLLA only, mixture of each with COL only and mixture of each with HA only and finally mixture of each polymer together with COL and HA in presence of growth factor (BMP7). Results revealed that phase separation of COL and polyester polymer (PisPLLA/ PLLA) took place leading to wide range of nanofibers diameter. PisPLLA mats or PisPLLA/HA mats showed increased viability results compared to PLLA and PisPLLA/COL composite.

PisPLLA has higher hydrophilic properties compared to PLLA and thus better cellular attachment and growth where the addition of COL enhanced the hydrophilicity to an extent that negatively affected the growth of the cells. Mineralization was observed in both PLLA scaffolds and PLLA composites, with no mineralization in any of PisPLLA composites. In conclusion addition of COL and HA to PisPLLA was found to enhance cellular growth and differentiation while their addition to PLLA enhanced ECM mineralization (Gonçalves et al., 2016).

Thesis scope and objectives

Collagen possesses exquisite properties that enhance tissue regeneration. It is one of the main components of the ECM, so its application in GTR was extensively investigated. Commercially available collagen membranes revealed to be a successful approach in GTR, however it showed drawbacks such as uncontrolled degradability and high cost.

In an attempt to fabricate an efficient bioresorbable membrane for periodontitis, gelatin was mixed with calcium carbonate at different concentrations using benign solvent. Gelatin is the hydrolysis product of collagen. It shares the majority of collagen exquisite properties, however it is less immunogenic and cost effective.

Based on literature review, the characteristics of successful bioresorbable membranes for periodontitis can be highlighted in the following requirements:

1. Being biocompatible.
2. Mimic the natural extracellular matrix.
3. Manipulated pore size essential for cell occlusivness with high vascularization.
4. Hydrophilic bioactive surface for enhanced cellular adhesion.
5. Controlled biodegradability for proper functioning.
6. Low cyotoxicity

To investigate Gn-CaCO₃ composite for healing periodontal pockets, the above requirements were studied via five main objectives:

1. Synthesis of high concentration of electrospun gelatin nanofibers using diluted acetic acid as benign water-based solvent.

2. The effect of different crosslinking time using gluteraldhyde vapors on pore size distribution within the mats.

3. Electrospinning of calcified gelatin nanofibers mixed calcium carbonate at different concentrations.

4. Chemical characterization of all fabricated mats by Fourier infrared transform spectroscopy (FTIR) to ensure that none of the following affected the original structure of gelatin.

    4.1. DAA concentration

    4.2. Electrospinning process

    4.3. Different concentrations of calcium carbonate.

5. *In vitro* characterization of crosslinked mats via swelling, biodegradation and viability test.

CHAPTER 3

MATERIALS AND METHODS

3.1. Materials

Gelatin from porcine skin; G6144; Bloom strength (90-110); Type A, Gluteraldhyde (25% in deionized water), glacial acetic acid; Fluka (≥99.7%); Molecular weight=60.05 gm/mole, ethanol anhydrous (≥ 99.5%); Molecular weight = 46.07 gm/mole and Dimethyl sulfoxide (DMSO); (≥99.9); Molecular weight = 78.13 gm/mole, were purchased from Sigma-Aldrich, Germany. Calcium carbonate ($CaCO_3$); powder; ≥99.9%; Molecular weight = 100.09 gm/mole; was purchased from Fisher scientific. Dulbecco's modified Eagle's medium (DMEM), Fetal Bovine Serum (FBS), Penicillin-Streptomycin and phosphate buffer saline (PBS), Trypsin-EDTA were obtained from Lonza, USA where (3-(4,5-Dimethylthiazol-2-yl)-2,5-Diphenyltetrazolium bromide) (MTT) was purchased from Serva, Germany. hTERT fibroblast cell line used was supplied by Dr. Andreas Kakarougkos as a kind gift.

3.2. Experimental methods

3.2.1. Gelatin nanofibers

3.2.1.1. Solution preparation

Dilute acetic acid solution (DAA) was prepared using distilled water to a final concentration of 40% (v%) where 40 ml of glacial acetic acid was added to 60ml of distilled water. Gn was dissolved in DAA to a final concentration of 30% (w/v %) where 3 gms of Gn powder was added to each 10ml of DAA. The solution was stirred at 40°C for about 15 minutes until Gn was completely dispersed in the solution then the temperature was lowered to room temperature. Solution was stirred until clear solution of honey color was obtained. The same procedure was followed for the preparation of 33%, 35% and 40% Gn solutions.

3.2.1.2. Electrospinning

Freshly prepared solutions were electrospun using SNAN electrospinning setup (MECC co., Ltd, Japan). 5 ml Teflon syringe filled with the electrospinning solution was loaded into the syringe pump. The syringe was connected through a teflon tubing to the needle tip placed on the electrospinning stage keeping the tip to collector distance unchanged at 13 cm. Solutions were electrospun by varying both the flow rate with the voltage in an attempt to obtain smooth fibers. At each flow

rate, the voltage was increased until a jet of fibers was showered on the stationary collector. Voltage was then increased for an attempt to optimize intermittent nanofibers to continuous smooth ones. The flow rate was then increased and kept constant while varying the voltage. The previous steps were repeated over a range of flow rate as shown in Table 3.1.

Table 3.1: Different electrospinning parameters used for different concentrations of Gn (30, 33, 35 and 40%) in 40% DAA.

Gn % (w/v %)	Flow rate (ml/h)	Voltage (KV)	Distance (cm)
30%	0.2-0.8	15-21	13
33%	0.2-0.8	15-21	13
35%	0.2-0.8	15-19	13
40%	0.4-1	17-24	13

The aforementioned procedure was repeated for each freshly prepared Gn concentration. Samples were collected on aluminum foil and left at least overnight at room temperature to be completely dried. Dried samples were imaged using Field emission scanning electron microscopy (FESEM, Leo Supra 55, ZeissInc., Oberkochen, Germany) at Youssef Jameel Science and Technology Research Center (YJSTRC) to determine the optimum gelatin concentration and electrospinning parameters used to obtain smooth nanofibers.

3.2.2. Gn-CaCO$_3$ nanofibers

3.2.2.1.Solution preparation

Different concentrations of CaCO$_3$ (2, 4, 5 and 6 w/v %), were prepared using 40% Gn concentration. Calcium carbonate was first dissolved in DAA until clear transparent solutions were obtained, then the temperature was raised to 40°C for 15 minutes to ensure the complete dispersion of Gn. The solutions stirred at room temperature until Gn completely dissolved and homogenous solutions obtained.

Solution of 40% gelatin denoted by Gn (0%), while that of Gn-CaCO$_3$ mixtures containing 2%, 4%, 5% and 6% CaCO$_3$ were denoted by 2%, 4%, 5% and 6%, respectively.

3.2.2.2. Electrospinning

Freshly prepared solutions of Gn-CaCO$_3$ mixtures were loaded in the electrospinning setup as mentioned earlier, where the tip-collector distance s maintained within 10-15 cm throughout the entire process. The voltage was varied at each flow rate, where a range of flow rate was investigated at each concentration as shown in Table 3.2.

Table 3.2: Electrospinning parameters used for different concentrations of Gn-CaCO3 mixtures, where the humidity ranged from 36-51 % at 22°C.

Gn-CaCO$_3$ mixture	Denoted by	Flow rate (ml/h)	Voltage (KV)	Distance (cm)
40% : 2%	2%	0.2-1	16-23	10-15 cm
40%: 4%	4%	0.2-1	16-23	10-15 cm
40%: 5%	5%	0.2-1.2	16-24	10-15 cm
40%: 6%	6%	0.2-1.2	16-24	10-15 cm

All samples collected on aluminum foil, dried overnight and imaged using FESEM to determine the optimum parameters used for smooth nanofibers. Smooth nanofibers then collected for further characterization.

3.2.2.3. EDX Analysis

Energy dispersion X-ray analysis was performed to ensure that the smooth Gn-CaCO$_3$ nanofibers (2% and 4%) contained calcium compared to Gn (0%) nanofibers.

3.2.2.4. Thickness measurement

Smooth nanofibers obtained at optimum parameters shown in Table 3.4 were collected. The thickness of these fibers was measured using ImageJ software. Three sets of measurements were done for each mat on three random positions. Each set of measurement includes at least 50 fibers. Statistical analysis for mean and standard error calculation performed using Sigma plot 10 software.

Table 3.3: Optimum electrospinning parameters used for smooth nanofibers at Gn (0%) and Gn-CaCO₃ mixtures (2% and 4%).

Solution Concentration	Flow rate (ml/h)	Voltage (KV)	Distance (cm)
Gn (0%)	0.5	19	13
Gn-CaCO$_3$ (2%)	0.6	20	13
Gn-CaCO$_3$ (4%)	0.7	21	13

3.2.3. <u>Solution characterization</u>

3.2.3.1.<u>Conductivity measurement</u>

Conductivity of the electrospinning solution is a crucial parameter for nanofibers synthesis (Bhardwaj & Kundu, 2010; Okutan et al., 2014). To determine the effect of CaCO$_3$ addition, 10 ml of freshly prepared Gn-CaCO$_3$ solutions (2%, 4%, 5% and 6% CaCO$_3$) was measured using conductivity meter.

Gn (0%) solution was prepared and used as reference solution to compare with Gn-CaCO$_3$ measurements. Three different samples were measured at the same temperature (22°C) for each concentration to ensure the accuracy of results.

3.2.3.2.<u>pH measurement</u>

Calibrated Adwa waterproof pH meter was used for measuring pH variation due to CaCO$_3$ addition together with the 40% DAA used. Although gelatin successfully dissolves in acidic solutions it may affects its structure through degradation (Ki et al., 2005; Mindru, Malutant, & Tura, 2007). 10ml of each freshly prepared Gn solution and Gn-CaCO$_3$ mixtures (2%, 4%, 5% AND 6%) was used and denoted by 0%, 2%, 4%, 5% and 6%, respectively. Each measurement was repeated in triplicates at constant temperature (22°C) for precision of measurements.

3.2.4. Nanofibers crosslinking

3.2.4.1.Crosslinking of Gn nanofibers

Crosslinking of Gn nanofibrous mats is an essential step to increase the mechanical properties of gelatin nanofibers and enhance its resistance to aqueous solutions. Chemical crosslinking using gluteraldhyde (GTA) was intensively employed for various biopolymers (Reddy, Reddy, & Jiang, 2015) with Gn on the top of the list (Nguyen & Lee, 2010; Rose et al., 2014; Sell et al., 2010). The optimized crosslinking time was investigated on four basic steps. First, 10ml of GTA was located at the bottom of the desiccator where crosslinking was performed. The mat was then placed on the rack of the desiccator where different crosslinking times (t= 8, 12 and 20 h) were tested each at a time for optimization. The mat was then removed after each time from the desiccator, dried and left at the fume hood for at least two hours to eliminate the extra GTA fumes. The dried crosslinked mat was placed in the oven at 100°c for an h to enhance crosslinking. The solubility of the mats was tested by their immersion in distilled water for three days at $37°C$, where the mats were observed daily to indicate its solubility (Y. Z. Zhang, Venugopal, Huang, Lim, & Ramakrishna, 2006).

3.2.4.2.Crosslinking of Gn-CaCO$_3$ nanofibers

The optimum crosslinking time resulted in stable apparent structure and best water resistance of Gn (0%) mats was then used for crosslinking of Gn-CaCO$_3$ mats (2% and 4%) using the same procedure mentioned earlier.

3.2.4.3.Morphology of crosslinked mats

All crosslinked mats were sputtered with gold nanoparticles at 15mA for 8 minutes to be imaged using FESEM. Images were obtained at accelerating voltage of 10 KV. Both Gn (0%) nanofibers crosslinked at different time intervals (t= 8, 12 and 20 h) and Gn-CaCO$_3$ (2% and 4%) mats crosslinked for 20 h were observed to investigate the relation between crosslinking time and mat's morphology.

3.2.5. Samples preparation for characterization

Samples of Gn (0%) and optimized mats of Gn-CaCO$_3$ composite (2% and 4%) were collected on gauze and then dried overnight followed by their crosslinking. The nanofibers mats were pealed from the gauze where Gn (0%) samples were crosslinked for (8, 12 and 20 h) as mentioned previously. The samples were cut into squares of (1cmx1cm) and were denoted by 8hrs, 12hrs and 20hrs respectively. Same procedure was performed for Gn-CaCO$_3$ composite (2% and 4%) mats donated by 2% and 4%, respectively. Samples were ready to be used for different characterizing techniques.

3.2.6. Pore size distribution

Pore size is a critical characteristic of GTR membrane barriers. It was determined for Gn (0%) crosslinked mats (t= 8, 12 and 20 h) and Gn-CaCO$_3$ composite (2% and 4%) crosslinked for 20 h. All prepared samples were further shredded into very small squares using scissors and were pretreated by applying vacuum at 34°C for four hours. All measurements were done using ASAP 2020 analyzer (Micromeritics instrument Corporation, Norcross, USA) where nitrogen gas flowed through the samples. During the flow of nitrogen gas, adsorption and desorption isotherms were recorded using 53-point pressure tables with 20 second equilibration intervals. Barrett, Joyner and Halenda (BJH) method was used to calculate the size distributions of mesopores and macropores using Kelvin model for pore filling.

3.2.7. Fourier transform infrared spectroscopy (FTIR)

It was performed to test the effect of using DAA as an electrospinning solvent, in addition to calcium carbonate on gelatin's chemical structure. All prepared samples were measured using Thermoscientific, Nicolet 380, USA. Transmission peaks of Gn (0%) and Gn-CaCO$_3$ mats (2% and 4%) were obtained in the range of 400- 4200 cm^{-1}.

3.2.8. *In vitro* characterization

3.2.8.1. Swelling test

Swelling properties of crosslinked mats determine their hydrophilic properties and their ability to retain water. Previously prepared Gn (0%) mats at different crosslinking time (t=8, 12 and 20 hrs) and crosslinked mats of Gn-CaCO$_3$ composite

(2% and 4%) were tested. Samples were weighed (W_d) then soaked in phosphate buffer saline solution (PBS at pH=7.4) at 37℃ (Del Gaudio et al., 2013). Soaked samples were removed at different time intervals (2, 4, 6, 8, 24, 48, 72, 96, 120, 144 and 168 h), where excess PBS on the surface of the samples was removed using filter paper. The samples were weighted and denoted as (W_w). The degree of swelling was calculated by the direct substitution of W_d and W_w for each sample in equation *(3.1)* (Bigi et.al., 2001; Nguyen & Lee, 2010).

$$Sw\% = \left(\frac{Ww-Wd}{Wd} \right) x100 \qquad (3.1)$$

W_d: Weight of dried samples before soaking

W_w: Weight of soaked samples.

3.2.8.2. Degradability test

As degradability test determines the rate of weight loss of the samples prepared, it plays a key role in the success of periodontal membranes. Samples of Gn (0%) and crosslinked Gn-CaCO$_3$ mats (2% and 4%) were prepared as aforesaid in section 3.2.5. Prepared samples were weighted (W_i) and soaked in PBS (pH=7.4) at 37℃ for three weeks (Qasim et.al., 2015). Every week, soaked samples were removed, washed twice with distilled water and dried in the vacuum oven at room temperature for 24 hours. Dried samples were weighted (W_s) and soaked again in PBS at 37℃. Weight loss (W%) was calculated at each time interval using equation *(3.2)* (Pan et. al., 2014; Tronci et al., 2015).

$$W\% = \left(\frac{Wi-Ws}{Wi} \right) x100 \qquad (3.2)$$

Where:

W_i: Weight of dried samples before soaking

W_s: Weight of dried samples after soaking

3.2.8.2.1. Field emission scanning electron microscopy

At the end of the first and the fourth week of PBS soaking, all the samples were washed using distilled water and dried at room temperature. Dried samples were gold sputtered using 15mA for 15 minutes and imaged using FESEM.

3.2.8.2.2. EDX Analysis

After the 1st and 4th week, all samples were washed, dried and gold sputtered using the same conditions mentioned earlier. Gold sputtered samples were analyzed using Inca software to reveal their chemical composition after the first week of the experiment and at the end of the fourth week.

3.2.8.3. MTT assay

The viability of prepared membranes was investigated on two consecutive steps. The first step was to test the viability of Gn (0%) mats at different crosslinking time (t= 0, 8, 12and 20 h). The second test was to investigate the cytotoxic effect of different concentration of calcium carbonate initially added to the electrospinning solutions

In the first experiment seeded tissue culture polystyrene wells (TCPs) were used as cell controls with 100% viability to evaluate the results obtained. The first experiment was designed to evaluate the cytotoxicity of different crosslinking time. The aim of the second experiment is to test the viability of Gn-CaCO$_3$ composites (2% and 4%). Crosslinked Gn (0%) mat that has revealed the best viability results from the first experiment was used as control during the second experiment. All Gn-CaCO$_3$ mats under investigation were crosslinked using the same optimized condition employed for the control. The aforesaid step was done to ensure that the effect of crosslinking time would not interfere with that due to different CaCO$_3$ concentration that was initially added.

Human telomerase reverse transcriptase immortalized fibroblasts cell line (hTERT) characterized with the reintroduction of telomerase reverse transcriptase (TERT) into human fibroblast cells. Normal cellular chromosomes were protected against terminal erosion via telomeres. The length of telomeres was normally shortened while aging. The reduction of the telomeres length to 4 kB activates cellular pathways that trigger cellular senescence. TERT gene affects the rate of cellular senescence by controlling erosion of the telomeres. (Smith, Goddard, Perusina Lanfranca, & Davido, 2013)

The cells were cultured in T75 tissue culture flasks using compound media (Dulbecco's modified Eagle's medium (DMEM) containing 10 % fetal bovine serum

(FBS) and 5 % penicillin-streptomycin, where 50ml of FBS and 25ml of penicillin-streptomycin were added to each 425 ml of DMEM. The cells were cultured in T75 flasks until the flask was 80% confluent, where trypsinization was performed using trypsin-EDTA. Viable cell count was performed via hemocytometer (Hausser, Scientific, USA) using trypan blue staining of the trypsinized cells. Viable cells appeared to be colorless while dead cells were stained with blue color.

All samples were punched into 1cm^2 circles for sterilization. During sterilization step, the scaffolds were washed using absolute ethanol followed by UV exposure for two hours; one hour for each side (Meng et al., 2010). Following sterilization, samples were immersed overnight in compound media in 5% CO_2 tissue culture incubator at 37°C. The aforesaid sterilization technique was used for all mats except for the uncrosslinked Gn (0%) mats at (t=0) where only UV exposure was applied for sterilization.

 After sterilization, the samples were placed in 24 well plates (Greiner Bio-one, Germany) and soaked in fresh compound media for 24 hours. The soaking media were then replaced by fresh media and trypsinized hTERT cells were seeded in each well (50x10^3 cells/well). Seeded mats were incubated in 5% CO_2 incubator at 37°C. Plates were removed from the incubator after a week for the 1st experiment and after 1 and 3 days for the second experiment for MTT assay.

In this assay, media were removed from each well followed by washing twice using PBS to ensure the complete removal of unattached cells. Each well was then filled with 420 µl of complete DMEM followed by 80µl of MTT; (3-(4,5-Dimethylthiazol-2-yl)-2,5-Diphenyltetrazolium bromide). The plates were placed back in the cell culture incubator under dark condition. After at least 3 hours, the wells were evacuated for the addition of dimethyl sulfoxide (DMSO) and moved back to the incubator for 30 minutes to solubilize formazan crystals formed. Aliquots of each sample were placed in 96 well plate and absorption intensities of solubilized formazan dye corresponding to the existed viable cells were measured using microplate reader FLUOstar OPTIMA (BMG LabTech, Germany) at 595 nm.

 The viability of the cells was calculated by the substitution of the absorbance (A) in equation 3.3.

$$Cell\ viability\ \% = \left(\frac{A\ sample - A\ Blank}{A\ control - A\ Blank} \right) x\ 100 \qquad (3.3)$$

Where:

A $_{sample}$: Absorbance reading of the tested sample.

A $_{Blank}$: Absorbance reading of the blank wells with no cells.

A $_{control}$: Absorbance of the control sample that represent 100% viability.

Three independent experiments were performed for each time interval, where each sample was done in triplicates. Cell viability was calculated and represented using the mean and standard deviation (mean ± standard deviation). Statistical analysis was done for the calculation of the P values and the comparison between two groups using t-test.

CHAPTER 4

RESULTS

4.1. Solution preparation

4.1.1. Gelatin solution preparation

The solubility of Gn in DAA was achieved by the addition of Gn to the solution at 40°C and keeping the heat for half an hour. The heat was lowered to room temperature and the solution was stirred for 2-3 hour or until clear solution was obtained. As the concentration of the solution was increased, the time for solution preparation was consequently increased.

4.1.2. Gn-CaCO$_3$ solution preparation

As CaCO$_3$ was added to DAA while preparing Gn-CaCO$_3$ mixtures, bubbles evolution was observed. The gas formed could be carbon dioxide resulted as a byproduct from the interaction of DAA together with CaCO$_3$. In addition to carbon dioxide gas, calcium acetate was produced and collected via forced evaporation and its structure was confirmed by XRD as shown in Figure 4.1 (B). FESEM images supported the XRD results shown in Figure 4.1 (A and C)

The increase of the added CaCO$_3$ caused an increase in the preparation time that reached overnight to ensure complete dispersion of acetate in the solution. Although clear solutions were obtained before the addition of Gn, only honey-like turbid solutions were formed at different concentrations of CaCO$_3$ initially added. Freshly prepared solutions were used for electrospinning to ensure an efficient mixing of all components and complete dispersion of acetate.
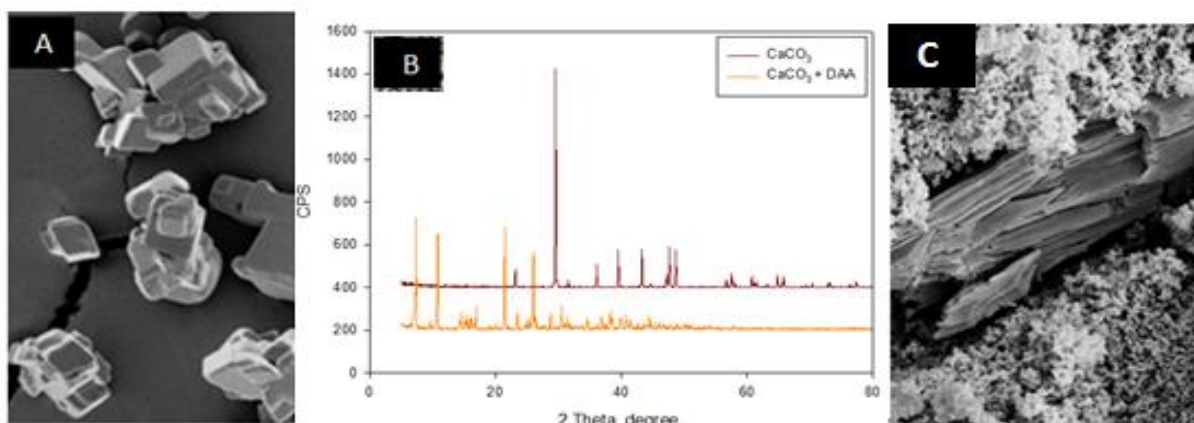
Figure 4.1: Calcium acetate hydrate produced during the first step of Gn-CaC0$_3$ mixtures preparation; (A) FESEM of Calcium carbonate powder, (B) XRD of calcium carbonate versus calcium acetate (C) FESEM of calcium acetate obtained.

4.2. Solution characterization

4.2.1. Conductivity measurement

Results showed the enhancement of the conductivity with the increase of $CaCO_3$ concentration within the solution. Gn (0%) solutions showed the least conductivity value, while 6% solutions showed the maximum value up to three times that of Gn (0%) as shown in Figure 4.2 (A).

4.2.2. pH measurement

All the measured values at different concentrations were less than pH=4. The pH was found to increase with decreasing the acidity of the solution on the addition of $CaCO_3$ as shown in the Figure 4.2 (B).
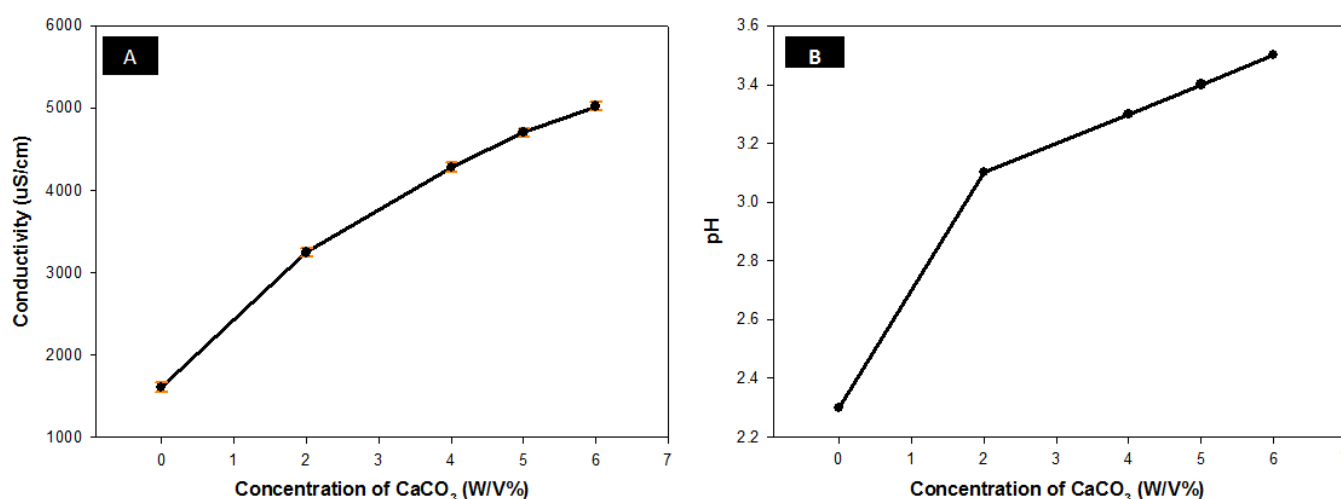
Figure 4. 2: Solution characterization of different samples prepared to investigate the effect of $CaCO_3$ addition where (A) conductivity measurement (B) pH measurements.

4.3. Electrospinning

4.3.1. Gelatin nanofibers

Electrospinning failed for Gn solutions with concentrations less than 35% as summarized in Table 4.1. During the electrospinning of 30% and 33% Gn solutions, no balance was achieved between the viscoelastic forces of the solution and the applied voltage. Consistent dropping took place throughout different flow rate variations even at 0.2 ml/h and was replaced by coagulation of the polymer droplet via its drying on the tip when the applied voltage was increased.

The 35% solution showed better results compared to that of 30% and 33% counterparts, where an unstable jet was observed. At low flow rates, the polymer ejection was too slow and was dried at the tip even on low voltage application. At high flow rates, the jet was disturbed with heavy dropping on low voltage application, while on increasing the applied voltage drying of the polymer took over.

Polymer jet showering fibers through Taylor cone was observed during the electrospinning of Gn 40% solutions over flow range of 0.4-1 ml/h. The jet was consistent with least/ no dropping at low flow rate, where the dropping was increased with increasing the flow rate. The dropping was affected by the applied voltage, where it was observed to decrease with the voltage increase at a given flow rate. Tip to collector distance variation from 10-15 cm significantly affected the formation of jet which was observed at 13 cm. Consistent dropping was observed at 10 cm while drying took place at 15 cm. Within the aforementioned range, flow rates of 0.4 ml/h and 0.5 ml/h showed to be the most promising ones at 13 cm tip-collector distance.

Table 4. 1: Electrospinning parameters where jetting of nanofibers were observed at different Gn concentrations.

Gn (0%)	Flow rate (ml/h)	Voltage (KV)	Distance (cm)	Jet observation	Smooth nanofibers
30%	X	X	X	X	X
33%	X	X	X	X	X
35%	0.2-0.8	16-18	13cm	√	X
40%	0.4-1	19-23	13cm	√	√

4.3.1.1. <u>Field emission scanning electron microscopy (FESEM)</u>

FESEM images of 35% samples showed consistent results with the observations taken during the electrospinning process as shown in Figure 4.3. The images showed least dropping at 0.2 ml/h, where the dropping was increased with increasing the flow rate. As shown in Figure 4.4 (1-3), smooth fibers separated by spheroids filled with solution appeared at all flow rates of 40% Gn solution where the spheroids completely disappeared at 0.5 ml/h, 19 KV shown in Figure 4.4 (2A). The spheroids

were found to decrease with decreasing the flow rate and with the increase of the applied voltage at a given flow rate as shown in Figure 4.4 (1(A-D), 2(A-D) and 3(A-B)). The aforementioned relation between the spheroid appearance and the voltage was found to persist at flow rates less than 0.8 ml/h and applied voltage not higher than 22 KV. At higher flow rate and/or voltages, spheroids appearance was found to be enhanced as shown in Figure 4.4 (3(C-D), 4(A-B) and 5(A-B)) for 0.6 ml/h at 22 and 23 KV, 0.8 ml/h at 18 and 19 KV, 1 ml/h at 18 and 19 KV, respectively. Continuously smooth nanofibers with no spheroids were obtained at 0.5 ml/h, with no dropping observed at 19 KV as shown in Figure 4.4 (2A) which was used as optimum Gn (0%) nanofibers throughout the experiments.
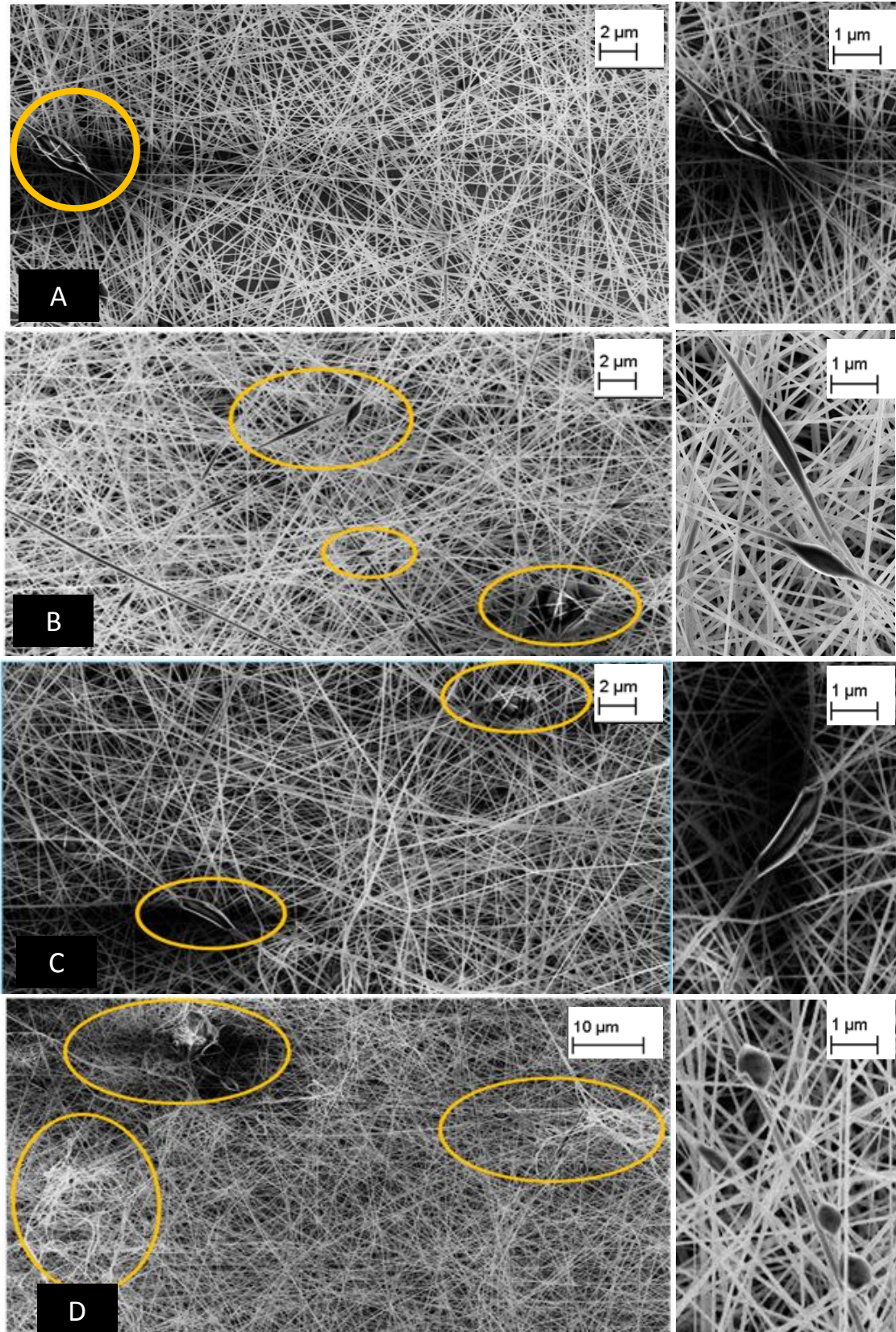
Figure 4.3: FESEM images of 35% nanofibers (A)0.2 ml/h at 16 KV, (B) 0.4 ml/h at 16 KV, where the least dropping and beaded fibers were obtained, (C) 0.6 ml/h at 18 KV, where dropping was increased and (D) 0.8 ml/h at 18 KV, where drying was observed.
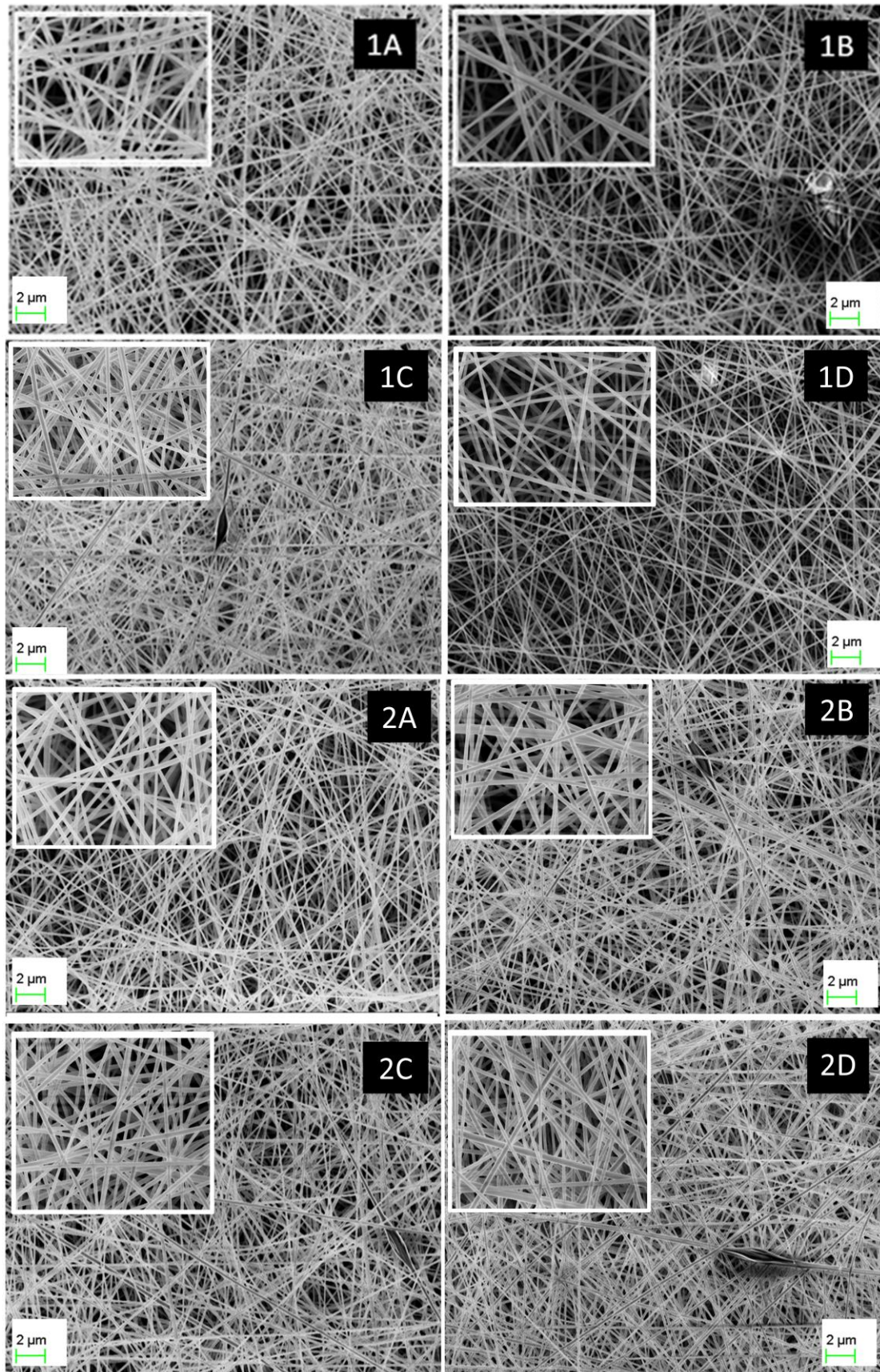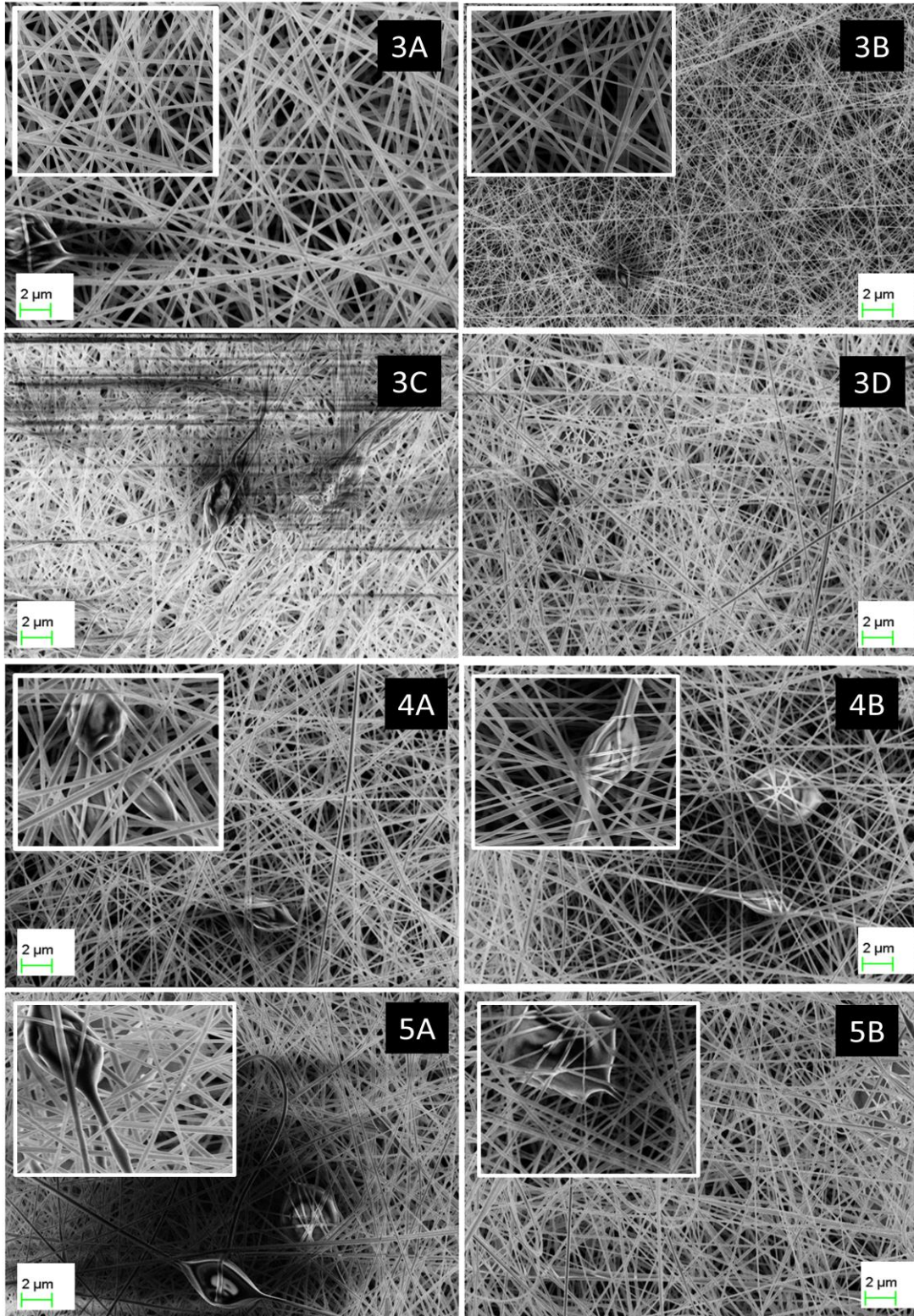
Figure 4.4: FESEM images for 40% Gn, where the optimization was done by varying the voltage together with the flow rate; (1(A-D)) 0.4 ml/h at different voltages 19 KV, 20 KV, 21 KV and 22 KV denoted by A, B, C and D respectively. (2(A-D)) 0.5 ml/h at different voltages 19 KV, 20 KV, 21 KV and 22 KV denoted by A, B, C and D, respectively. (3(A-D)) 0.6 ml/h at different voltages 19 KV, 20 KV, 21 KV and 22 KV denoted by A, B, C and D, respectively. (4(A-B)) 0.8 ml/h at 18 KV and 19 KV denoted by A and B, respectively. (5(A-B)) 1 ml/h at 18 KV and 19 KV denoted by A and B, respectively.

4.3.1.2. Thickness measurement

The thickness of smooth 40% Gn nanofibers was measured and found in the range of 204±31.3 nm, with the thickness distribution illustrated in Figure 4.5. Most nanofibers produced at 0.5 ml/h contained spheroids, which were found to be affected by the applied voltage. The thickness was found to decrease with increasing of the voltage as shown in Table 4.2.

Table 4.2: Thickness variation with the applied voltage at 0.5 ml/h.

Voltage (KV)	19 KV	20 KV	21 KV	22 KV
Thickness (nm)	204±31.3	233.6±36.06	199.84±36.87	193.64±54.41
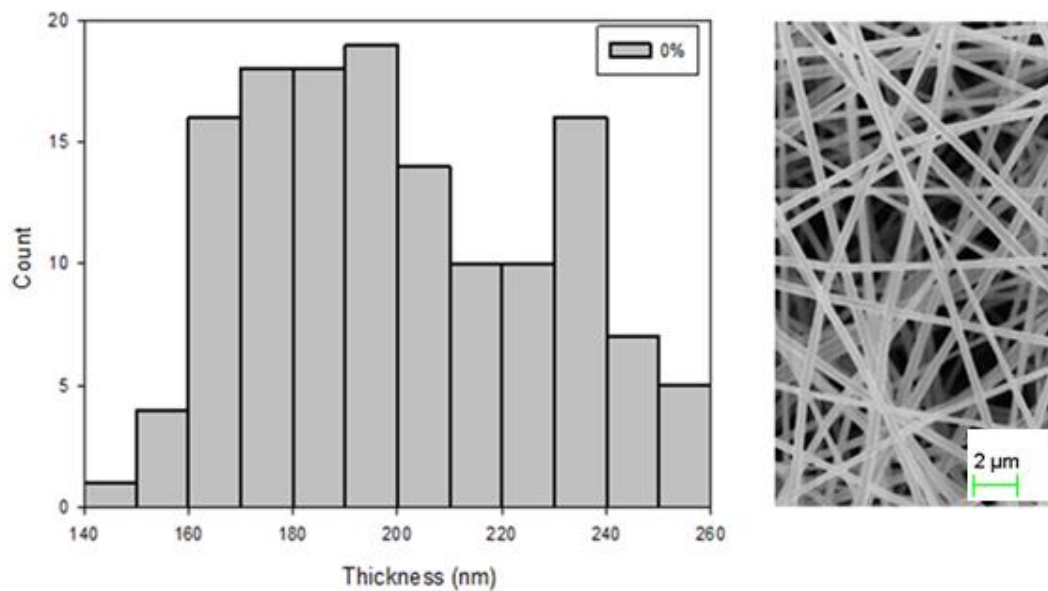
Figure 4.5: Thickness distribution of optimized 40% nanofibers obtained at 0.5 ml/h, 19 KV.

4.3.2. Gn-CaCO₃ nanofibers

Electrospinning using freshly prepared solutions was a crucial step to ensure that all calcium acetate was completely dispersed especially at higher concentrations of initially added $CaCO_3$. Humidity was found to greatly affect the ease of electrospinning and the stability of the jet formed, where at humidity range 46-51% the electrospinning was found to be efficient and dropping throughout

electrospinning of different concentrations was relatively low compared to that at 33-36%.

4.3.2.1. <u>Field emission scanning electron microscopy (FESEM)</u>

Intermittent nanofibers together with mushroom like structures were noticed in mats from different concentrations of Gn-CaCO$_3$ mixtures as shown in Figures 4.6, 4.7, 4.8 and 4.9. Optimization was done by the variation of flow rate together with the applied voltage. Intermittent nanofibers were successfully replaced by smooth continuous nanofibers in case of 2% and 4% samples as shown in Figure 4.6 (1A, 1C and 2D) and 4.7 (2D), respectively while smooth nanofibrous mats with decreased mushroom-like structures were obtained from 5% and 6% samples as shown in Figure 4.8 and 4.9. The mushroom-like structures of calcium acetate left outside the nanofibers prevailed with increasing the flow rate at a given CaCO$_3$ concentration or increasing of CaCO$_3$ content from one mixture to another. The decrease of air humidity was found to greatly affect the electrospinning parameters at which optimum smooth fibers can be obtained. 2% Gn-CaCO$_3$ mixture smooth nanofibers were found to be obtained at 0.7 ml/h (19 KV) and 0.8 ml/h (20 KV) as shown in Figure 4.6 (1C) and (2D), respectively at humidity ranged from 46-51%. As the humidity decreased to 33-36%, the dropping of the electrospinning solution through the electrospun mat appeared as shown in Figure 4.6 (6A). To overcome the effect of humidity, optimization was done again by lowering the flow rate to 0.6 ml/h where smooth nanofibers appeared at 20 KV. All mats used throughout different experiments were collected for 2% at 0.6 ml/h (20 KV) and for the 4% at 0.7 ml/h (21 KV), with humidity carefully monitored at maintained (36-51%).
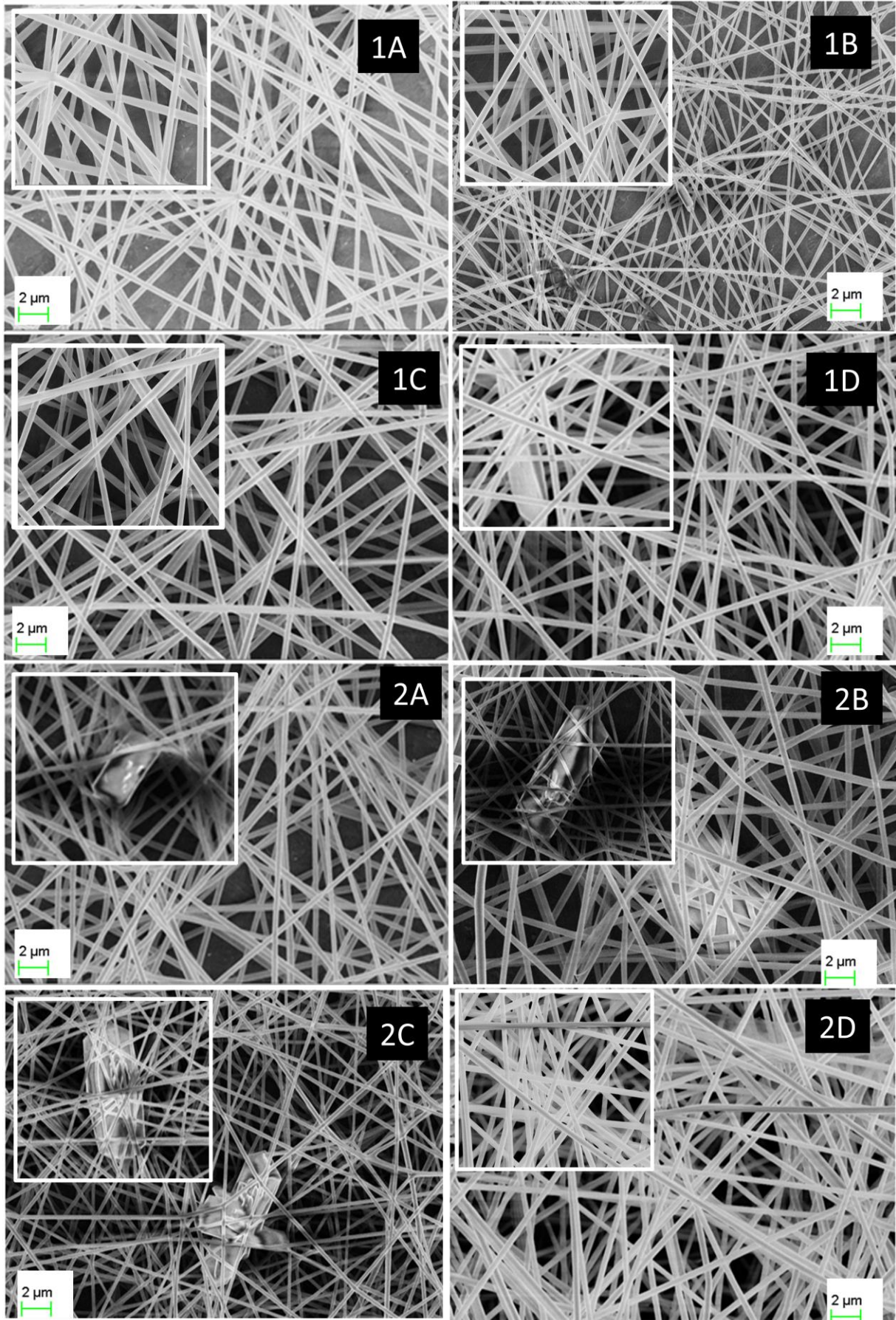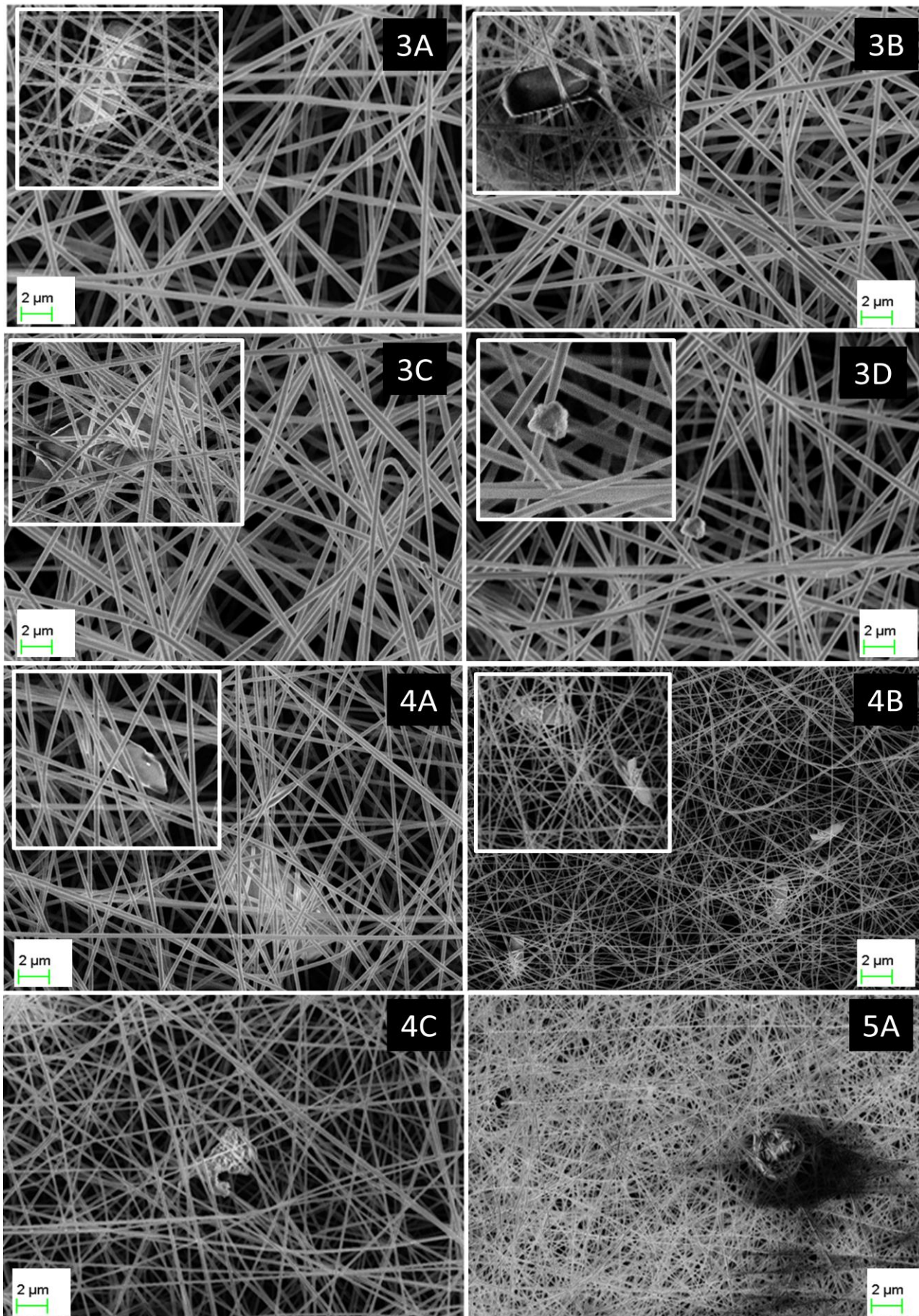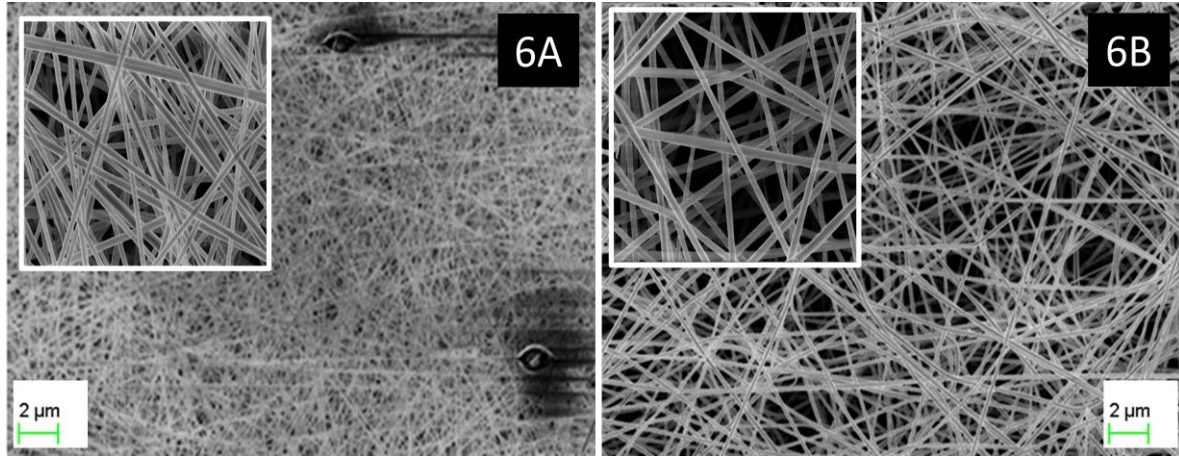
Figure 4.6: FESEM images of 2% Gn-CaCO₃; (1(A-D)) 0.7 ml/h at different voltages 16 KV, 17 KV, 18 KV and 19 KV denoted by A, B, C and D, respectively. (2(A-D)) 0.8 ml/h at different voltages 17 KV, 18 KV, 19 KV and 20 KV denoted by A, B , C and D, respectively. (3(A-D)) 0.9 ml/h at different voltages 19 KV, 20 KV, 21 KV and 22 KV denoted by A, B, C and D, respectively. (4(A-C)) 1 ml/h at 20 KV, 21 KV and 22 KV denoted by A, B and C, respectively. (5(A)) 1.2 ml/h at 23 KV denoted by A. (6(A-B)) shows the effect of humidity decrease leading to dropping at 0.7 ml/h, 19 KV shown at (6A), where optimization was done once again by decreasing the flow rate and dropping disappeared at (6B) 0,6 ml/h, 20 KV.
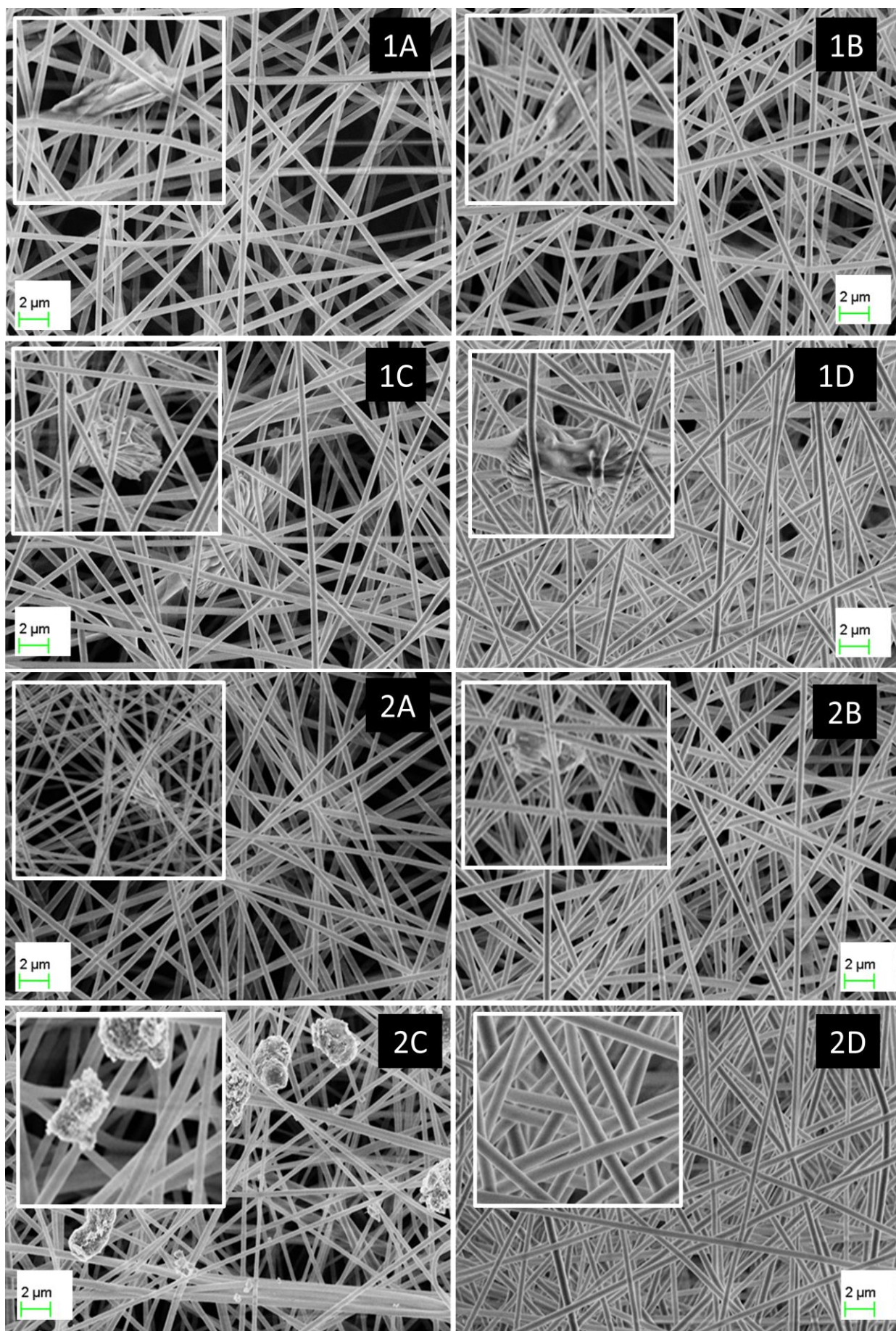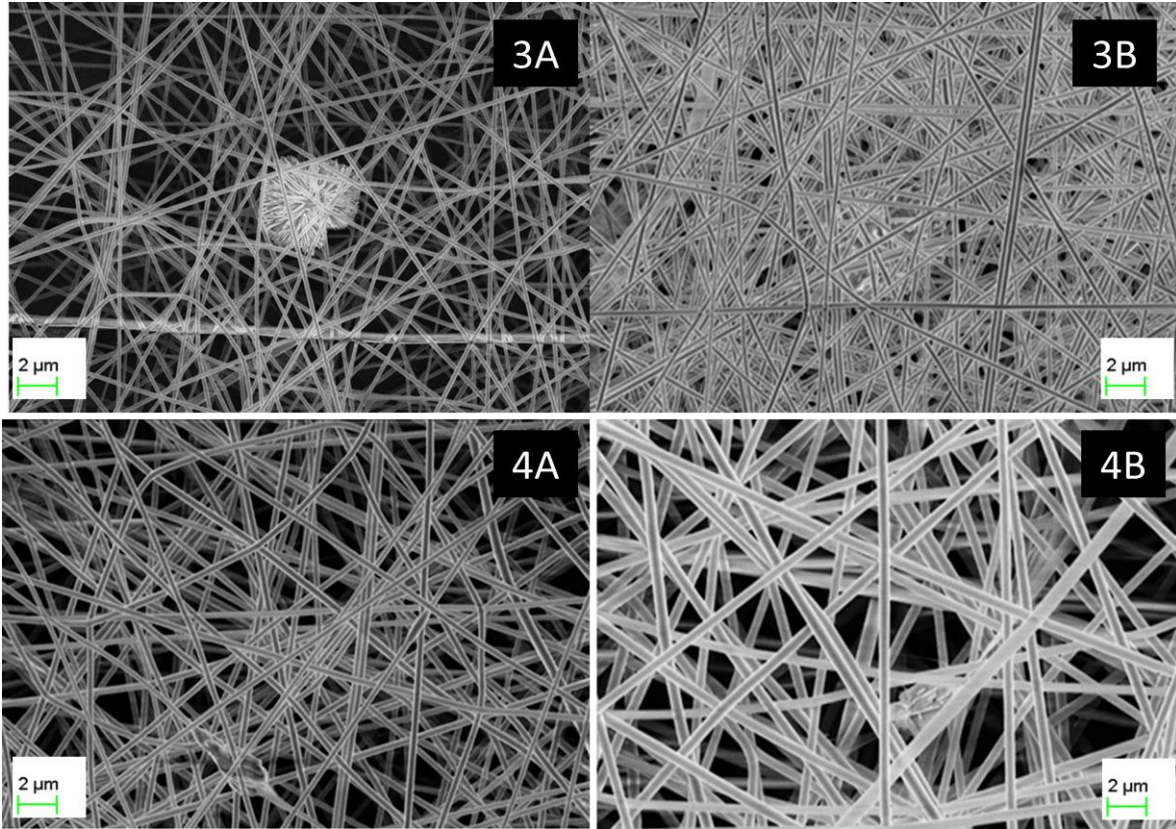
Figure 4.7: FESEM images for 4% Gn-CaCO₃; (1(A-D)) 0.6 ml/h at different voltages 17 KV, 18 KV, 19 KV and 20 KV denoted by A, B, C and D, respectively. (2(A-D)) 0.7 ml/h at different voltages 17 KV, 18 KV, 19 KV and 20 KV denoted by A, B, C and D, respectively. (3(A-B)) 0.8 ml/h at different voltages 19 KV and 20 KV denoted by A and B, respectively. (4(A-B)) 0.9 ml/h a 19 KV and 20 KV denoted by A and B, respectively.
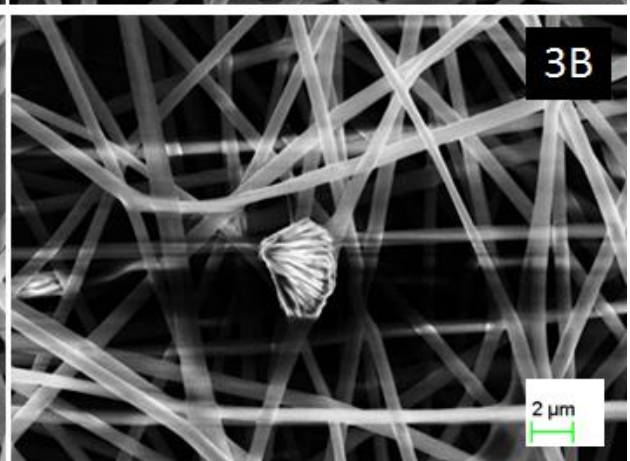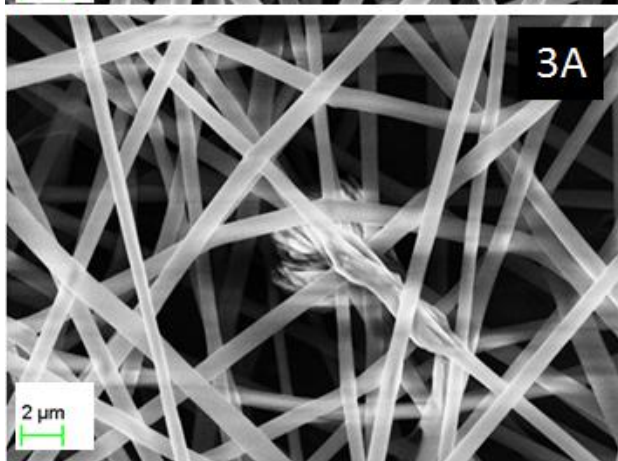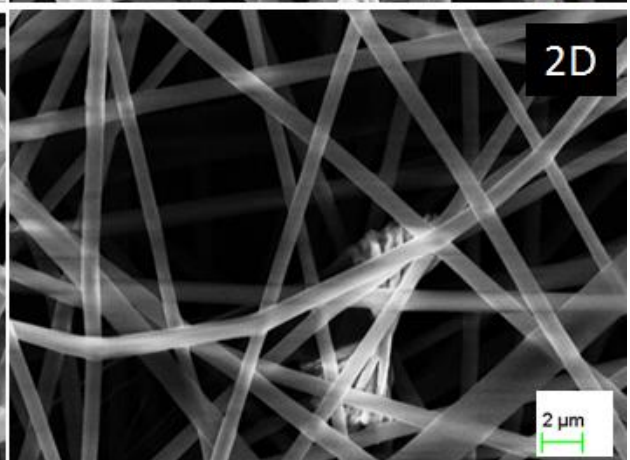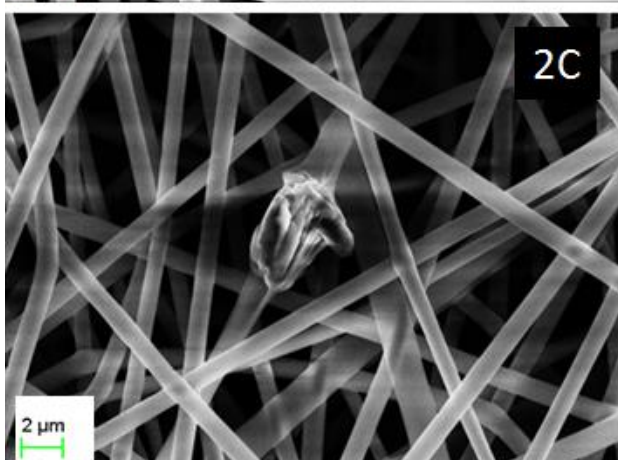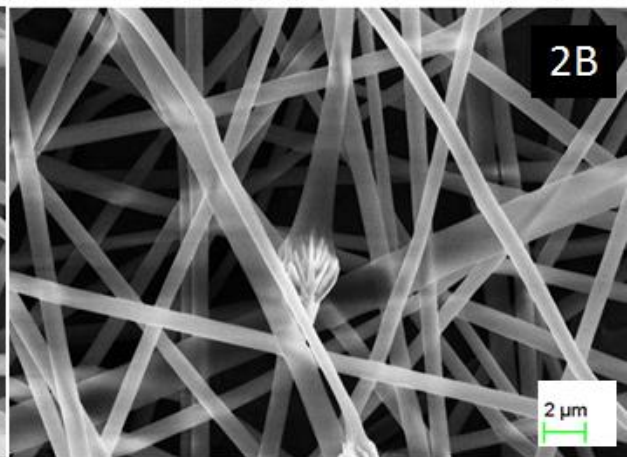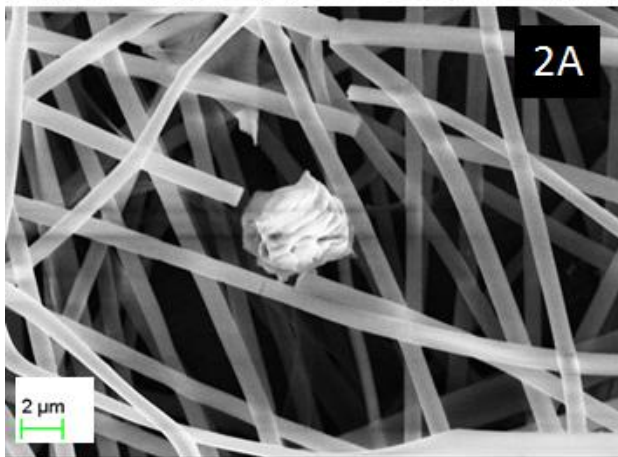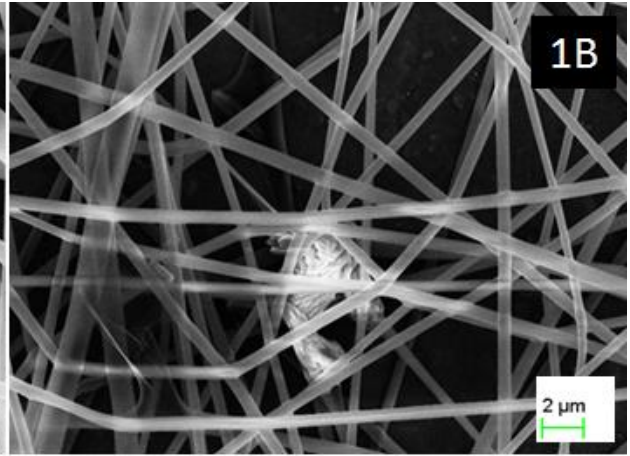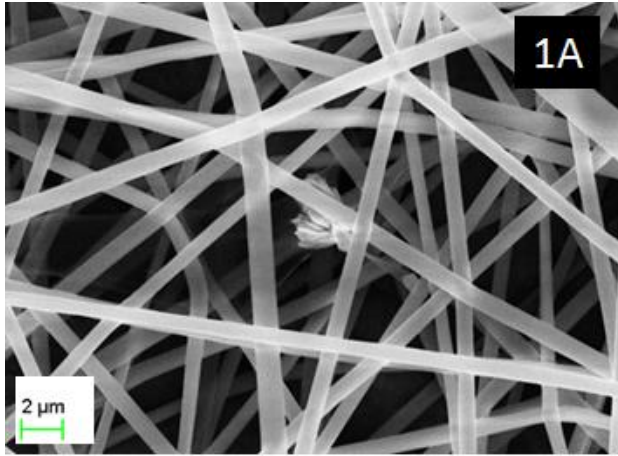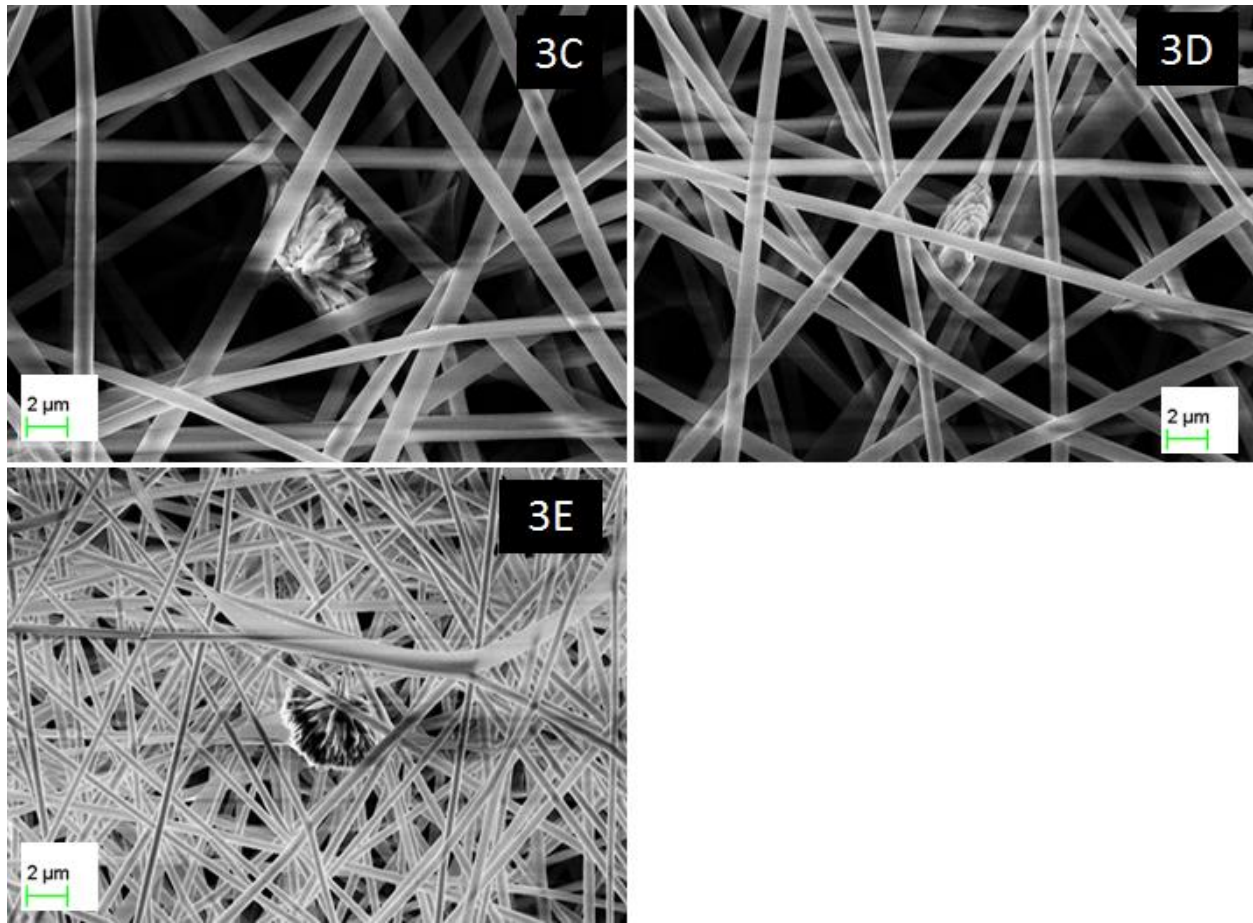
Figure 4.8: FESEM images for 5% Gn-CaCO₃ showing calcium acetate whether clogged within nanofibers or dispersed within the mats; (1(A-B)) 0.4 ml/h at different voltages 19 KV and 20 KV denoted by A and B, respectively. (2(A-D)) 0.6 ml/h at different voltages 18 KV, 19 KV, 20 KV and 21 KV denoted by A, B, C and D, respectively. (3(A-E)) 0.8 ml/h at different voltages 19 KV, 20 KV, 21 KV, 22 KV, 23 KV and 24 KV denoted by A, B, C, D and E, respectively.
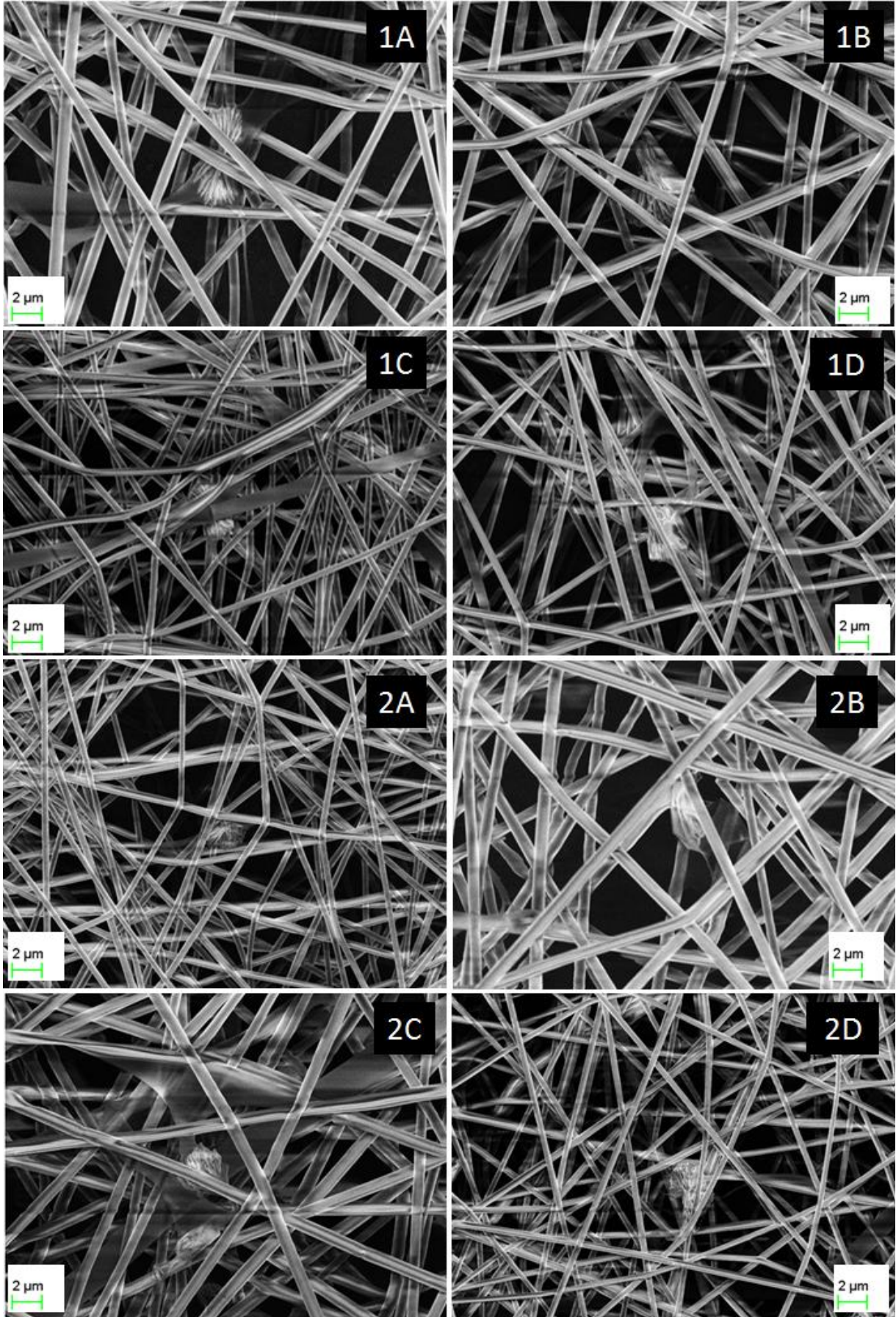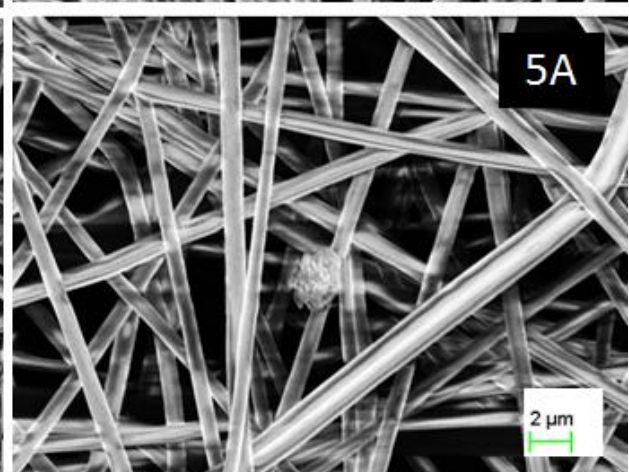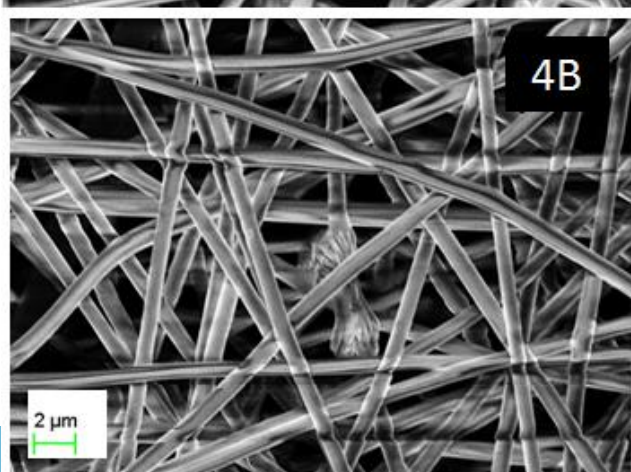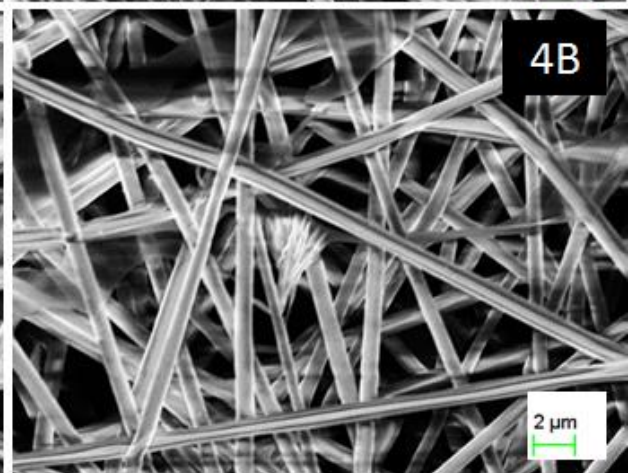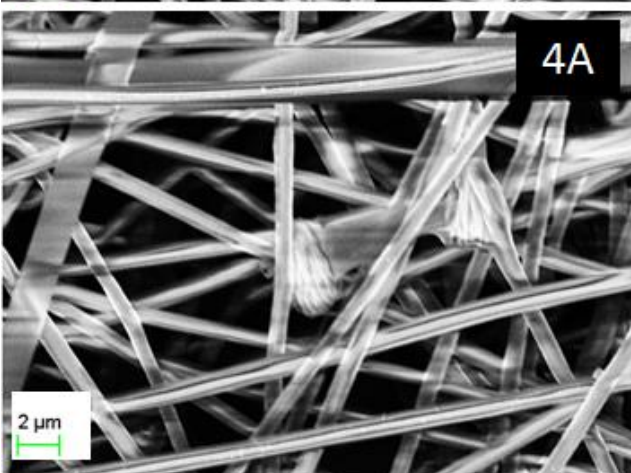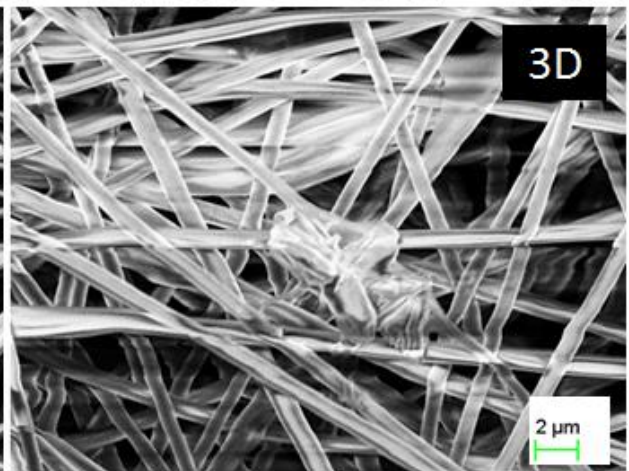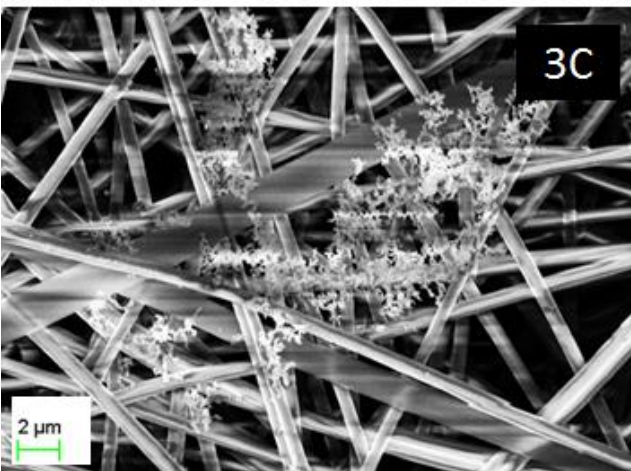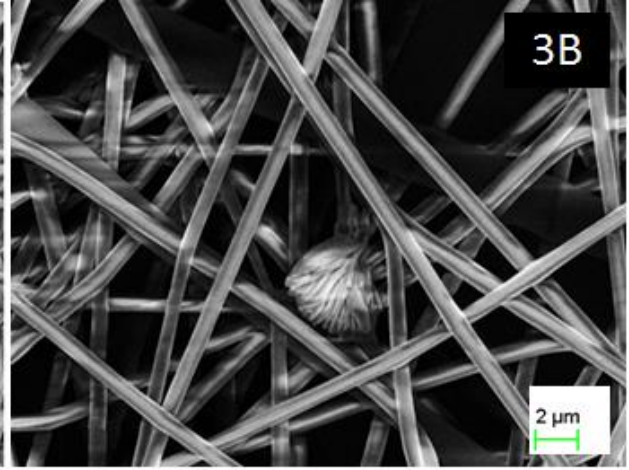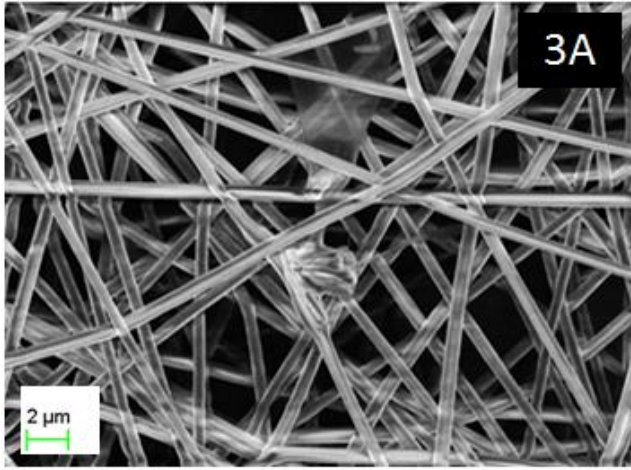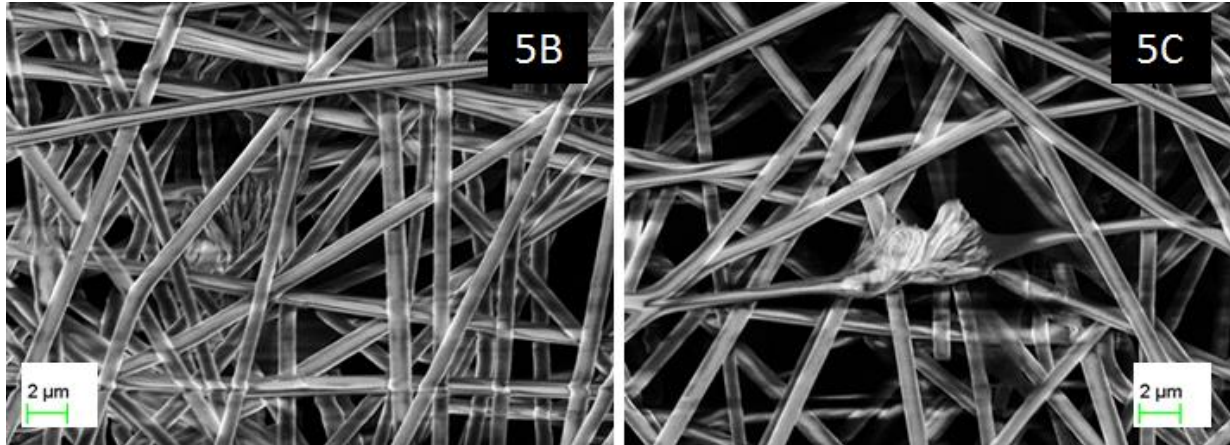
Figure 4.9: FESEM images of 6% Gn-CaCO₃ showing calcium acetate whether dispersed within the nanofibers mats or emerging from the nanofibers; (1(A-B)) 0.6 ml/h at different voltages 17 KV, 18 KV, 19 KV and 20 KV denoted by A, B, C and D, respectively. (2(A-D)) 0.7 ml/h at different voltages 17 KV, 18 KV, 19 KV and 20 KV denoted by A, B , C and D, respectively. (3(A-D)) 0.8 ml/h at different voltages 18 KV, 19 KV, 20 KV and 21 KV denoted by A, B, C, D and E, respectively, (4(A-C)) 0.9 ml/h at different voltages 19 KV, 20 KV and 21 KV denoted by A, B and C, respectively. (5(A-C)) 1 ml/h at different voltages 19 KV, 20 KV and 21 KV denoted by A, B and C, respectively.

4.3.2.2. Thickness measurement

Thickness measurement was done for Gn-CaCO$_3$ smooth nanofibers collected at optimized and were tabulated in Table 4.3 together with that of Gn 40% results denoted by Gn (0%). The thickness of smooth nanofibers was increased with the increase of calcium content from one concentration to another. Thickness distribution at each concentration was shown in Figure 4.10 (A) and (B) for 2% and 4%, respectively.

Table 4. 3: Thickness of the nanofibers estimated using Image J software for 0%, 2% and 4% smooth nanofibers.

Sample	Minimum thickness	Maximum thickness	Mean
Gn (0%)	141 nm	287 nm	204±31.3 nm
Gn-CaCO$_3$ (2%)	185 nm	398 nm	280±37.5 nm
Gn-CaCO$_3$ (4%)	209 nm	472 nm	332±38.7 nm
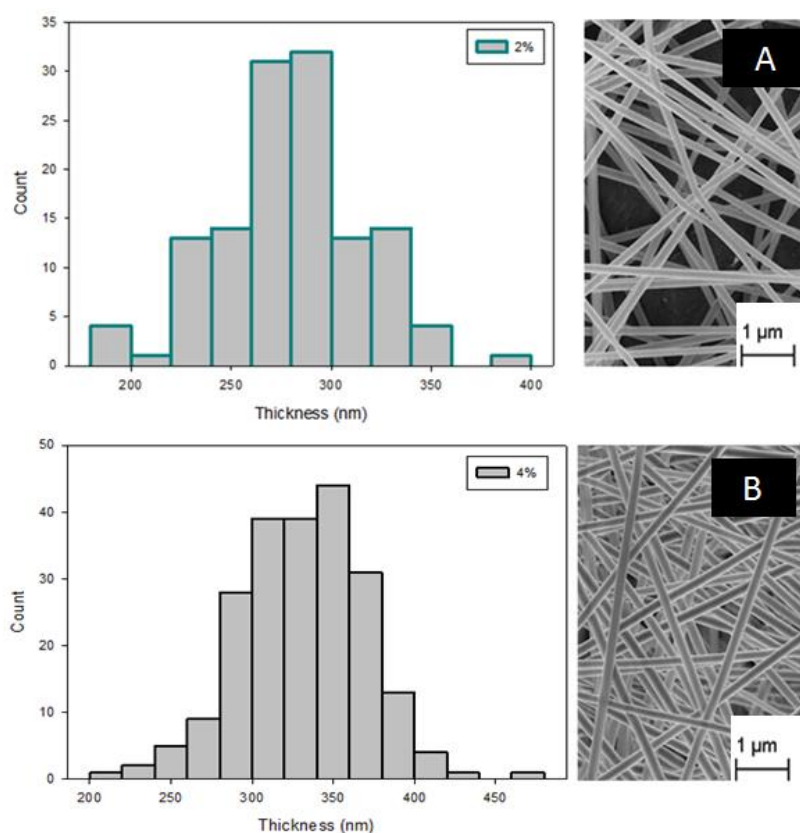
Figure 4.10: Thickness distribution of smooth nanofibers; (A) 2% and (B) 4%.

4.3.2.3. EDX Analysis

EDX results of 2% and 4% nanofibers showed calcium peak in addition to the carbon and oxygen ones that appeared for the Gn (0%) mats as shown in Figure 4.11 (A-B) where EDX mapping of 4% mats was shown in Figure 4.12.

4.4. Nanofibers crosslinking

Crosslinking using GTA vapors added chemical crosslinks within the fibrous mats enhancing its properties and correspondingly affected its architecture and morphological structures. Soft nanofibrous mats with its white color was shrunk and solidified into yellowish colored mats on exposure to GTA vapors. The yellow color in addition to the rigidity of the mats was found to increase with prolonged crosslinking time.

4.4.1. Field emission scanning electron microscopy

Images prevailed porous structures aligned into woven architectures with well-distributed pores along the mats. The crosslinking time affected the degree of crosslinks formed along the mats that can be seen as networking between nanofibers as illustrated in Figure 4.13 (A-C).

Both 2% and 4% crosslinked mats revealed similar morphology to Gn (0%) mats crosslinked for 20 h as shown in Figure 4.13 (D) and (E) respectively.

4.4.2. Pore size distribution

Results obtained for different mats showed that pore size distribution of Gn (0%) mats was ranging up to 300 nm. The pore size fraction up to 50 nm was found to increase with increasing the crosslinking time from 8 hours to 20 hours as illustrated in Figure 4.14.

Although the presence of calcium acetate within the nanofibers significantly affected the thickness of nanofibers as shown in Table 4.3, it did not affect the pore size range as shown in Figure 4.14.
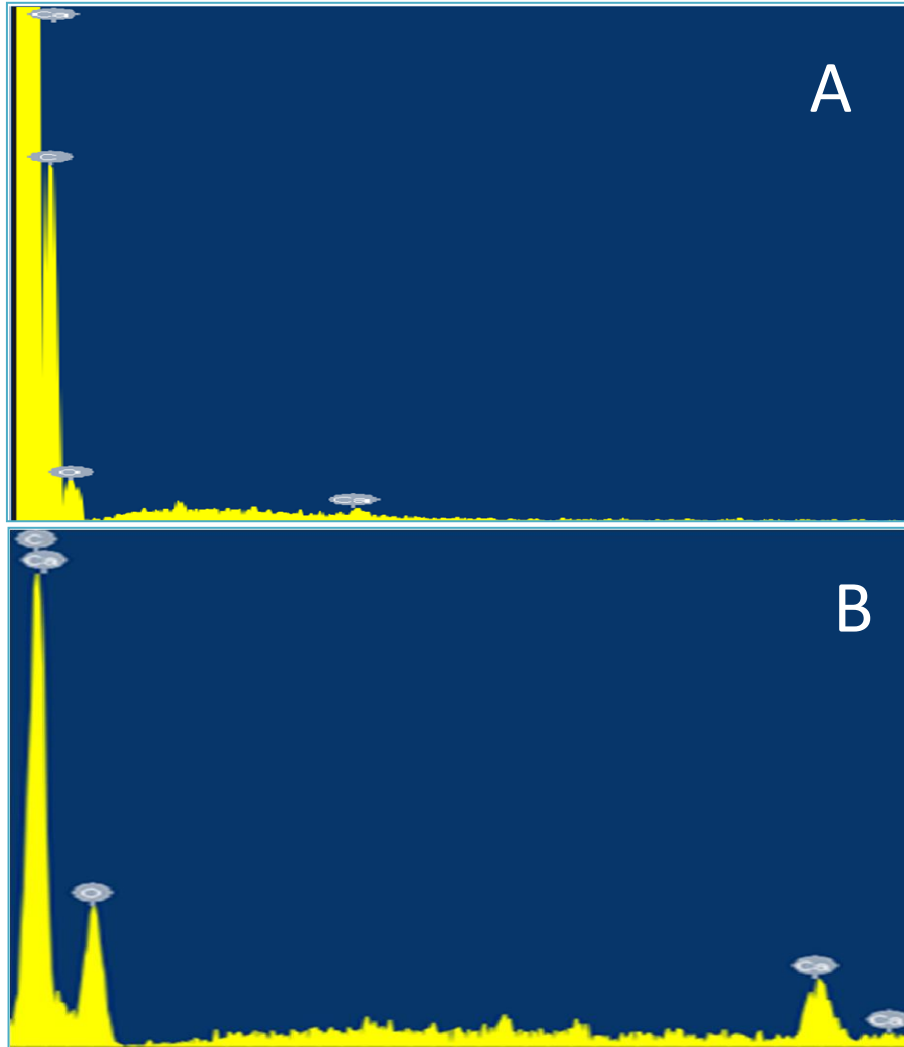
Figure 4 .11: EDX analysis showing calcium peaks at both 2% and 4% samples at (A) and (B) respectively.
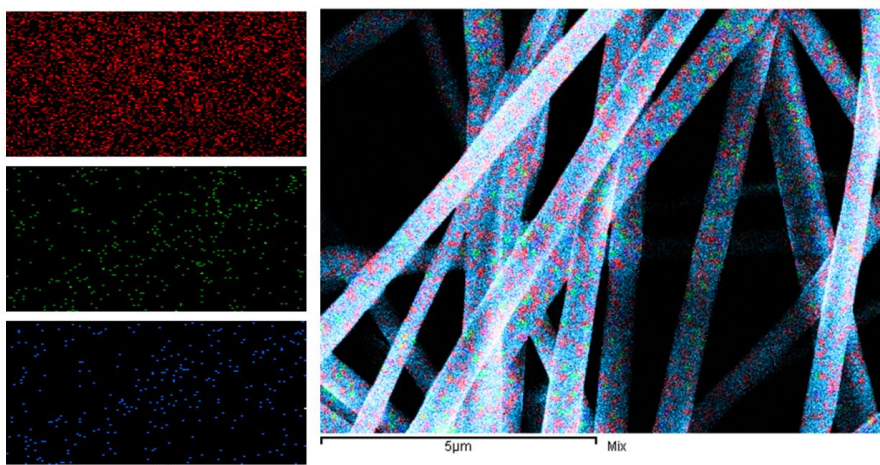
Figure 4 .12: EDX mapping of 4% mats showing carbon in red color, oxygen element in green color and calcium element in purple.

.
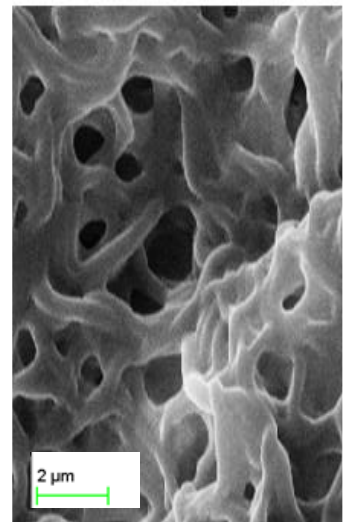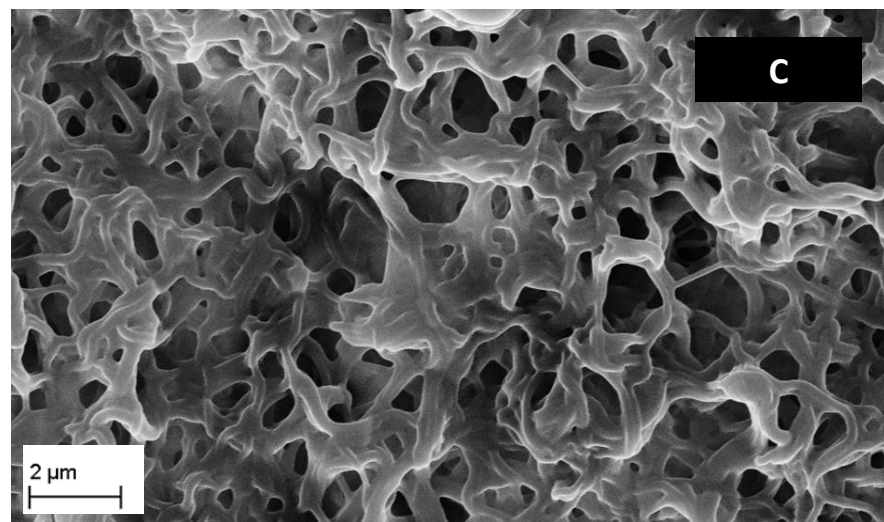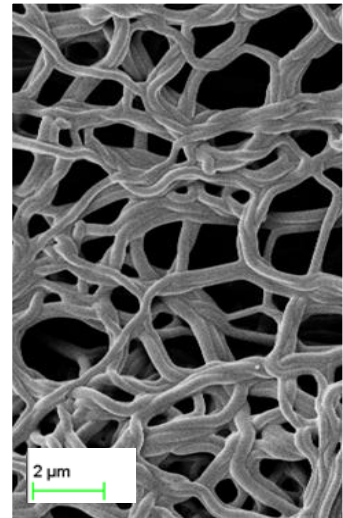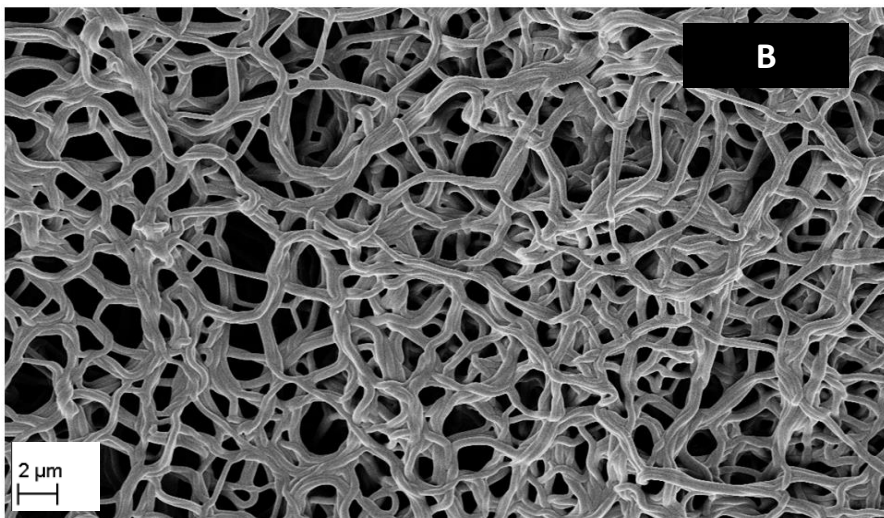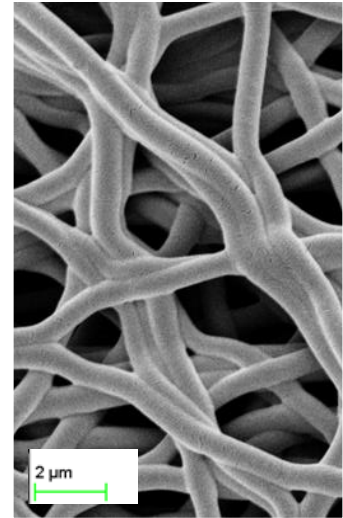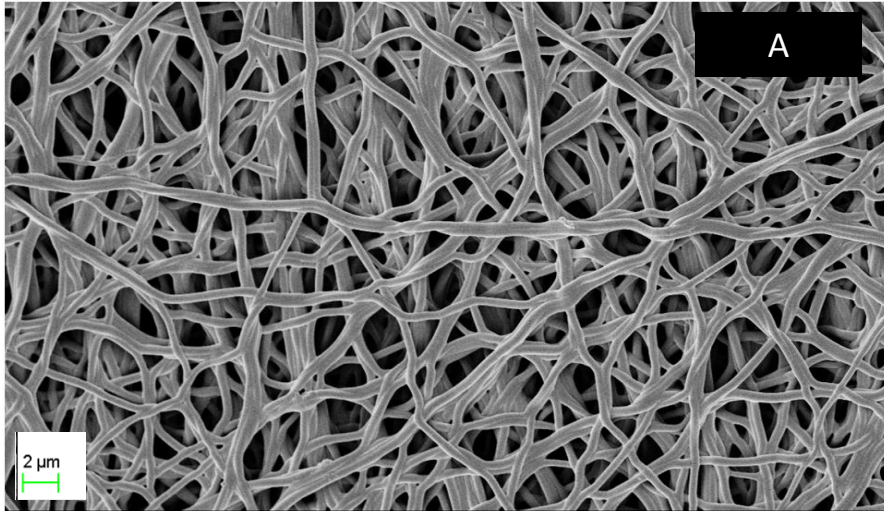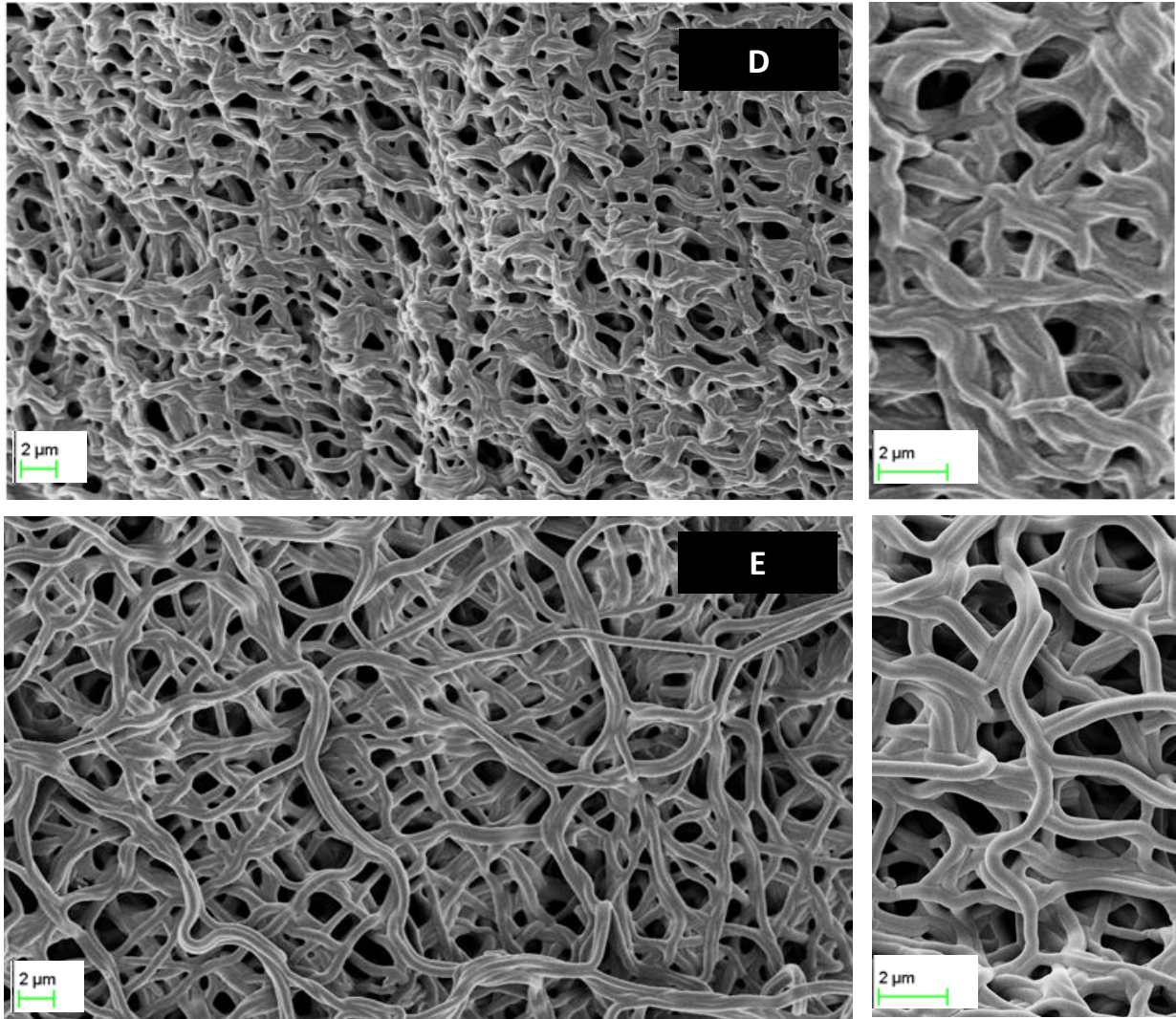
Figure 4.13: Crosslinked mats; (A) Gn (0%) crosslinked for 8h, (B) Gn (0%) crosslinked for 12 h, (C) Gn (0%) crosslinked for 20 h, (D) 2% mat crosslinked for 2o h and (E) 4% mat crosslinked for 20 h.
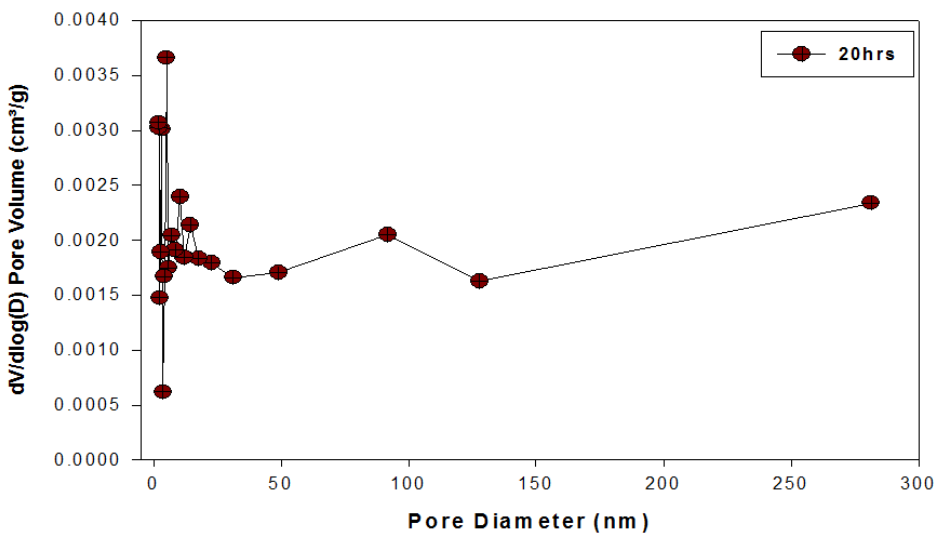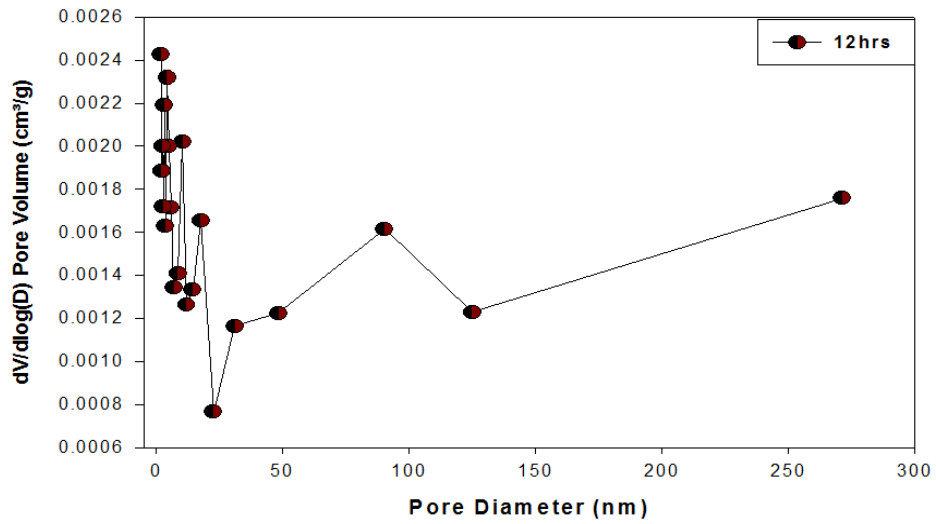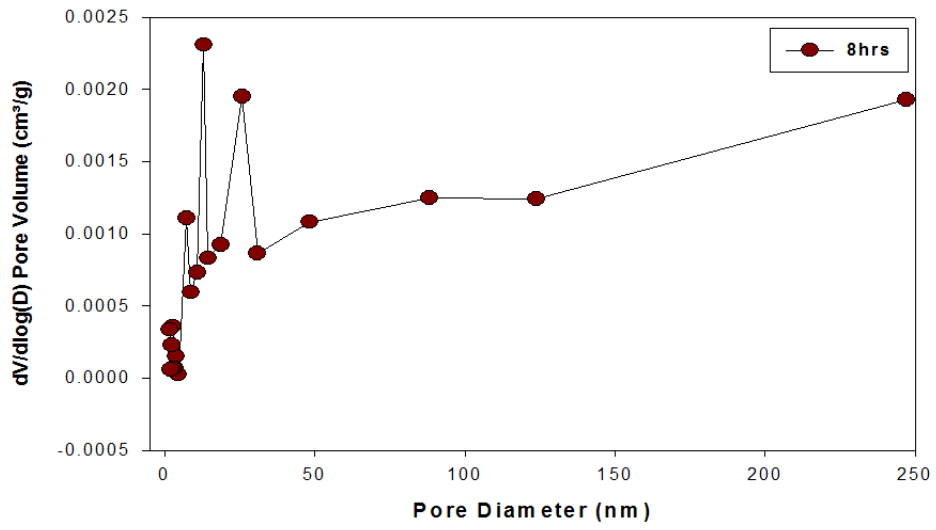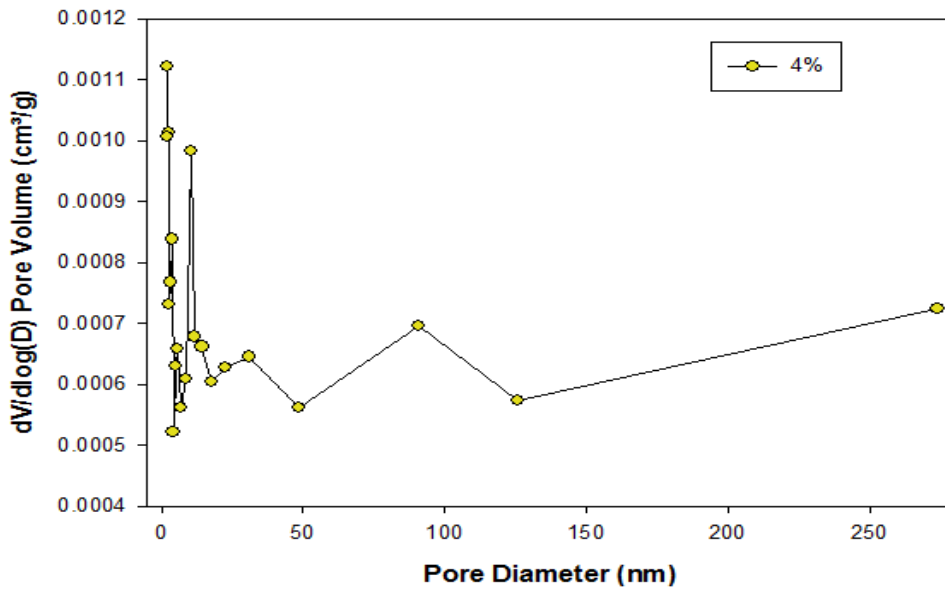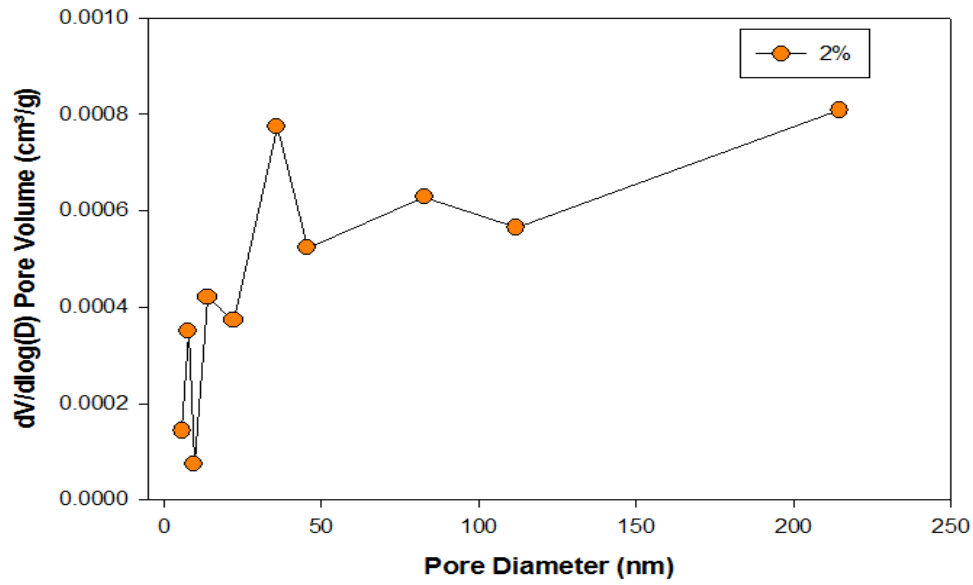
Figure 4.14: Pore size distribution of different crosslinked mats; Gn (0%) crosslinked at different time intervals (8, 12 and 20 h), Gn-CaCO₃ mats crosslinked for 20 h; 2% and 4%

4.4.3. Dissolvability test

The dissolvability results revealed that all Gn (0%) crosslinked mats at different crosslinking time (t=8, 12 and 20 h) existed after 3 days from its immersion in PBS. Gn (0%) mats (t= 8 h) showed debris suspended in PBS together with fractures

formation within the mats, where the 12 h and 20 h crosslinked mats showed no apparent change except for water retention.

In consequence, crosslinking the mats for 20 h appeared to be the optimum crosslinking time for Gn-CaCO$_3$ crosslinking to preserve prolonged resistance.

4.5. Fourier transform infrared spectroscopy (FTIR)

Gelatin has four characteristic peaks corresponding to peak A, Amide I, II and III peaks, respectively that acts as finger print of its structure (Erencia et al., 2015). The FTIR results of all mats (0%, 2% and 4%) showed the four peaks specific for Gn (0%); peak A at 3292 cm^{-1} (N-H stretching vibration), Amide I peak at 1640 cm^{-1} (C=O stretching), Amide II peak at 1536 cm^{-1} (C-H stretching) and Amide III peak at 1240 cm^{-1} (C-H stretching and N-H bending) as shown in Figure 4.16 (Siimon, Siimon, & Jarvekulg, 2015). In addition to the four peaks, additional peak was observed at 1450 cm^{-1} specific to the aldimine linkage (CH=N). The aldimine linkage was formed between the aldehyde group of GTA and the amino group of lysine within gelatin backbone.

Calcium containing mats showed the four specific peaks, however some were slightly shifted toward lower wave numbers. The shift was observed to increase with the increase of CaCO$_3$ initially added to Gn as shown in Figure 4.15. Peak A was shifted from 3292 cm^{-1} for Gn (0%) to 3288 cm^{-1} for 2% and 4%, which could be attributed to water adsorption on the surface of gelatin. Another peak shift was observed from 1535 cm^{-1} at 0% to a broadened peak at 1537 cm^{-1} for the 2% and 1547 cm^{-1} for the 4%. This peak shift could be attributed to the insertion of calcium acetate which has specific peak at 1550 cm^{-1} for (COO$^-$) asymmetric stretches (Bullen et.al., 2008). Shifting of 1448 cm^{-1} peak initially appeared for Gn (0%) mat to 1438 cm^{-1} at 2% and 1432 cm^{-1} at 4%, with the broadening of the shoulder appeared in 1394- 1417 cm^{-1} region could be an indication for the 1412 cm^{-1} peak characteristic for calcium acetate.
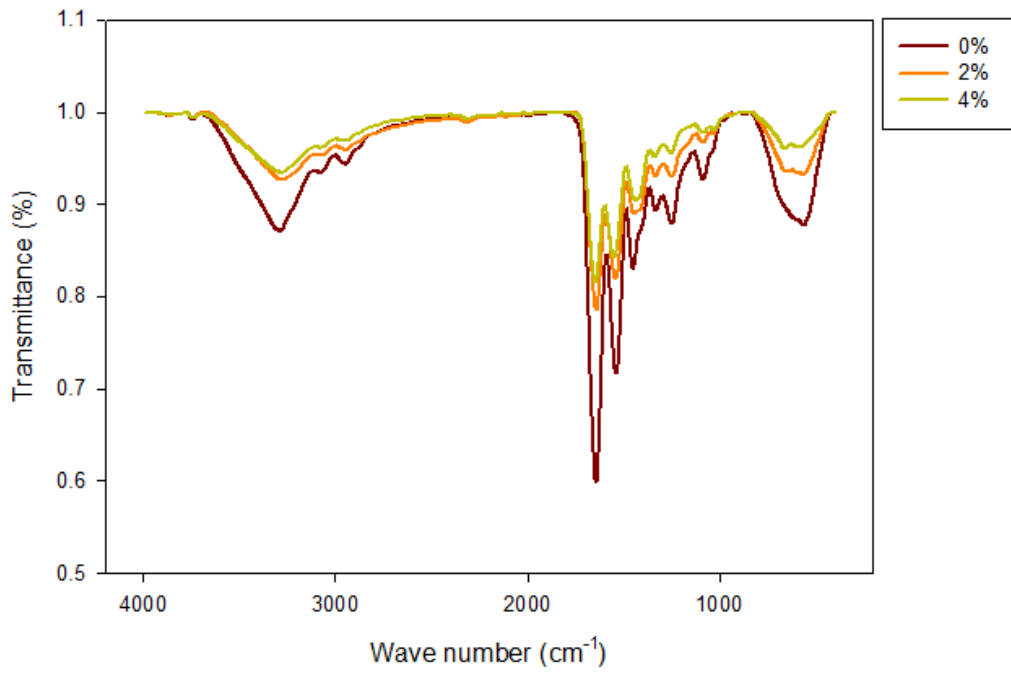
Figure 4.15: FTIR spectra showing transmittance spectrum in the region of 400- 4200 cm^{-1} for crosslinked Gn mats having different concentration of CaCO$_3$ initially added; 0%, 2% and 4%.
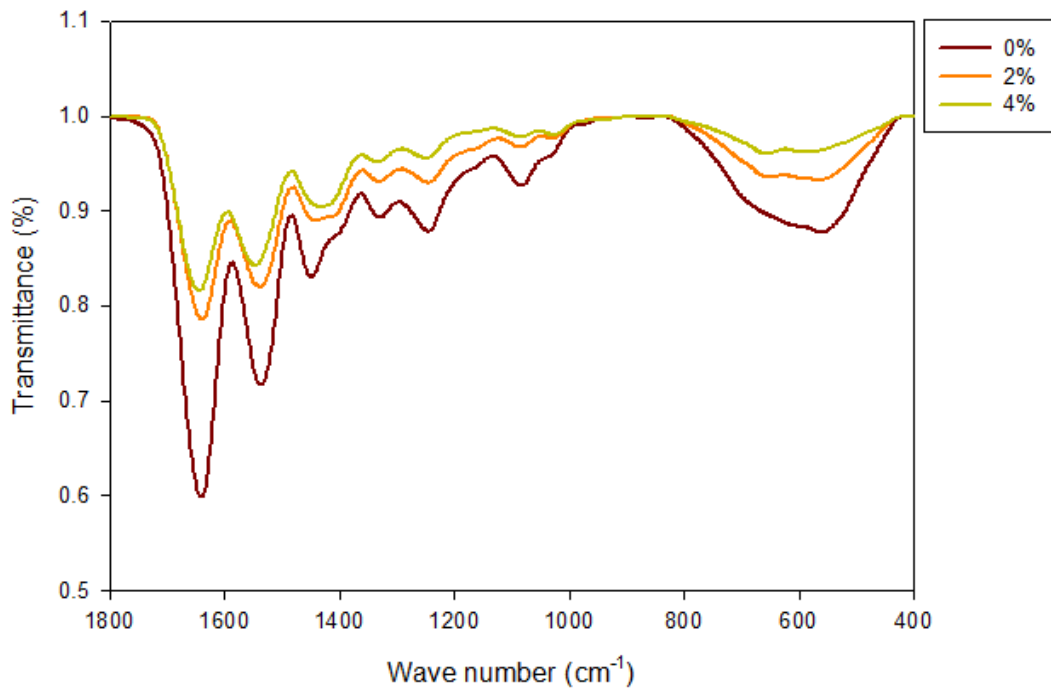
Figure 4.16: FTIR transmittance spectra in the region of 400- 1800 cm-1 for Gn- CaCO$_3$ mats; 0%, 2% and 4%.

4.6. *In vitro* characterization

4.6.1. Swelling test

Swelling was calculated for all mats immersed in PBS solution along the entire week of the experiment. Gn (0%) crosslinked mats for different time interval (t=8, 12 and 20 h) have reached maximum swelling percentage (Sw%) after 1 day of immersion in PBS as tabulated in Table 4.4. Throughout the entire week of their soaking, the Sw% was found to decrease with the increase of the crosslinking time except for the 8h crosslinked mats which possessed the least swelling profile as shown in Figure 4.17.

Table 4. 4: Maximum swelling percentage for each crosslinked Gn (0%) reached at different crosslinking time.

Crosslinking time (h)	Maximum Sw (%)	Soaking time (h)
8	528	24
12	925	24
20	884	24

During the 1st day of the experiment, Gn (0%) crosslinked for 20 h showed increased swelling compared to both Gn-CaCO$_3$ (2% and 4%) crosslinked mats reaching maximum value of 884% as shown in Figure 4.18. The swelling was then declined throughout the second day of immersion for the Gn (0%) mats, where both 2% and 4% mats reached their maximum swelling values; 695% and 688% respectively. Diminished swelling persisted starting from the 3rd day till the end of the week, where Gn (0%) mats lost up to three quarters of the maximum retained PBS while both Gn-CaCO$_3$ (2% and 4%) reserved almost 75% of the retained PBS . In conclusion, addition of CaCO$_3$ did not enhance swelling properties compared to Gn (0%) mats but it showed a relatively stable swelling profile throughout the experiment.
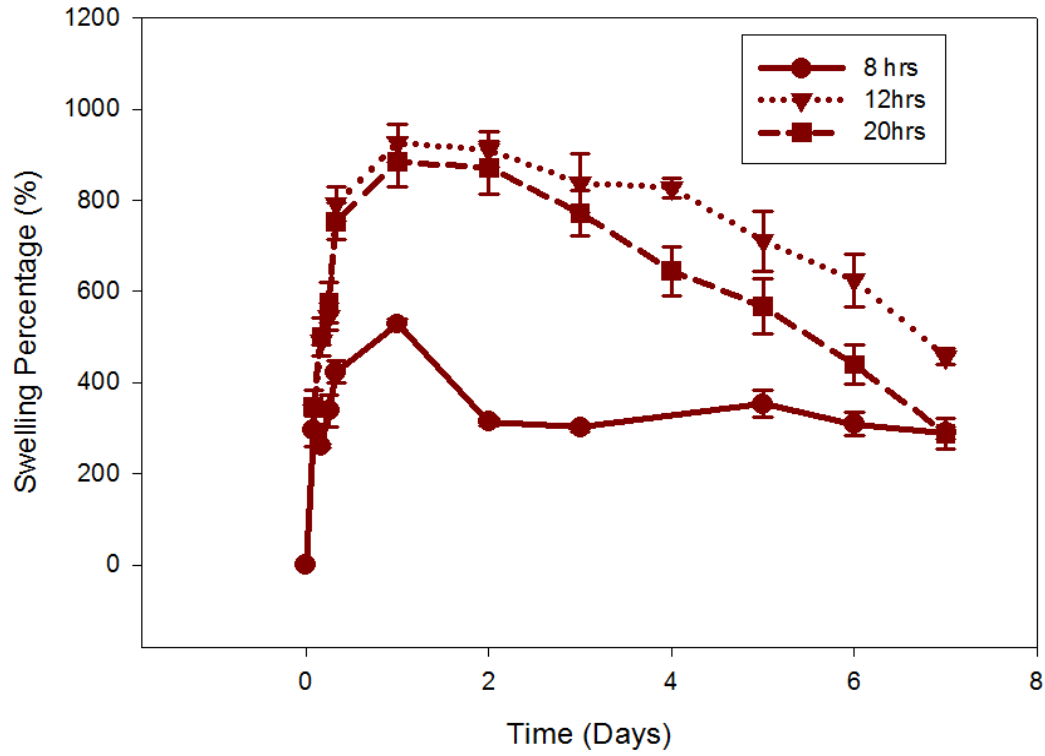
Figure 4.17: Swelling rate of Gn (0%) mats crosslinked at different time intervals; 8, 12 and 20 h.
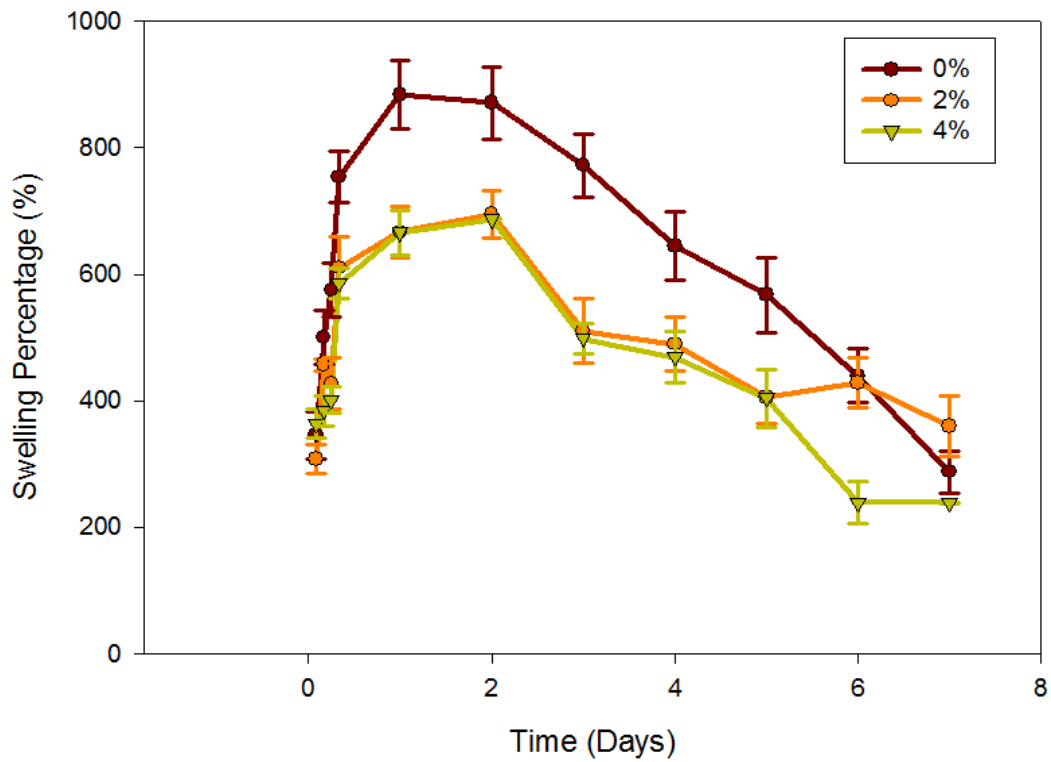
Figure 4.18: Swelling behavior of Gn-CaCO₃ mats; 0, 2and 4% crosslinked for 20 h using GTA.

4.6.2. Degradability test

Weight loss is a crucial property that indicates the dissolvability of the mats in simulated body fluid at 37°C. Crosslinking enhanced the resistance of the mats to dissolve in PBS as shown by the dissolvability test in section 4.4.3 and thus an expected prolonged degradation. All mats showed weight gain during the 1st week as shown in Figure 4.19, where Gn (0%) mats crosslinked for 20 h preserved weight gain throughout the entire experiment.

During the second week, the 2% and 4% mats lost up to 12% and 7 % of their dry weights. Weight gain was maintained for the 0% mats during the third week, where weight loss was almost doubled for the 2% and was slightly decreased for the 4% mats reaching 22% and 6%, respectively. The results showed that the presence of calcium acetate within the mats enhanced the weight loss compared to Gn (0%) mats where doubling of acetate concentration suppressed the rate of degradation. Over all, the consistency of the degradation results of both 0% mats and 2% mats cannot be guaranteed especially during the first two weeks.
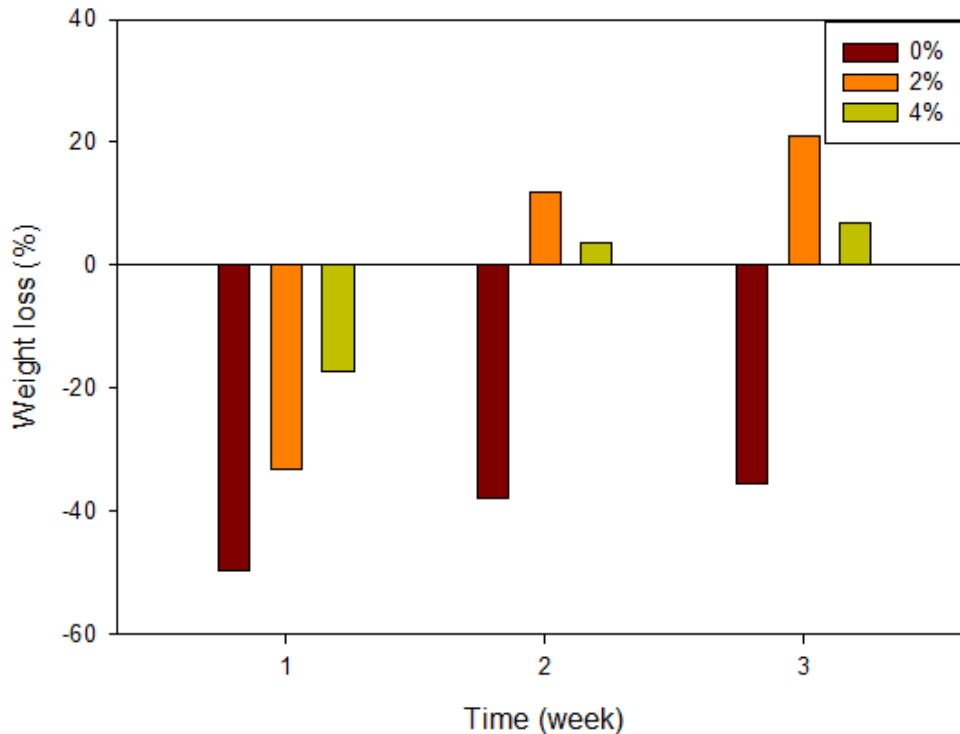
Figure 4.19: Histogram showing the rate of degradability of different Gn-CaCO₃ mats; 0, 2and 4% crosslinked for 20 h.

4.6.2.1. Field emission scanning electron microscopy

Images of the 1st week samples showed that all mats were somehow swollen but still keeping their original structure. In addition, the images revealed the presence of tiny particles along the surface of Gn (0%) mats while needle like structures were dispersed within the pores of both 2% and 4% mats as shown in Figure 4.20 (A), (B) and (C) respectively.

The four week samples of Gn (0%) mats showed increased dispersion of tiny particles that was observed along the mats as shown in Figure 4.21 (A). Soaked 2% and 4% samples showed growth of flower like structures scattered in form of colonies along the surface of the mats as illustrated by FESEM images in Figure 4.21 (B) and (C) respectively.

4.6.2.2. EDX analysis

The analyses of all mats revealed the presence of two peaks specific to sodium and chloride elements in both the 1st week and 4th week samples, with extra two peaks appeared for the 2% and 4% mats corresponding to calcium and phosphorus elements shown in Figure 4.21.

4.6.3. MTT assay

The first experiment investigated the cyotoxicity of DAA and GTA used for Gn (0%) crosslinking at different time intervals (t=8, 12 and 20 h). Gn nanofibers at (t=0) denoted by NFs showed significant viability compared to the cell control (TCPs) as illustrated in Figure 4.22 where $P<0.05$. All crosslinked mats at different time intervals showed no significant difference compared to TCPs except for the 20 h crosslinked mats, where the viability was significantly enhanced as shown in Figure 4.22 (B), where $P<0.001$. Both NFs and gelatin crosslinked mats (t=20 h) revealed significant growth, however the viability of the 20 h crosslinked mats was more significant compared to NFs as shown in Figure 4.22 (B), where $P<0.001$.

As aforementioned, the viability of Gn (0%) mats crosslinked for 20 h was significant amongst other samples, Gn-CaCO$_3$ mats (2% and 4%) were crosslinked for 20 h and prepared for the second experiment. The aim of this experiment was to test

the cytotoxicity of calcium acetate, Gn (0%) mats crosslinked for 20 h were used as control to ensure that all results obtained was due to the effect of calcium acetate.

After the first day of seeding, the absorbance was increased with increasing the concentration of calcium within the mats. Both concentrations (2% and 4%) had significant viability compared to Gn (0%) mats as shown in Figure 4.23 (B). This increased viability could be attributed to the presence of calcium within the mats, which stimulated the mineralization of the mats and enhanced cellular growth.

Absorbance measured after the third day of seeding showed enhanced cellular growth among both the control and the 2% samples, with the slight decrease of absorbance for the 4% mats. Although the increase of calcium in the 4% mats slightly affected their absorbance, the viability was found to significantly decrease compared to the control and the 2% mats.

In conclusion, the viability of Gn-CaCO$_3$ mats revealed significant difference compared to the control shown in Figure 4.23 (B) where P<0.05. The calcium content in the 2% mats showed significant increase in the viability of the cells, while its increase in the 4% mats revealed significant decrease in the cellular viability.
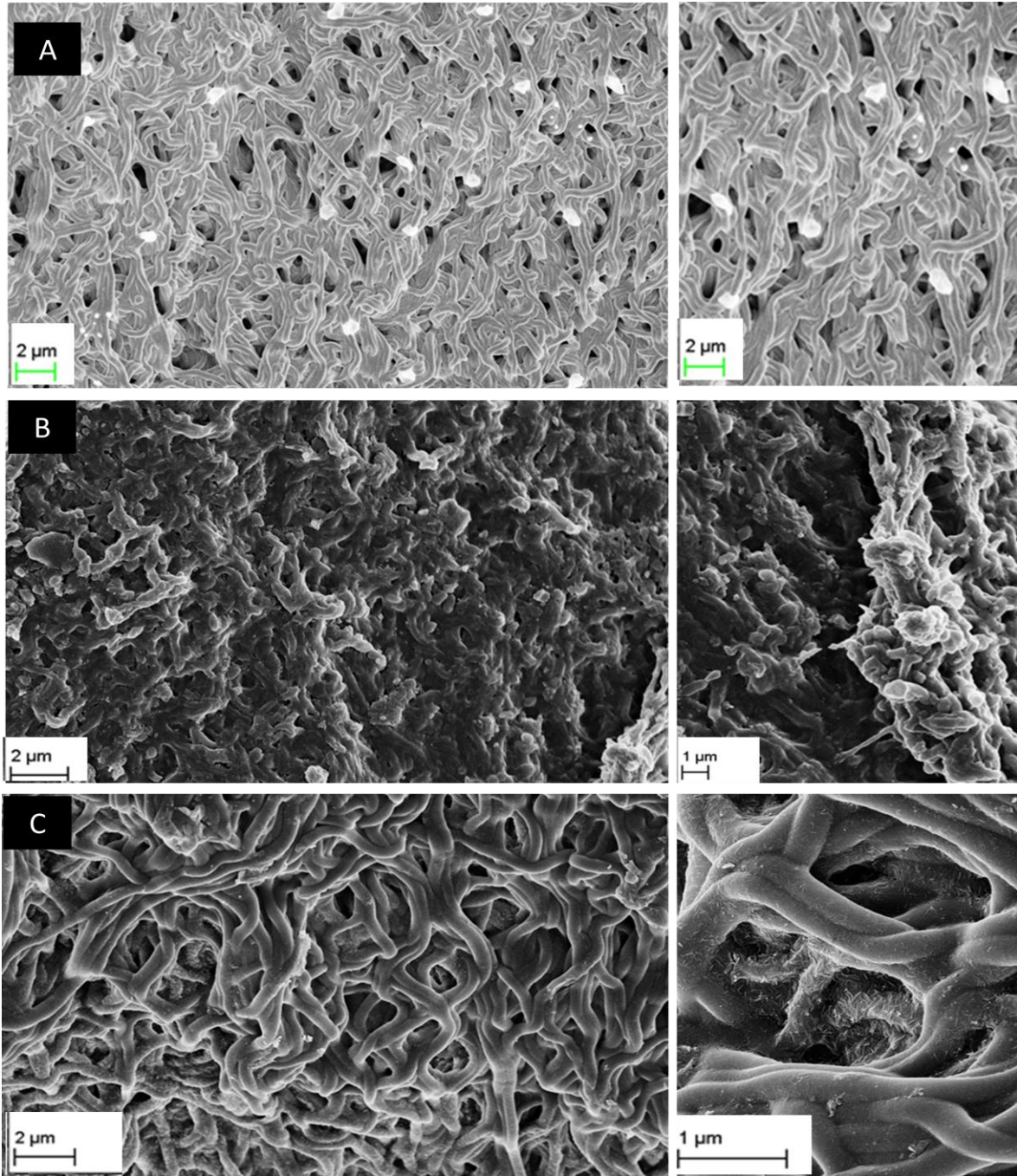
Figure 4.20: Degradability samples Gn (0%), 2% and 4% crosslinked for 20 h shown in A, B and C, respectively after soaking in PBS for a week.
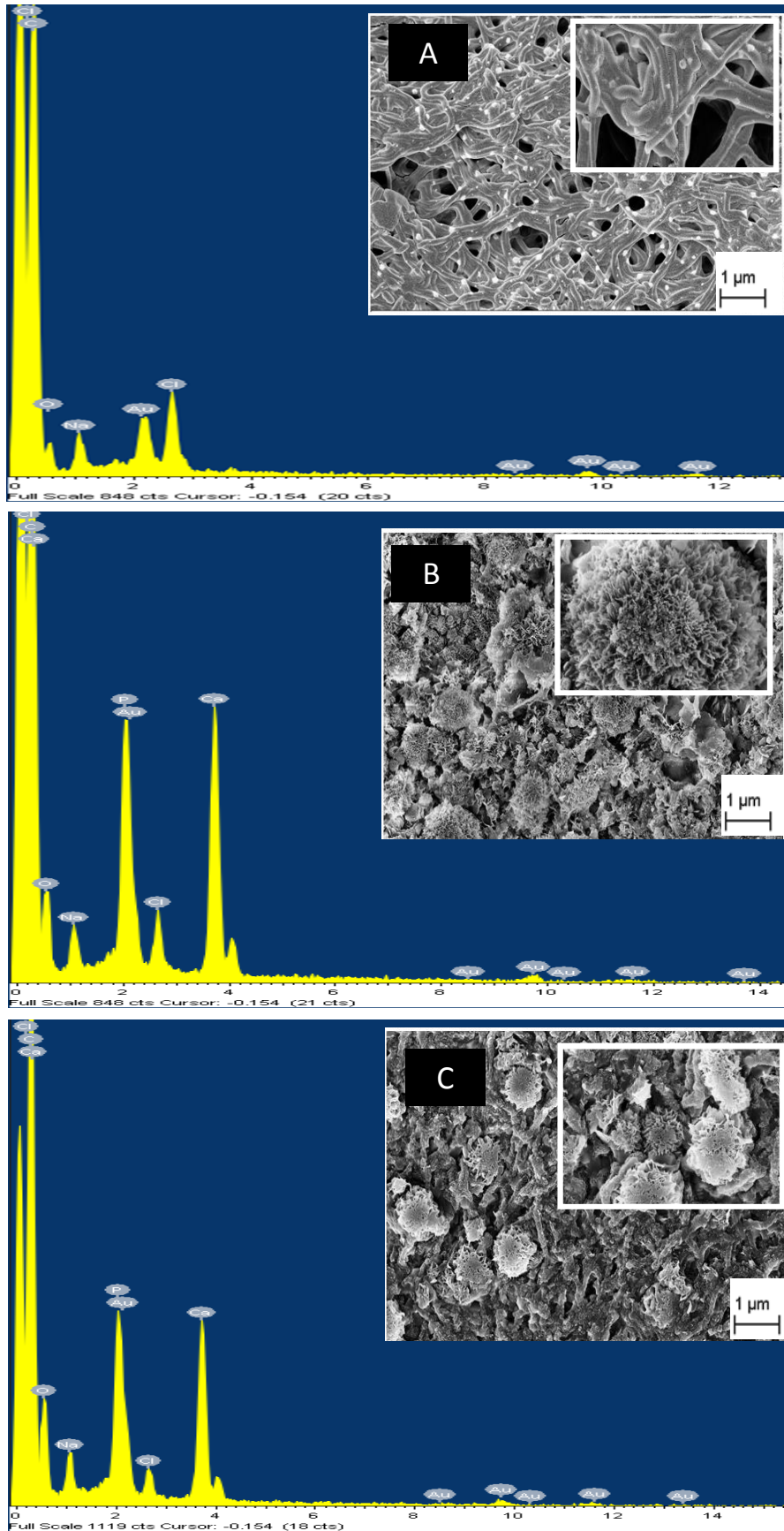
Figure 4.21: FESEM and EDX analysis of Gn-CaCO₃ mats; 0, 2 and 4% soaked for a month in PBS at 37°C.
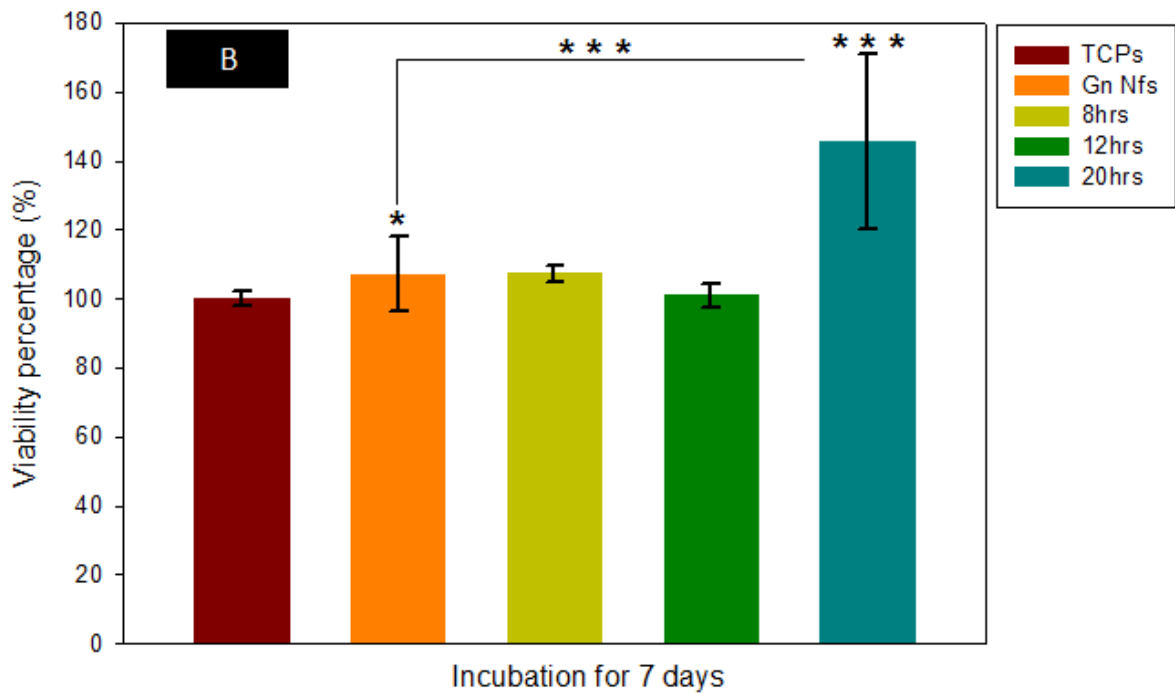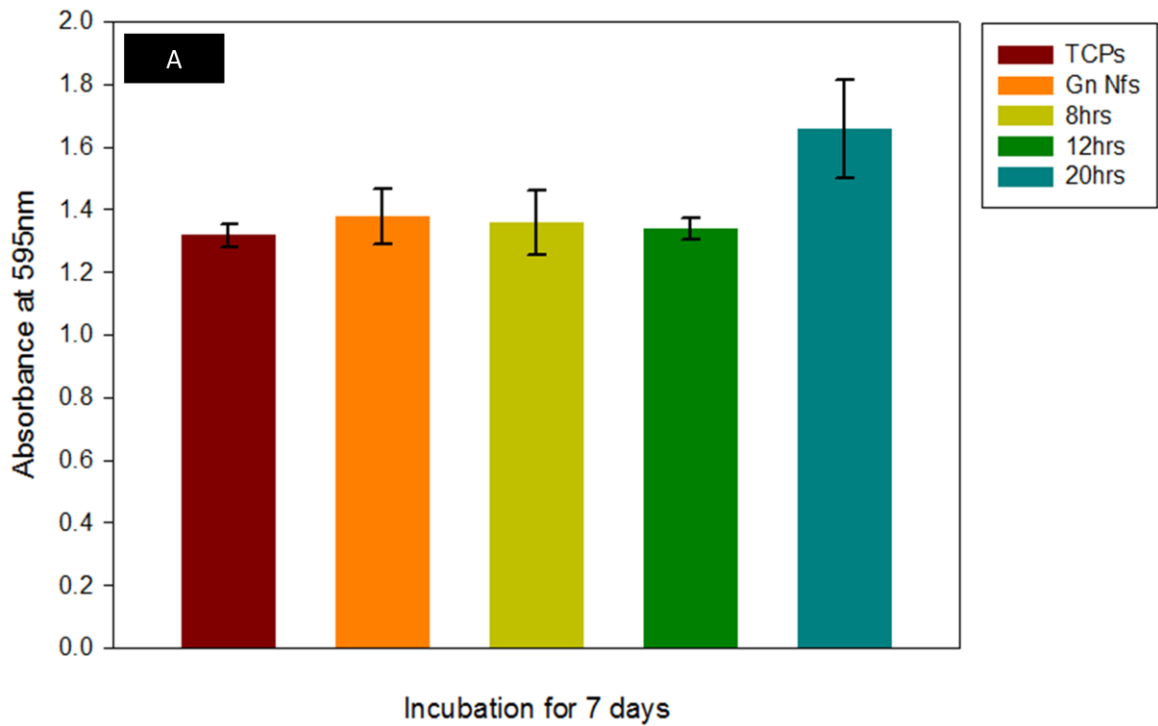
Figure 4.22: Results of the first experiment where Gn (0%) nanofibers crosslinked at different time intervals using GTA and uncrosslinked gelatin mats were investigated for the cytotoxic effect of GTA in crosslinked mats and DAA in uncrosslinked ones; (A) Absorbance at 595 nm and (B) Viability percent representing cellular growth. Data are presented as a mean of at least three independent experiments (mean±SD), where (* P<0.05, *** P<0.001).
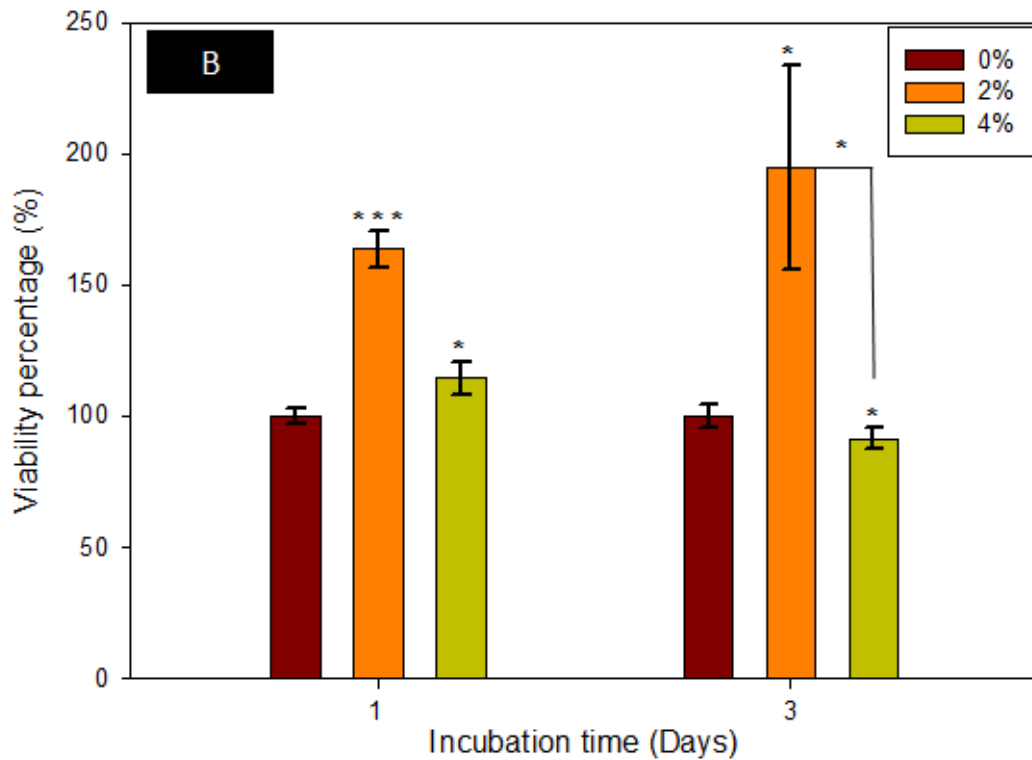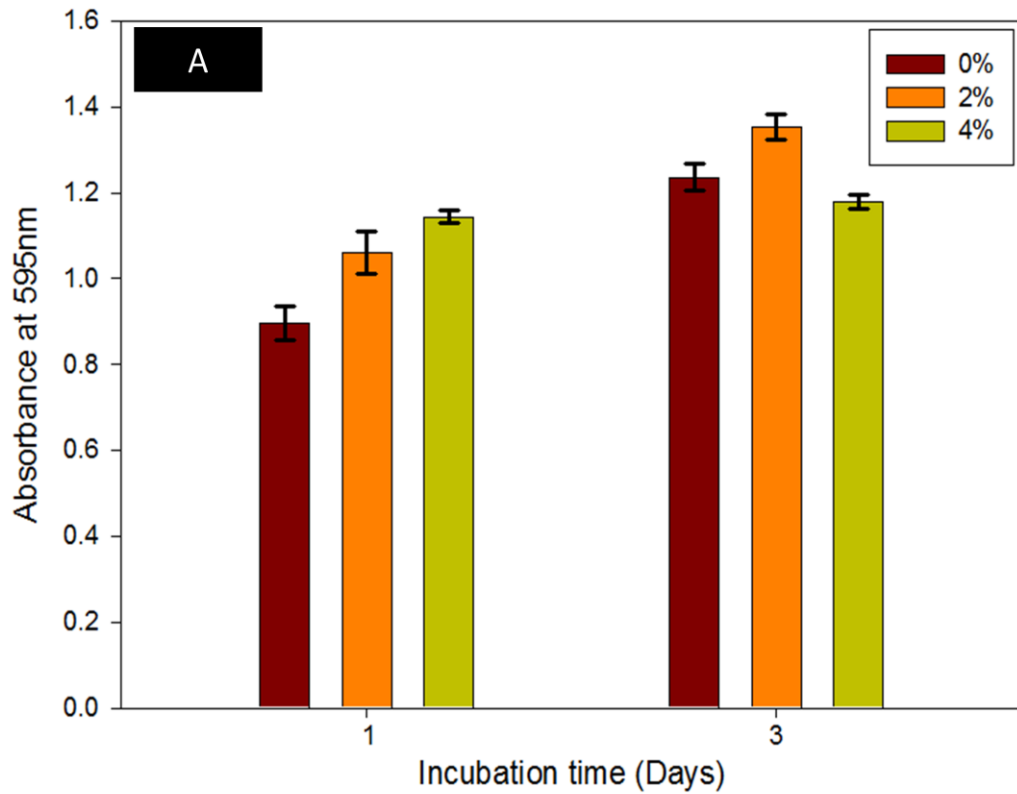
Figure 4.23: Results of the second experiment where Gn-CaCO₃ mats; 2 and 4% were investigated for the cytotoxic effect of increased concentration of calcium acetate within the mats after 1 and 3 days from seeding; (A) Absorbance at 595nm and (B) Viability percent representing cellular growth. Data are presented as a mean of at least three independent experiments (mean±SD) where (* $P<0.05$, *** $P<0.001$).

CHAPTER 5

DISCUSSION

5.1. <u>Solution preparation and characterization</u>

Calcium carbonate greatly affected the physical properties of the Gn (0%) solution. Mixing of calcium carbonate together with DAA while solution preparation at different concentrations of $CaCO_3$ (2, 4, 5 and 6%) led to the formation of calcium acetate. The reaction mechanism was shown in Figure 5.1.
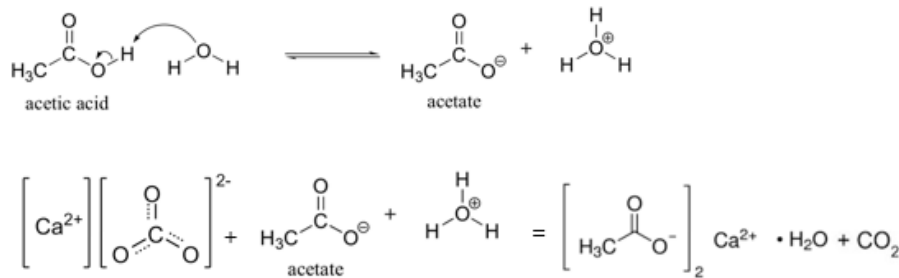
Figure 5. 1: Reaction mechanism of DAA with CaCO₃ while preparing Gn-CaCO₃ mixtures.

The release of water caused the increase of the pH of the solution and consequently the pH increased with increasing the concentration of $CaCO_3$ initially added as previously shown in Figure 4.2B.

Not only calcium acetate formation affected the pH value of the solution, but also it greatly enhanced the conductivity of the solution. According to literature, both the pH and the concentration of gelatin greatly affect the conductivity of gelatin solutions (Palmer W. Walter, 1921). At acidic medium, where the pH is less than gelatin's isoelectric point it became protonated and experience intermolecular repulsive forces (Bukhari et.al., 2015; Texas, 2015). These repulsive forces affected the structure of gelatin and the consequence ease of ions flow (Johlin, 1930; Palmer W. Walter, 1921). Doubling the initial calcium carbonate concentration added from 2% to 4% caused doubling of the conductivity where continuous increase resumed reaching maximum value at 6%.

5.2. <u>Electrospinning and nanofibers crosslinking</u>

Different parameters greatly affect the efficiency of the electrospinning process and the formation of bead-free nanofibers. The concentration of prepared solution greatly affects its viscosity. As the concentration increases, the tangling of the polymeric network consequently increases. The concentration of gelatin solution

greatly affected the success of the electrospinning process to yield smooth nanofibers. With concentrations less than 40% (w/v %), solutions were electrospun into beaded fibers with increased dropping. The thickness of smooth nanofibers obtained from 40% Gn solutions was smaller than that reported by Zhang et al. using almost same Gn concentration in aqueous solution (S. Zhang et al., 2009).

The decrease of the thickness of Gn (0%) nanofibers at 0.5 ml/h from 204±31.3 nm at 19 KV to 193.64±54.41 nm at 22 KV can be explained by the increased charge injection to the polymeric solution, leading to increased repulsive forces between the nanofibers formed. Repulsive electric forces led to the consequent accelerating toward the collector undergoing whipping forces and thickness was decreased (Bhardwaj & Kundu, 2010).

The increased thickness of Gn-$CaCO_3$ nanofibers fibers formed could be explained by the incorporation of calcium acetate with Gn nanofibers formed as previously confirmed by EDX analysis for 2% and 4% mats.

Crosslinking of the mats using GTA vapors enhanced the resistance of mats to aqueous solutions. The increased crosslinking time enhanced the chemical crosslinks formed within the gelatin mats leading to increased resistance. The presence of Gn (0%) crosslinked mats at different crosslinking time (t= 8, 12 and 20 h) after three days conflicted the results reported by Zhang et.al (2006), although both experiments were performed under same conditions and using same concentration of GTA. They reported that only prolonged exposure to GTA vapors for more than 2 days revealed proper crosslinking degree, with those mats crosslinked for less than 2 days were completely dissolved after three days of immersion (Y. Z. Zhang et al., 2006). This contradiction in results could be attributed to the difference in structure of gelatin nanofibers due to the different solvents used, which in turn affected the extent of crosslinking.

Pores size distribution for Gn (0%) mats (crosslinked at t= 8, 12 and 20 h) revealed that the pore sizes were in the range of 250 nm with the majority are up to 50 nm. Small pore size is suitable for periodontal membranes to prevent the in growth of fibroblast and permits vascularization at the same time. The pore distribution was not greatly affected by the crosslinking time, however water resistance and the

stability of the mats was affected. Crosslinking for 20 h seemed to be the ultimate choice for crosslinking of Gn-CaCO₃ nanofibers to enhance the stability of the mats.

5.3. <u>Fourier transform infrared spectroscopy</u>

Gelatin has four peaks that reveal its conformational structure, where the absence of any of those peaks could be a sign of degradation and decreased molecular weight. Different solvents succeeded in gelatin electrospinning, however some solvents affected its chemical composition via degradation. Formic acid was reported to change the conformational structure of gelatin from helical to random coiled structure (Ki et al., 2005; Mindru, Mindru et.al., 2007).

FTIR spectra of the fabricated mats revealed their molecular composition ensuring that all mats preserved the initial structure of gelatin. The four characteristic peaks of gelatin (peak A, Amide I, Amide II and Amide III), in addition to a strong peak at 1450 cm^{-1} (aldimine absorption), were identified for all mats (Nguyen & Lee, 2010; Y. Z. Zhang et al., 2006). The presence of both the Amide I and Amide II peaks indicates that the mats reserved its helical structure as reported by Li et.al. (H. Li et al., 2016).

None of the acetic acid peaks previously reported by Erencia et al. was observed in any of the mats revealing the absence of any DAA residuals (Erencia et al., 2015). In conclusion, DAA used during the electrospinning process did not affect the gelatin helical structure.

FTIR spectra of Gn-CaCO₃ mats showed slight shift in majority of the bands toward lower wavelength compared to Gn (0%) mats. This shift could be attributed to the insertion of calcium acetate within the gelatin matrix. The aforementioned explanation could be supported by the shift of Amide II peak at 1535 cm^{-1} for 0% to 1539 cm^{-1} for 2% and reaching 1546 cm^{-1} for 4% mats. This shift could be assigned to the (COO^-) asymmetric stretches specific to calcium acetate at 1550 cm^{-1} (Bullen et al., 2008). All mats showed the absence of acetic acid specific peak at 1702 cm^{-1} which was previously reported in gelatin nanofibers using DAA as an electrospinning solvent (Erencia et al., 2015).

All results revealed that neither the use of 40% DAA as electrospinning solvent nor the addition of calcium carbonate affected the conformational structure of gelatin.

5.4. *In vitro* characterization

5.4.1. Swelling

As crosslinking time increases, the degree of crosslinking increases, resulting in a decrease in consequently the degree of swelling (Y. Chen, Zhou, Lin, & Jiang, 2014). The swelling of Gn (0%) mats crosslinked at different time intervals revealed that the swelling was increased with decreasing the crosslinking time interval, where the mats crosslinked for 8 h showed the least swelling percentage. The aforementioned results is consistent with what was previously reported in literature for the use of chemical crosslinkers in different gelatin composites (Dash, Foston, & Ragauskas, 2013; Liao, Zhang, & Chen, 2009; Nguyen & Lee, 2010b; Xing et al., 2014)

The swelling of the 12-hours-crosslinked mats was the maximum followed by the 20-hours-crosslinked mats where both reached maximum values after 1 day of PBS soaking. The 8-hours-crosslinked mats showed the least degree of swelling unlike what was expected, reaching its maximum within 24 h of immersion. The unstable swelling profile of the 8-hours-crosslinked mats compared to the 12- and 20-hours ones could be attributed to the decreased degree of crosslinking along with the weight loss during the week of the experiment. The debris of the mats that was observed during the dissolvability test indicated weight loss. These results reassured that crosslinking for 20 h was suitable for the stability of the mats.

For Gn-CaCO$_3$ mats, previously shown in Figure 4.18, the swelling of the 0% mats crosslinked for 20 h reached a maximum value of 884% at the 1st day, where the 2% and the 4% mats reached maximum values of 695% and 686%, respectively at the 2nd day. The decrease in swelling with the increase in CaCO$_3$ concentration initially added to the mats compared to Gn (0%) could be explained by Donnan effect. The increase of the metal ions concentration within the mats decreased the concentration difference of ions between the mats and PBS leading to the decreased PBS diffusion and ceased its retention (Xing et al., 2014).

5.4.2. Degradability

The rate of degradability of membranes is very crucial for the success of periodontal healing. All mats were soaked in PBS solution and due to the difference in ions concentration between the solution and the mats, diffusion took place. Mats were removed after the first week; washed, dried and weighed where weight gain was perceived. The initial increase in the weight of the mats was found to be consistent with what was previously reported by Xing et al. (2014). Although the increase of the weight observed rather than its loss was explained by salt entrapment, a closer look was essential to understand the reasons for the high standard of deviation calculated for different mats.

FESEM imaging together with EDX analysis gave a closer look on all soaked samples. Weight increase together with the inconsistency of the results among triplicate samples used for each concentration can be explained by two justifications; salt entrapment within the mats (Xing et al., 2014) and apatite growth (Meng, Li, Sun, Zheng, & Zheng, 2013; Nirmala, Nam, Navamathavan, Park, & Kim, 2011; Zhan & Lan, 2012).

Salt entrapment was observed via FESEM and confirmed by EDX analysis as shown earlier in Figure 4.20 and 4.21. This salt entrapment is consistent with the aforementioned explanation of weight gain and represents a justification for the inconsistency of the results throughout the samples tested as the concentration of entrapped salt may vary from one sample to another creating an increased deviation.

Although FESEM revealed that all mats preserved their initial morphology, flower-like structures in form of colonies were observed along the calcium containing mats where tiny particles were dispersed through the surface of Gn mats. Salt entrapped together with calcium initially present within the Gn-CaCO$_3$ mats led to Ca-P growth in the form of needles, which progressed to flower like structures in the 4th week. Ca-P growth along the mats could be attributed to more than one factor such as, the released calcium to PBS during degradation, in addition to calcium within the mats. The presence of calcium acted as nucleation sites for mineralization

of the mats and the growth of Ca-P (Oliveira, Malafaya, & Reis, 2003; Yang et al., 2009). In addition, enhancing Ca-P growth and the initiation of nucleation sites were greatly affected by the swelling degree of the mats. Swelling enhances the presence of OH group on the surface of mats, which can bind to calcium followed by Ca-P growth.

Both FESEM imaging and EDX analysis confirmed Ca-P growth along the mats. According to literature, Ca-P growth increases the weight of the soaked mats, with increasing the soaking time. Thus, the weight increased due to Ca-P growth imposed with the expected weight loss due to mats degradation (Meng et al., 2013). In conclusion, degradation experiment using PBS as a soaking solution was not informative for the actual degradation rate of Gn-CaCO$_3$ mats

5.4.3. <u>Viability test</u>

According to literature, the cytotoxicity of the gelatin nanofibers prepared using DAA found to increase with the increase of the initial concentration of the acetic acid used. This was attributed to the traces of the solvent maintained within the mats (Erencia et al., 2015). Results of the 1st experiment revealed that gelatin nanofibers prepared using 40% DAA showed enhanced viability compared to TCPS, which can be attributed to the complete drying of the mats before their use and the absence of solvent traces. This explanation was consistent with the FTIR results that lacked acetic acid peaks previously reported by Erencia et.al. (2015).

The good viability of gelatin nanofibers is consistent with literature as gelatin is renowned by its cell recognition sites, enabling cell adhesion and proper functioning (Liu & Ma, 2009; Woo, Chen, & Ma, 2003; S. Zhang et al., 2009)

The closely equal viability of Gn crosslinked mats (t= 8, 12 and 20 h) with that of cell control indicated that neither the concentration of GTA used nor the crosslinking intervals tested have cytotoxic effect. The significance of 20- hours-crosslinked mats could be attributed to the preserved apparent structure of the mats and mechanical properties, which could greatly affect the viability of the cells.

The second experiment revealed that the presence of calcium within the mats greatly affect the viability compared to Gn (0%). Both Gn-CaCO$_3$ containing mats showed enhanced growth compared to Gn (0%) mats, with the viability of the 4% mats was found to be greater than that of the 2% mats for the 1st day. The viability of the 4% mats was decreased during the third day that could be explained by its cytotoxic effect on the cells. The presence of calcium within the mats enhanced the cellular growth which can be attributed to improving the signaling pathways within the cells that in turn increases cellular adhesion (Cheng et al., 2013; X. Zhang et al., 2015).

In conclusion, presence of calcium within the mats greatly affected the viability of the cells, where the 2% concentration of initially added CaCO$_3$ showed the best significant growth compared to both Gn (0%) and 4% mats.

CHAPTER 6

CONCLUSION AND FUTURE PERSPECTIVES

6.1. <u>Conclusion</u>

Gelatin nanofibers successfully synthesized via electrospinning from 40% Gn solution in 40% DAA, where beaded fibers obtained at lower concentrations of gelatin. Different concentrations of $CaCO_3$ (2%, 4%, 5% and 6 %) added each at a time for preparation of Gn-$CaCO_3$ solutions. $CaCO_3$ addition enhanced both the conductivity and the pH values of the prepared solutions.

Various factors found to affect the success of electrospinning process. The macro size of the calcium carbonate used affected the efficacy of nanofibers synthesis when used at higher concentrations. Smooth nanofibers synthesized from 2% and 4% solutions, where beaded broken fibers produced from 5% and 6% solutions. In addition to $CaCO_3$ concentration, the humidity greatly affected the success of obtaining smooth nanofibers from Gn-$CaCO_3$ mixtures.

Calcium retained within the electrospun Gn-$CaCO_3$ mats found to be in form of acetate rather than carbonate due to the interaction of $CaCO_3$ with DAA during solution preparation. The presence of calcium acetate was confirmed via XRD analysis.

Prepared Gn nanofibers are considered a new achievement compared to what previously reported in literature, as the used concentration of gelatin in 40% DAA has not been reported before for gelatin electrospinning. As gelatin nanofibers are highly soluble in water, crosslinking appealed to be an essential step for proper functioning. Different crosslinking time intervals were investigated to determine the optimum crosslinking duration required for better water resistivity and least GTA exposure. Twenty hours crosslinked mats were the most stable mats and thus crosslinking of collected 2% and 4% mats was done for 20 h.

Fourier transforms infrared spectra of all crosslinked mats; Gn (0%) and Gn-$CaCO_3$ (2% and 4%) confirmed the preservation of Gn intrinsic structures, which ensured that neither DAA nor the electrospinning affected its chemical structure. In addition to conservation of Gn structure, DAA completely evaporated from the crosslinked

mats. The complete evaporation of DAA was further confirmed via FTIR results that lacked the 1702 cm^{-1} peak specific for acetic acid.

Although different crosslinking time greatly affected the resistance of the mats to aqueous solution, no dramatic differences in pore size was observed using BJH analysis. All mats possessed pore size distribution up to 250 nm that is suitable for infiltration of gingival epithelia.

Swelling profiles of Gn mats crosslinked at different time intervals coincided with the dissolvability results. Mats crosslinked for 8 h were unstable, with the least resistance to PBS. The presence of calcium within Gn-CaCO$_3$ mats decreased their swelling compared to Gn mats crosslinked for the same time interval.

As degradation rate is a characteristics property of successful periodontal membranes, degradation of calcified gelatin mats was investigated for three weeks. The results implied that investigation of weight loss using PBS solution could lead to misleading results due to salts entrapment and Ca-P growth.

MTT assay employed for different mats confirmed the biocompatibility of prepared Gn nanofibers. Cellular viability slightly affected with the crosslinking time, as all crosslinked mats showed close absorbance to TCPs where Gn mats crosslinked for 20 h possessed significant viability compared to TCPs and other samples. Further addition of calcium to Gn found to enhance cell viability, where 2% mats revealed significant results.

Concisely, calcified gelatin mats can be considered as promising prototypes that with further optimization can be a new member in bioresorbable membranes for healing of periodontitis.

6.2. Future perspectives

- As humidity appealed to be a critical parameter for the production of smooth nanofibers at low concentrations of calcium carbonate, Studying of the effect of humidity variation at high CaCO$_3$ concentrations could be promising in fabrication of smooth nanofibers with high calcium content.

- Investigation on the rate of degradation of calcified crosslinked mats must be repeated using deionized water to have a closer look on weight loss profiles together with the stability of membranes.

- As mineralization found to increase with the soaking time, the effect of mineralization on the pore size must be completely investigated. Full investigation can be done by measuring pore size distribution at different soaking time to determine whether the observed superficial layer could block pores over prolonged PBS immersion.

- As crosslinked calcified gelatin mats promoted mineralization, further investigation on uncrosslinked calcified gelatin nanofibers (2% and 4%) appeals to be promising for their application in surface coating of synthetic polymers especially polyesters, cell culture flasks and metallic biomaterials to enhance cellular adhesion.

- The effect of different crosslinking time used on the pore size distribution and the mineralization of different concentrations of calcium containing mats as a further optimization of the investigated calcified gelatin mats (2% and 4%) crosslinked for 20 h.

7. <u>References</u>

Aldousiri, B., Shalwan, a., & Chin, C. W. (2013). A review on tribological behaviour of polymeric composites and future reinforcements. *Advances in Materials Science and Engineering*, *2013*. doi:10.1155/2013/645923

Andersen, T., Strand, B. L., Formo, K., Alsberg, E., & Christensen, B. E. (2012). Alginates as biomaterials in tissue engineering. *Carbohydrate Chemistry*, *37*, 227–258. doi:10.1039/9781849732765-00227

Annabi, N., Mithieux, S. M., Camci-unal, G., Dokmeci, M. R., Weiss, A. S., & Khademhosseini, A. (2013). Elastomeric recombinant protein-based biomaterials. *Biochemical Engineering Journal*, *77*, 110–118. doi:10.1016/j.bej.2013.05.006

Annabi, N., Vrana, E., & Zorlutuna, P. (2006). *Engineering Biomimetic Scaffolds Approaches to Engineer Biomimetic Constructs* (Vol. 1).

Aurer, A., & JorgiE-Srdjak, K. (2005). Membranes for Periodontal Regeneration. *Acta Stomatologica Croatica*, *39*(1), 107–112.

Avérous, L. (2008). Polylactic Acid : Synthesis , Properties and Applications. *Synthesis*, 2006–2008. doi:10.1055/s-2005-861867

Babu, R. P., O'Connor, K., & Seeram, R. (2013). Current progress on bio-based polymers and their future trends. *Progress in Biomaterials*, *2*(1), 8. doi:10.1186/2194-0517-2-8

Baji, A., Mai, Y. W., Wong, S. C., Abtahi, M., & Chen, P. (2010). Electrospinning of polymer nanofibers: Effects on oriented morphology, structures and tensile properties. *Composites Science and Technology*, *70*(5), 703–718. doi:10.1016/j.compscitech.2010.01.010

Bansal, V., Sharma, P. K., Sharma, N., Pal, O. P., & Malviya, R. (2011). Applications of Chitosan and Chitosan Derivatives in Drug Delivery. *Advanced in Biological Research*, *5*(1), 28–37.

Basu, S., Jana, S., Gandhi, A., & Sen, K. (2011). Natural Polymers and their Application in Drug Delivery and Biomedical Field. *PharmaSciTech*, *1*(1), 16–27. Retrieved from http://scholar.google.com/scholar?hl=en&btnG=Search&q=intitle:Natural+Polymers+and+their+Application+in+Drug+Delivery+and+Biomedical+Field#0

Bergmann, C. P., & Stumpf, A. (2013). *Dental Ceramics*. Berlin, Heidelberg: Springer Berlin Heidelberg. doi:10.1007/978-3-642-38224-6

Berthiaume, F., Maguire, T. J., & Yarmush, M. L. (2011). Tissue engineering and regenerative medicine: history, progress, and challenges. *Annual Review of*

Chemical and Biomolecular Engineering, *2*, 403–30. doi:10.1146/annurev-chembioeng-061010-114257

Bhardwaj, N., & Kundu, S. C. (2010). Electrospinning: A fascinating fiber fabrication technique. *Biotechnology Advances*, *28*(3), 325–347. doi:10.1016/j.biotechadv.2010.01.004

Bigi, A., Cojazzi, G., Panzavolta, S., Rubini, K., & Roveri, N. (2001). Mechanical and thermal properties of gelatin films at different degrees of glutaraldehyde crosslinking. *Biomaterials*, *22*(8), 763–768. doi:10.1016/S0142-9612(00)00236-2

Bottino, M. C., Kamocki, K., Yassen, G. H., Platt, J. a, Vail, M. M., Ehrlich, Y., … Gregory, R. L. (2013). Bioactive nanofibrous scaffolds for regenerative endodontics. *Journal of Dental Research*, *92*(11), 963–9. doi:10.1177/0022034513505770

Bottino, M. C., Thomas, V., Schmidt, G., Vohra, Y. K., Chu, T. M. G., Kowolik, M. J., & Janowski, G. M. (2012). Recent advances in the development of GTR/GBR membranes for periodontal regeneration - A materials perspective. *Dental Materials*, *28*(7), 703–721. doi:10.1016/j.dental.2012.04.022

Bottino, M. C., Yassen, G. H., Platt, J. A., Labban, N., Windsor, L. J., Spolnik, K. J., & Bressiani, A. H. A. (2015). A novel three-dimensional scaffold for regenerative endodontics: materials and biological characterizations. *Journal of Tissue Engineering and Regenerative Medicine*, *9*(11), E116–23. doi:10.1002/term.1712

Bukhari, S. M. H., Khan, S., Rehanullah, M., & Ranjha, N. M. (2015). Synthesis and Characterization of Chemically Cross-Linked Acrylic Acid/Gelatin Hydrogels: Effect of pH and Composition on Swelling and Drug Release. *International Journal of Polymer Science*, *2015*. doi:10.1155/2015/187961

Bullen, H. A., Oehrle, S. A., Bennett, A. F., Taylor, N. M., & Barton, H. A. (2008). Use of attenuated total reflectance fourier transform infrared spectroscopy to identify microbial metabolic products on carbonate mineral surfaces. *Applied and Environmental Microbiology*, *74*(14), 4553–4559. doi:10.1128/AEM.02936-07

Chan, B. P., & Leong, K. W. (2008). Scaffolding in tissue engineering: General approaches and tissue-specific considerations. *European Spine Journal*, *17*(SUPPL. 4). doi:10.1007/s00586-008-0745-3

Chandra, R., & Rustgi, R. (1998a). Biodegradable Polymers. *Prog. Polym. Sci.*, *23*(97), 1273–1335.

Chandra, R., & Rustgi, R. (1998b). Pergamon BIODEGRADABLE POLYMERS. *Progress in Polymer Science*, *23*(97), 1273–1335.

Chen, D. W. C., Lee, F. Y., Liao, J. Y., Liu, S. J., Hsiao, C. Y., & Chen, J. K. (2013). Preclinical experiments on the release behavior of biodegradable nanofibrous multipharmaceutical membranes in a model of four-wall intrabony defect. *Antimicrobial Agents and Chemotherapy*, *57*(1), 9–14. doi:10.1128/AAC.00506-12

Chen, S., Hao, Y., Cui, W., Chang, J., & Zhou, Y. (2013). Biodegradable electrospun PLLA/chitosan membrane as guided tissue regeneration membrane for treating periodontitis. *Journal of Materials Science*, *48*(19), 6567–6577. doi:10.1007/s10853-013-7453-z

Chen, Y., Zhou, X., Lin, Q., & Jiang, D. (2014). Bacterial cellulose/gelatin composites: In situ preparation and glutaraldehyde treatment. *Cellulose*, *21*(4), 2679–2693. doi:10.1007/s10570-014-0272-9

Cheng, S., Wang, W., Lin, Z., Zhou, P., Zhang, X., Zhang, W., … Lu, C. (2013). Effects of extracellular calcium on viability and osteogenic differentiation of bone marrow stromal cells in vitro. *Human Cell*, *26*(3), 114–120. doi:10.1007/s13577-012-0041-8

Chung, H. J., & Park, T. G. (2007). Surface engineered and drug releasing pre-fabricated scaffolds for tissue engineering. *Advanced Drug Delivery Reviews*, *59*(4-5), 249–62. doi:10.1016/j.addr.2007.03.015

Dash, R., Foston, M., & Ragauskas, A. J. (2013). Improving the mechanical and thermal properties of gelatin hydrogels cross-linked by cellulose nanowhiskers. *Carbohydrate Polymers*, *91*(2), 638–645. doi:10.1016/j.carbpol.2012.08.080

Del Gaudio, C., Baiguera, S., Boieri, M., Mazzanti, B., Ribatti, D., Bianco, A., & Macchiarini, P. (2013). Induction of angiogenesis using VEGF releasing genipin-crosslinked electrospun gelatin mats. *Biomaterials*, *34*(31), 7754–7765. doi:10.1016/j.biomaterials.2013.06.040

Dhandayuthapani, B., Yoshida, Y., Maekawa, T., & Kumar, D. S. (2011). Polymeric Scaffolds in Tissue Engineering Application: A Review. *International Journal of Polymer Science*, *2011*(ii), 1–19. doi:10.1155/2011/290602

Di Martino, A., Sittinger, M., & Risbud, M. V. (2005). Chitosan: a versatile biopolymer for orthopaedic tissue-engineering. *Biomaterials*, *26*(30), 5983–90. doi:10.1016/j.biomaterials.2005.03.016

Draget, K. I., Smidsrùd, P. O., & Skjåk-brñk, P. G. (2005). Alginates from Algae. *Wiley-VCH*, 1–30.

Draget, K. I., & Taylor, C. (2011). Chemical, physical and biological properties of alginates and their biomedical implications. *Food Hydrocolloids*, *25*(2), 251–256. doi:10.1016/j.foodhyd.2009.10.007

Dupoirieux, L., Pourquier, D., Picot, M. C., & Neves, M. (2001). Comparative study of three different membranes for guided bone regeneration of rat cranial defects. *International Journal of Oral and Maxillofacial Surgery*, *30*(1), 58–62. doi:http://dx.doi.org/10.1054/ijom.2000.0011

Erencia, M., Cano, F., Tornero, J. A., Fernandes, M. M., Tzanov, T., Macan??s, J., & Carrillo, F. (2015). Electrospinning of gelatin fibers using solutions with low acetic acid concentration: Effect of solvent composition on both diameter of electrospun fibers and cytotoxicity. *Journal of Applied Polymer Science*, *132*(25), 1–11. doi:10.1002/app.42115

Freeman, J. W., & Kwansa, A. L. (2008). Recent Advancements in Ligament Tissue Engineering : The Use of Various Techniques and Materials for ACL Repair. *Recent Patents on Biomedical Engineering*, 18–23.

Fujihara, K., Kotaki, M., & Ramakrishna, S. (2005). Guided bone regeneration membrane made of polycaprolactone/calcium carbonate composite nano-fibers. *Biomaterials*, *26*(19), 4139–4147. doi:10.1016/j.biomaterials.2004.09.014

Gómez-Guillén, M. C., Giménez, B., López-Caballero, M. E., & Montero, M. P. (2011). Functional and bioactive properties of collagen and gelatin from alternative sources: A review. *Food Hydrocolloids*, *25*(8), 1813–1827. doi:10.1016/j.foodhyd.2011.02.007

Gonçalves, F., de Moraes, M. S., Ferreira, L. B., Carreira, A. C. O., Kossugue, P. M., Boaro, L. C. C., … Catalani, L. H. (2016). Combination of Bioactive Polymeric Membranes and Stem Cells for Periodontal Regeneration: In Vitro and In Vivo Analyses. *PloS One*, *11*(3), e0152412. doi:10.1371/journal.pone.0152412

Gunatillake, P. A., & Adhikari, R. (2003). Biodegradable synthetic polymers for tissue engineering. *European Cells and Materials*, *5*, 1–16.

Halley, P. J., & Averous, L. (2014). Starch Polymers. In *Starch Polymers: From Genetic Engineering to Green Applications* (First., pp. 3–10). Elsevier. doi:10.1016/B978-0-444-53730-0.00018-X

Ham, J., & Miller, P. J. (2003). Expanded Polytetrafluoroethylene Implants in Rhinoplasty: Literature Review, Operative Techniques, and Outcome. *Facial Plastic Surgery*, *19*(4), 331–339. doi:10.1055/s-2004-815653

Huang, L., Liu, B., Cha, J. Y., Yuan, G., Kelly, M., Singh, G., … Helms, J. A. (2016). Mechanoresponsive Properties of the Periodontal Ligament. *Journal of Dental Research*. doi:10.1177/0022034515626102

Huang, Z. M., Zhang, Y. Z., Ramakrishna, S., & Lim, C. T. (2004). Electrospinning and mechanical characterization of gelatin nanofibers. *Polymer*, *45*(15), 5361–5368. doi:10.1016/j.polymer.2004.04.005

Humenik, M., Smith, A. M., & Scheibel, T. (2011). Recombinant Spider Silks—Biopolymers with Potential for Future Applications. *Polymers*, *3*, 640–661. doi:10.3390/polym3010640

Irvine, S. a., Agrawal, A., Lee, B. H., Chua, H. Y., Low, K. Y., Lau, B. C., … Venkatraman, S. (2015). Printing cell-laden gelatin constructs by free-form fabrication and enzymatic protein crosslinking. *Biomedical Microdevices*, *17*(1), 1–8. doi:10.1007/s10544-014-9915-8

Izwan, S., Razak, A., Fadzliana, N., Sharif, A., Aizan, W., & Abdul, W. (2012). Biodegradable Polymers and their Bone Applications : A Review. *International Jounrnal of Basic and Applied Sciences*, *12*(February), 31–49.

Jafari, M., Paknejad, Z., Rad, M. R., Motamedian, S. R., Eghbal, M. J., Nadjmi, N., & Khojasteh, A. (2015). Polymeric scaffolds in tissue engineering: A literature review. *Journal of Biomedical Materials Research - Part B Applied Biomaterials*. doi:10.1002/jbm.b.33547

Jia, J., Liu, G., Guo, Z. X., Yu, J., & Duan, Y. (2012). Preparation and characterization of soluble eggshell membrane protein/PLGA electrospun nanofibers for guided tissue regeneration membrane. *Journal of Nanomaterials*, *2012*. doi:10.1155/2012/282736

Johlin, J. M. (1930). Isoelectric Point of Gelatin. *Journal of Biological Chemistry*, *86*, 231–234.

Kalia, S., Dufresne, A., Cherian, B. M., Kaith, B. S., Avérous, L., Njuguna, J., & Nassiopoulos, E. (2011). Cellulose-Based Bio- and Nanocomposites: A Review. *International Journal of Polymer Science*, *2011*, 1–35. doi:10.1155/2011/837875

Kamel, S., Ali, N., Jahangir, K., Shah, S. M., & El-Gendy, A. A. (2008). Pharmaceutical significance of cellulose: A review. *eXPRESS Polymer Letters*, *2*(11), 758–778. doi:10.3144/expresspolymlett.2008.90

Ki, C. S., Baek, D. H., Gang, K. D., Lee, K. H., Um, I. C., & Park, Y. H. (2005). Characterization of gelatin nanofiber prepared from gelatin-formic acid solution. *Polymer*, *46*(14), 5094–5102. doi:10.1016/j.polymer.2005.04.040

Kim, Y. K., & Park, J. B. (2003). *Biomaterials: Principles and Applications* (Vol. 12).

Lee, K., Yoon, K. U. K. R. O., Woo, S. I. H. L., & Choi, I. S. (2003). Surface Modification of Poly (glycolic acid) (PGA) for Biomedical Applications. *Journal of Pharmaceutical Sciences*, *92*(5), 933–937.

Li, H., Wang, M., Williams, G. R., Wu, J., Sun, X., Lv, Y., & Zhu, L.-M. (2016). Electrospun gelatin nanofibers loaded with vitamins A and E as antibacterial wound dressing materials. *RSC Adv.*, *6*(55), 50267–50277. doi:10.1039/C6RA05092A

Li, Z., Ramay, H. R., Hauch, K. D., Xiao, D., & Zhang, M. (2005). Chitosan-alginate hybrid scaffolds for bone tissue engineering. *Biomaterials*, *26*(18), 3919–28. doi:10.1016/j.biomaterials.2004.09.062

Liao, H., Zhang, H., & Chen, W. (2009). Differential physical, rheological, and biological properties of rapid in situ gelable hydrogels composed of oxidized alginate and gelatin derived from marine or porcine sources. *Journal of Materials Science: Materials in Medicine*, *20*(6), 1263–1271. doi:10.1007/s10856-009-3694-4

Liu, X., & Ma, P. X. (2009). Phase separation, pore structure, and properties of nanofibrous gelatin scaffolds. *Biomaterials*, *30*(25), 4094–4103. doi:10.1016/j.biomaterials.2009.04.024

Ma, P. X. (2004). Scaffolds for tissue fabrication. *Materials Today*, *7*(5), 30–40. doi:10.1016/S1369-7021(04)00233-0

Mao, J., Kondu, S., Ji, H.-F., & McShane, M. J. (2015). Response of chitosan/gelatin-coated microcantilever to small pH change. *Biotechnol Bioeng*, *95*(June 2016), 333–341. doi:10.1002/bit.20755.Study

Mediaswanti, K., Wen, C., Ivanova, E. P., Berndt, C. C., Malherbe, F., Thi, V., … Wang, J. (2013). Biomimetics Biomaterials and Tissue Engineering A Review on Bioactive Porous Metallic Biomaterials, *18*(1), 1–8. doi:10.4172/1662-100X.1000104

Meng, Z. X., Li, H. F., Sun, Z. Z., Zheng, W., & Zheng, Y. F. (2013). Fabrication of mineralized electrospun PLGA and PLGA/gelatin nanofibers and their potential in bone tissue engineering. *Materials Science and Engineering C*, *33*(2), 699–706. doi:10.1016/j.msec.2012.10.021

Meng, Z. X., Wang, Y. S., Ma, C., Zheng, W., Li, L., & Zheng, Y. F. (2010). Electrospinning of PLGA/gelatin randomly-oriented and aligned nanofibers as potential scaffold in tissue engineering. *Materials Science and Engineering C*, *30*(8), 1204–1210. doi:10.1016/j.msec.2010.06.018

Mindru, T. B., Mindru, I. B., Malutant, T., & Tura, V. (2007). Electrospinning of high concentration gelatin solutions. *Journal of Optoelectronics and Advanced Materials*, *9*(11), 3633–3638.

Mobini-Dehkordi, M., & Javan, F. A. (2012). Application of alpha-amylase in biotechnology. *Biology and Today's World*, *1*(1), 39–50.

Moon, R. J., Martini, A., Nairn, J., Simonsen, J., & Youngblood, J. (2011). *Cellulose nanomaterials review: structure, properties and nanocomposites. Chemical Society reviews* (Vol. 40). doi:10.1039/c0cs00108b

Nagarajan, R., Miller, C. S., Dawson, D., Al-Sabbagh, M., & Ebersole, J. L. (2015). Patient-specific variations in biomarkers across gingivitis and periodontitis. *PLoS ONE*, *10*(9), 1–16. doi:10.1371/journal.pone.0136792

Nair, L. S., & Laurencin, C. T. (2007). Biodegradable polymers as biomaterials. *Progress in Polymer Science*, *32*, 762–798. doi:10.1016/j.progpolymsci.2007.05.017

Nasab, M. B., & Hassan, M. R. (2010). Metallic Biomaterials of Knee and Hip - A Review. *Trends in Biomaterials and Artificial Organs*, *24*(1), 69–82.

Nguyen, T.-H., & Lee, B.-T. (2010). Fabrication and characterization of cross-linked gelatin electro-spun nano-fibers. *Journal of Biomedical Science and Engineering*, *03*(12), 1117–1124. doi:10.4236/jbise.2010.312145

Nirmala, R., Nam, K. T., Navamathavan, R., Park, S. J., & Kim, H. Y. (2011). Hydroxyapatite Mineralization on the Calcium Chloride Blended Polyurethane Nanofiber via Biomimetic Method. *Nanoscale Research Letters*, *6*(1), 1–8. doi:10.1007/s11671-010-9737-4

Norowski, P. A., Babu, J., Adatrow, P. C., Garcia-Godoy, F., Haggard, W. O., & Bumgardner, J. D. (2012). Antimicrobial Activity of Minocycline-Loaded Genipin-Crosslinked Nano-Fibrous Chitosan Mats for Guided Tissue Regeneration. *Journal of Biomaterials and Nanobiotechnology*, *03*(04), 528–532. doi:10.4236/jbnb.2012.324054

O'Brien, F. J. (2011). Biomaterials & scaffolds for tissue engineering. *Materials Today*, *14*(3), 88–95. doi:10.1016/S1369-7021(11)70058-X

Okutan, N., Terzi, P., & Altay, F. (2014). Affecting parameters on electrospinning process and characterization of electrospun gelatin nanofibers. *Food Hydrocolloids*, *39*, 19–26. doi:10.1016/j.foodhyd.2013.12.022

Oliveira, A. L., Malafaya, P. B., & Reis, R. L. (2003). Sodium silicate gel as a precursor for the in vitro nucleation and growth of a bone-like apatite coating in compact and porous polymeric structures. *Biomaterials*, *24*(15), 2575–2584. doi:10.1016/S0142-9612(03)00060-7

Oryan, A., Alidadi, S., Moshiri, A., & Maffulli, N. (2014). Bone regenerative medicine: classic options, novel strategies, and future directions. *Journal of Orthopaedic Surgery and Research*, *9*(1), 18. doi:10.1186/1749-799X-9-18

Palmer W. Walter, A. D. and L. R. F. (1921). The effect of increasing concentrations of Gelatin on the conductivity of sodium chloride solution. *Journal of General Physiology*, 341.

Pan, J., Liu, N., Sun, H., & Xu, F. (2014). Preparation and characterization of electrospun PLCL/Poloxamer nanofibers and dextran/gelatin hydrogels for skin tissue engineering. *PloS One*, *9*(11), e112885. doi:10.1371/journal.pone.0112885

Patel, H., Bonde, M., & Srinivasan, G. (2011). Biodegradable Polymer Scaffold for Tissue Engineering. *Trends Biomater. Organs*, *25*(1), 20–29.

Pellegrini, G., Pagni, G., & Rasperini, G. (2013). Surgical approaches based on biological objectives: GTR versus GBR techniques. *International Journal of Dentistry*, *2013*. doi:10.1155/2013/521547

Pham, Q. P., Sharma, U., & Mikos, A. G. (2006). Electrospinning of polymeric nanofibers for tissue engineering applications: a review. *Tissue Engineering*, *12*(5), 1197–211. doi:10.1089/ten.2006.12.1197

Pilliar, R. M., & Metals, I. W. (2009). *Biomedical Materials*. (R. Narayan, Ed.). Boston, MA: Springer US. doi:10.1007/978-0-387-84872-3

Puppi, D., Chiellini, F., Piras, A. M., & Chiellini, E. (2010). Progress in Polymer Science Polymeric materials for bone and cartilage repair. *Progress in Polymer Science*, *35*(4), 403–440. doi:10.1016/j.progpolymsci.2010.01.006

Qasim, S. B., Delaine-Smith, R. M., Fey, T., Rawlinson, A., & Rehman, I. U. (2015). Freeze gelated porous membranes for periodontal tissue regeneration. *Acta Biomaterialia*, *23*, 317–28. doi:10.1016/j.actbio.2015.05.001

Qiu, X., & Hu, S. (2013). "Smart" Materials Based on Cellulose: A Review of the Preparations, Properties, and Applications. *Materials*, *6*(3), 738–781. doi:10.3390/ma6030738

Rakhmatia, Y. D., Ayukawa, Y., Furuhashi, A., & Koyano, K. (2013). Current barrier membranes: Titanium mesh and other membranes for guided bone regeneration in dental applications. *Journal of Prosthodontic Research*, *57*(1), 3–14. doi:10.1016/j.jpor.2012.12.001

Ramakrishna, S., Mayer, J., Wintermantel, E., & Leong, K. W. (2001). Biomedical applications of polymer-composite materials: a review. *Composites Science and Technology*, *61*(9), 1189–1224. doi:10.1016/S0266-3538(00)00241-4

Reddy, N., Reddy, R., & Jiang, Q. (2015). Crosslinking biopolymers for biomedical applications. *Trends in Biotechnology*. doi:10.1016/j.tibtech.2015.03.008

Rehm, B. H. A. (2009). Alginates: Biology and Applications. *Microbiology Monographs, Springer*, *13*. doi:10.1007/978-3-540-92679-5

Ren, J. (2010). Lactic Acid. *Biodegradable Poly (Lactic Acid): Synthesis, Modification, Processing and Applications*, 4–14. doi:10.1007/978-3-642-17596-1_2

Rinaudo, M. (2006). Chitin and chitosan : Properties and applications. *Prog. Polym. Sci.*, *31*, 603–632. doi:10.1016/j.progpolymsci.2006.06.001

Rispoli L, Fontana F, Beretta M, P. Ce. M. C. (2015). Surgery Guidelines for Barrier Membranes in Guided Bone Regeneration (GBR). *Otolaryngology and Rhinology ClinMed*, *1*(2), 1–8.

Rose, J. B., Pacelli, S., El Haj, A. J., Dua, H. S., Hopkinson, A., White, L. J., & Rose, F. R. A. J. (2014). Gelatin-based materials in ocular tissue engineering. *Materials*, *7*(4), 3106–3135. doi:10.3390/ma7043106

Rucker, M., Laschke, M. W., Junker, D., Carvalho, C., Tavassol, F., Mulhaupt, R., … Menger, M. D. (2008). Vascularization and biocompatibility of scaffolds consisting of different calcium phosphate compounds. *Journal of Biomedical Materials Research - Part A*, *86*(4), 1002–1011. doi:10.1002/jbm.a.31722

Sachlos, E., & Czernuszka, J. T. (2003). Making tissue engineering scaffolds work. Review on the application of solid freeform fabrication technology to the production of tissue engineering scaffolds. *European Cells and Materials*, *5*, 29–40.

Sam, G., & Madhavan Pillai, B. R. (2014). Evolution of barrier membranes in periodontal regeneration-"Are the third generation membranes really here?" *Journal of Clinical and Diagnostic Research*, *8*(12), ZE14–ZE17. doi:10.7860/JCDR/2014/9957.5272

Scantlebury, T., & Ambruster, J. (2012). The development of guided regeneration: Making the impossible possible and the unpredictable predictable. *Journal of Evidence-Based Dental Practice*, *12*(3 SUPPL.), 101–117. doi:10.1016/S1532-3382(12)70022-2

Seal, B., Otero, T., & Panitch, A. (2001). Polymeric biomaterials for tissue and organ regeneration. *Materials Science and Engineering: R: …*, *34*, 147–230. Retrieved from http://www.sciencedirect.com/science/article/pii/S0927796X01000353

Sell, S. A., Wolfe, P. S., Garg, K., McCool, J. M., Rodriguez, I. A., & Bowlin, G. L. (2010). The use of natural polymers in tissue engineering: A focus on electrospun extracellular matrix analogues. *Polymers*, *2*(4), 522–553. doi:10.3390/polym2040522

Shastri, V. P. (2003). Non-degradable biocompatible polymers in medicine: past, present and future. *Current Pharmaceutical Biotechnology*, *4*(5), 331–337. doi:10.2174/1389201033489694

Shue, L., Yufeng, Z., & Mony, U. (2012). Biomaterials for periodontal regeneration: a review of ceramics and polymers. *Biomatter*, *2*(4), 271–277. doi:10.4161/biom.22948

Siimon, K., Siimon, H., & Jarvekulg, M. (2015). Mechanical characterization of electrospun gelatin scaffolds cross-linked by glucose. *Journal of Materials Science. Materials in Medicine*, *26*(1), 5375. doi:10.1007/s10856-014-5375-1

Smith, M. C., Goddard, E. T., Perusina Lanfranca, M., & Davido, D. J. (2013). hTERT Extends the Life of Human Fibroblasts without Compromising Type I Interferon Signaling. *PLoS ONE*, *8*(3), 1–11. doi:10.1371/journal.pone.0058233

Song, J. H., Kim, H. E., & Kim, H. W. (2008). Production of electrospun gelatin nanofiber by water-based co-solvent approach. *Journal of Materials Science: Materials in Medicine*, *19*(1), 95–102. doi:10.1007/s10856-007-3169-4

Srivastava, S., Tandon, P., Gupta, K. K., Srivastava, A., Kumar, V., & Shrivastava, T. (2015). A comparative clinico-radiographic study of guided tissue regeneration with bioresorbable membrane and a composite synthetic bone graft for the treatment of periodontal osseous defects. *Journal of Indian Society of Periodontology*, *19*(4), 416–421. doi:10.4103/0972-124X.154544

Subia, B., Kundu, J., & Kundu, S. (2010). Biomaterial scaffold fabrication techniques for potential tissue engineering applications. *Tissue Engineering*, (3), 141–159. doi:10.5772/189

Sun, J., & Tan, H. (2013). Alginate-Based Biomaterials for Regenerative Medicine Applications. *Materials*, *6*(4), 1285–1309. doi:10.3390/ma6041285

Tawakkal, I. S. M. a, Cran, M. J., Miltz, J., & Bigger, S. W. (2014). A review of poly(lactic acid)-based materials for antimicrobial packaging. *Journal of Food Science*, *79*(8). doi:10.1111/1750-3841.12534

Tronci, G., Kanuparti, R. S., Arafat, M. T., Yin, J., Wood, D. J., & Russell, S. J. (2015). Wet-spinnability and crosslinked fibre properties of two collagen polypeptides with varied molecular weight. *International Journal of Biological Macromolecules*, *81*, 112–120. doi:10.1016/j.ijbiomac.2015.07.053

V, G. U., & A, P. S. (2013). REVIEW ARTICLE . A review of biopolymer chitosan blends in polymer system. *Int. Res. J of Science & Engineering*, *1*(1), 13–16.

Viktor, M. J., Rose, S. H., van Zyl, W. H., & Viljoen-Bloom, M. (2013). Raw starch conversion by Saccharomyces cerevisiae expressing Aspergillus tubingensis amylases. *Biotechnology for Biofuels*, *6*(1), 167. doi:10.1186/1754-6834-6-167

Vroman, I., & Tighzert, L. (2009). Biodegradable Polymers. *Materials*, *2*(2), 307–344. doi:10.3390/ma2020307

Wang, J., Wang, L., Zhou, Z., Lai, H., Xu, P., Liao, L., & Wei, J. (2016). Biodegradable Polymer Membranes Applied in Guided Bone/Tissue Regeneration: A Review. *Polymers*, *8*(4), 115. doi:10.3390/polym8040115

Woo, K. M., Chen, V. J., & Ma, P. X. (2003). Nano-fibrous scaffolding architecture selectively enhances protein adsorption contributing to cell

attachment. *Journal of Biomedical Materials Research. Part A*, *67*, 531–537. doi:10.1002/jbm.a.10098

Woodruff, M. A., & Hutmacher, D. W. (2010). Progress in Polymer Science The return of a forgotten polymer — Polycaprolactone in the 21st century. *Progress in Polymer Science*, *35*, 1217–1256. doi:10.1016/j.progpolymsci.2010.04.002

Xia, Y., Yao, J., Li, N., Shao, C.-H., Shen, X.-Y., Xie, L.-Z., … Gu, N. (2014). Electrospun poly(butylene carbonate) membranes for guided bone regeneration: In vitro and in vivo studies. *Journal of Bioactive and Compatible Polymers*, *29*(5), 486–499. doi:10.1177/0883911514543055

Xing, Q., Yates, K., Vogt, C., Qian, Z., Frost, M. C., & Zhao, F. (2014). Increasing mechanical strength of gelatin hydrogels by divalent metal ion removal. *Scientific Reports*, *4*, 4706. doi:10.1038/srep04706

Xue, J., He, M., Liang, Y., Crawford, A., Coates, P., Chen, D., … Zhang, L. (2014). Fabrication and evaluation of electrospun PCL–gelatin micro-/nanofiber membranes for anti-infective GTR implants. *J. Mater. Chem. B*, *2*(39), 6867–6877. doi:10.1039/C4TB00737A

Yang, F., Both, S. K., Yang, X., Walboomers, X. F., & Jansen, J. A. (2009). Development of an electrospun nano-apatite/PCL composite membrane for GTR/GBR application. *Acta Biomaterialia*, *5*(9), 3295–3304. doi:10.1016/j.actbio.2009.05.023

Zhan, J., & Lan, P. (2012). The Review on Electrospun Gelatin Fiber Scaffold. *Journal of Research Updates in Polymer Science*, *1*(2), 59–71. doi:10.6000/1929-5995.2012.01.02.1

Zhang, S., Huang, Y., Yang, X., Mei, F., Ma, Q., Chen, G., … Deng, X. (2009). Gelatin nanofibrous membrane fabricated by electrospinning of aqueous gelatin solution for guided tissue regeneration. *Journal of Biomedical Materials Research. Part A*, *90*, 671–679. doi:10.1002/jbm.a.32136

Zhang, X., Meng, S., Huang, Y., Xu, M., He, Y., Lin, H., … Deng, X. (2015). Electrospun Gelatin / ? -TCP Composite Nanofibers Enhance Osteogenic Differentiation of BMSCs and In Vivo Bone Formation by Activating Ca 2 + - Sensing Receptor Signaling, *2015*.

Zhang, Y. Z., Venugopal, J., Huang, Z. M., Lim, C. T., & Ramakrishna, S. (2006). Crosslinking of the electrospun gelatin nanofibers. *Polymer*, *47*(8), 2911–2917. doi:10.1016/j.polymer.2006.02.046

Zhang, Y., Zhang, X., Shi, B., & Miron, R. (2013). Membranes for guided tissue and bone regeneration. *Annals of Oral and Maxillofacial Surgery*, *1*(1), 1–10. doi:10.13172/2052-7837-1-1-451